AD-A256 560

TD 91-3982

report no.
FEL-91-A375
PH9066FEL

copy no.

3

title

Definition study PHARUS: final report

author(s):

(see page 2)

date   :

November 1991

DTIC
S ELECTE D
OCT 29 1992
E

classification

title	: unclassified
abstract	: unclassified
report text	: unclassified
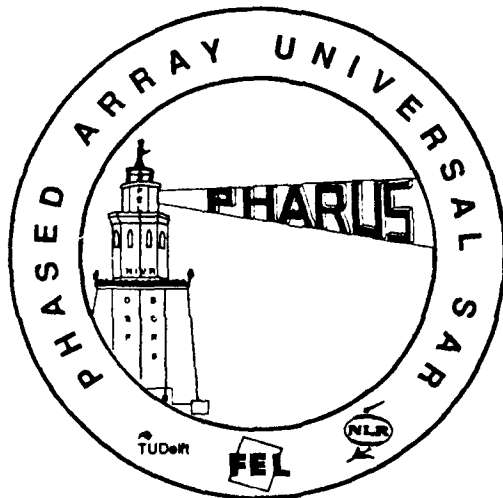
no. of copies   : 75

no. of pages   : 107   (excl. RDP & distribution list)

appendices   : -

All information which is classified according to Dutch regulations shall be treated by the recipient in the same way as classified information of corresponding value in his own country. No part of this information will be disclosed to any party.

PHASED ARRAY UNIVERSAL SAR
PHARUS
TUDelft   FEL   NLR

92-28368

92 10 27 173

NLR — TNO — **TU**Delft

AUTHORS:		
FEL-TNO:	**NLR**	**TU Delft**
Ir. P. Hoogeboom	Ir. H. Pouwels	Ir. P.J. Snoeij
Ir. P.J. Koomen	Dr. G. van der Burg	J.L.Tauritz M.Sc
Ir. W.P.M.N. Keizer	Ir. H.J. Breeman	Ir. A. Vellekoop
Ir. M.P.G. Otten		
Ir. M.H.A. Paquay		
Ir. H.J. Visser		
Ing. A.P. de Hek		

TNO report

report no.	:	FEL-91-A375
title	:	Definition study PHARUS: final report
author(s)	:	(see page 2)
institute	:	TNO Physics and Electronics Laboratory
date	:	November 1991
NDRO no.	:	-
no. in pow '91	:	715.3
Research supervised by:		Ir. P. Hoogeboom
Research carried out by :		(see page 2)

ABSTRACT (UNCLASSIFIED)

This report describes the results of the PHARUS definition stage, which can be distinguished in three main parts:

- Antenna technology study,
- Motion compensation study,
- Realisation of a SAR testbed.

The antenna technology study was mainly focussed on the theory and design of patch antennae. Further the study included the theory of internal calibration of SAR systems, microwave components under pulsed conditions and measurements of phased arrays under operational conditions.

The second study was focussed on finding a solution for the motion compensation in PHARUS. The study included the development of a SAR data simulator to evaluate the degradation of the SAR image by the motion of the aircraft. A motion sensor package for PHARUS was proposed. For verification, this motion sensor package was used in the SAR testbed.

The third study consisted of the design and development of a SAR testbed and processor to gain experience with airborne SAR technology. The SAR testbed had an active eight element antenna with distributed solid state power generation. Innovative microwave technology was used in the design of the radarsystem.
A real time digital azimuth filter was developed to reduce the large data stream to such a level that maximum recording capacity was not overdrawn. A personal computer enabled full control over the radarsystem.
Algorithms are developed for the use in the SAR processor. In combination with the results of the motion compensation study the requirements for PHARUS were met.

The results of the definition study are used for the pre-design of the PHARUS system.

NLR ——————— TNO ——————— TUDelft

rapport no.	:	FEL-91-A375
titel	:	Definitie studie PHARUS: eindrapport
auteur(s)	:	(zie pagina 2)
instituut	:	Fysisch en Elektronisch Laboratorium TNO
datum	:	november 1991
hdo-opdr.no.	:	-
no. in iwp '91	:	715.3
Onderzoek uitgevoerd o.l.v.	:	Ir. P. Hoogeboom
Onderzoek uitgevoerd door	:	(see page 2)

SAMENVATTING (ONGERUBRICEERD)

Dit rapport geeft een overzicht van de resultaten uit de PHARUS definitie fase, die opgedeeld kan worden in drie hoofdstukken:

- Antenne technologie studie
- Bewegingscompensatie studie
- Realisatie van een SAR testbed.

The antenne technologie studie richtte zich voornamelijk op de theorie en ontwerp van patch antennes. In deze studie kwamen ook interne calibratie van SAR systemen, microgolf componenten onder gepulste condities en metingen van phased arrays onder operationele condities aan de orde.

De tweede studie richtte zich op een oplossing voor het bewegingscompensatie probleem in PHARUS. De studie bevatte tevens de ontwikkeling van een SAR data simulator om de degradatie van een SAR afbeelding door de bewegingen van het vliegtuig te kunnen evalueren. Een combinatie van bewegingssensoren werd voor PHARUS voorgesteld. Voor de verificatie van de resultaten werd deze combinatie toegepast in het SAR testbed.

De derde studie bestond uit het ontwerp en de ontwikkeling van een SAR testbed en een SAR processor om ervaring op te bouwen met vliegtuig SAR technologie. Het SAR testbed bestond uit een acht elements aktieve antenne met gedistribueerde solid state vermogensopwekking. Innovatieve microgolf technologie werd gebruikt bij het ontwerp van het radarsysteem.
Een real time digitaal azimuth filter werd ontwikkeld om de grote datastroom zodanig te reduceren dat de maximale recording capaciteit niet overschreden werd. Een personal computer werd gebruikt om het radarsysteem te bedienen.

Voor de SAR processor werden algoritmes ontwikkeld die, in combinatie met de resultaten uit de bewegingscompensatie studie, aan de gestelde PHARUS eisen konden voldoen.

De resultaten uit de definitie studie zijn gebruikt in het voorontwerp van het PHARUS systeem.

TNO report

TNO report

1   INTRODUCTION

The PHased ARray Universal Synthetic Aperture Radar (PHARUS) project started in 1988 as a Netherlands national project, after preparatory studies in the previous years. The initiative for this project came from the remote sensing community, which in the years before performed extensive studies using an X-band SLAR and groundbased scatterometers. Furthermore international airborne campaigns offered data from various radar sensors.

Remote sensing studies indicated the need for stable, accurate and calibrated radar systems. These properties were not obvious, since radar was originally developed as a detection and ranging device, without pertinent attention to radiometric performance.
The Dutch X-band SLAR for instance had an internal loop to calibrate its unstabilized magnetron signal. However the need for a coherent, stable radar system became stronger over the years.

A "coherent radar" study, performed for the BCRS (National Remote Sensing Board) in 1985/1986 [Krul, 1986], was the basis for the PHARUS project. At that time polarimetric SAR technology was introduced for the first time in the U.S. This technology was taken into account in the coherent radar study, even though a full understanding of the added value in remote sensing was missing.

An important factor in the development of microwave remote sensing systems is the choice of frequency. Although the coherent radar study initially aimed for a detailed analysis of pro's and con's of possible frequencies and polarisations, the final choice was based on the ERS-1, ESA's remote sensing satellite for the nineties. For ERS-1 the C-band (5.3 GHz, wavelength 5.6 cm) was selected. The frequency analysis in the coherent radar study was limited to what could be expected from a C-band radar for remote sensing applications.

The PHARUS project had to become much more than the simple and straightforward construction of a C-band SAR. The Dutch community that developed the plans had no experience in SAR technology and SAR processing. Furthermore there was a lack of knowledge on polarimetric antennae and radar systems. Finally for the realisation of an airborne SAR the development of systems capable of measuring the aircraft motions with high accuracy was necessary (.1 wavelength, 5 mm).

TNO report

The set-up of the PHARUS project reflects the above mentioned points. It is illustrated in figure 1.1. The complete PHARUS project consists of two parts, a definition study and a realisation phase. The definition study had to solve the problems that were encountered in the coherent radar study and it's aim was to gain experience with SAR technology and with airborne SAR problems. The realisation phase will profit from the gained experience and will lead to a straightforward and riskfree development of a polarimetric SAR system.

```
Projectmanagement          Antennatechnology
FEL       WP 0             FEL, TUD    WP 1
P.Hoogeboom                P.Snoeij

                           Ant.motion & comp.
                           FEL, NLR    WP 2
                           H.Pouwels

                           PHARS, SAR testbed
                           FEL,NLR     WP 3
                           P.Koomen

                           PHARUS design
                           FEL,NLR,TUD  WP 4
                           P.Hoogeboom
```
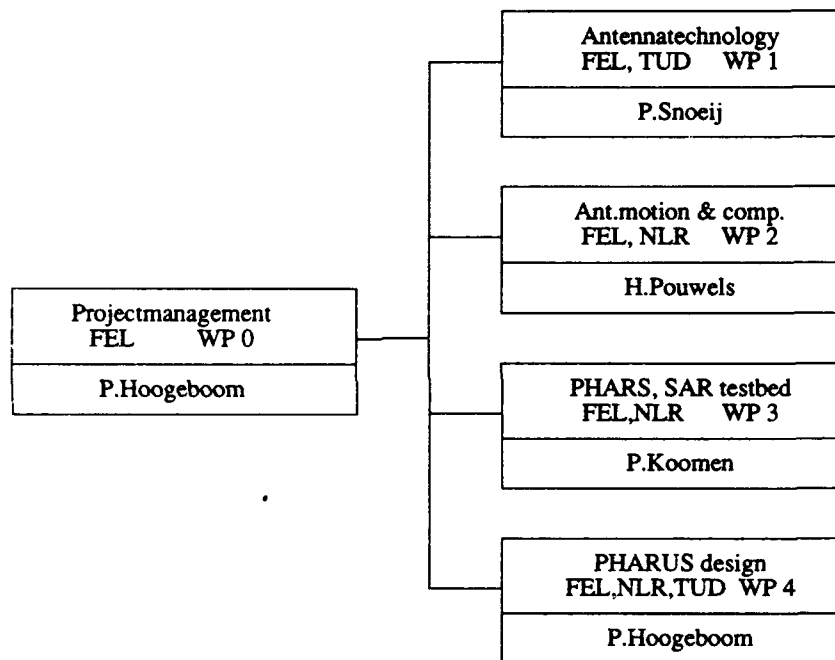
Fig. 1.1:   Work breakdown structure for the PHARUS project in the the definition study.

The work breakdown structure in figure 1.1 shows the workpackages for the definition study. The results of these workpackages are discussed in the separate chapters of this report. The antenna technology study was mainly focused on the theory and design of patch antennae, including polarimetric designs. Other items were microwave switches and components for the T/R modules, internal calibration schemes and antenna measurements of phased arrays under pulsed conditions. The PHARUS project is focused to new, innovative microwave technology, including active antennae, equipped with distributed solid state power generation. This strategy will not only lead to experience in the field of SAR, but also in the state of the art microwave technology, nowadays

being developed for space applications: a distinct, but humble jump to the space technology market.

The second study was focused on motion compensation and is reported in chapter 3. First a computer based simulator of raw SAR data was developed. This simulator was used to study the impact of aircraft motions, resulting in a precise definition of the motion compensation requirements. An experimental verification was performed with the SAR testbed, developed in the third study. In the verification program a combination was used of inertial sensors, which were mounted close to the SAR antenna in order to achieve a very high measurement accuracy necessary for this application.

The third study consisted of the realisation of a SAR testbed (simple SAR system for experimental and verification purposes). The development of the radar, the data handling and the recording hardware is described in chapter 4. This study was also focussed on the development of SAR processing algorithms including so-called autofocus algorithms, which determine the aircraft trajectory from the radar data. This strategy enabled a comparison with the results of the motion compensation study and allowed to determine whether the achievable motion compensation level met our demands set for PHARUS. Chapter 4 also discusses the results obtained from a testflight with the PHARS SAR testbed. Both the radar performance and the motion compensation system performance are evaluated.

The results of the three studies are used for the pre-design of the PHARUS system, described in chapter 5.

The PHARUS study was carried out by the Physics and Electronics Laboratory of TNO in The Hague, The National Aerospace Laboratory in Amsterdam and Marknesse, and by the Delft University of Technology, Laboratory for Telecommunication and Remote Sensing Technology. FEL-TNO had the lead and was responsible for the project management. On behalf of the Ministry of Defence and the National Remote Sensing Board, who were the prime sponsors of the project, the Netherlands Agency for Aerospace Programs in Delft was responsible for the program management.

The definition study PHARUS was started in the first half of 1988 and ended early 1991. The project execution was close to the project plans in every respect (time, money, results). The completion of the studies was rewarded with a successful testflight of the PHARS testbed on 8 November 1990.

2   RESULTS FROM THE ANTENNA TECHNOLOGY STUDY

2.1   Patch antennae

2.1.1   Microstrip Antennae

Among all available types of radiators, antennae based on microstrip technology have many constructional advantages. Especially the fact that it is a flat and lightweight structure makes it very suited for application with airborne radar. The manufacturing of microstrip antennae is similar to the etching of printed circuit boards which implies that there is an enormous flexibility in possible configurations. Unfortunately, not much experience with this antenna-type was available. The lack of experience with polarimetric SAR systems complicated the derivation of design parameters. Consequently it was difficult to set up realistic requirements for the antenna performance. Only the major parameters were defined at the start of the study:

-    centre frequency   : 5.3 GHz
-    bandwidth   : 100 MHz (max. 1 dB variation)
-    two orthogonal linear polarisations

Other parameters were defined as guide-lines:

-    polarisation decoupling : 20 dB
-    elevation scan range   : 60 degrees (near swath till far swath)
-    elevation beam width   : far swath : 6 degrees
     (two way -3 dB)   near swath: 25 degrees.
-    azimuth scan range   : ± 12 degrees
-    azimuth beam width   : 6 degrees (two way -3 dB, as flat as possible)
-    sidelobes   : as low as possible.

Antenna tuning is difficult with this technique. For each combination of design parameters a new antenna has to be made and tested. A pure experimental approach is a long (and maybe never ending) road to success. A supporting theory is preferable to design microstrip antennae. Such a theory or software was not available at the start of the project. So this had to be the first step, followed by experimental verification.

2.1.2 Theoretical Model

In literature, a variety of methods and models is described. A surveying book of Bahl and Bhartia [Bahl, Bhartia, 1980] served as a guide. Based on some diagrams, several conclusions could already be drawn:

- The optimum relative dielectric constant ε_r of the antenna substrate has to be between 2 and 3. Lower ε_r-values give a too narrow beam, higher values result in a low gain.
- The substrate thickness has to be less than 2 mm. Thicker substrates have a rapid degradation of the beam for great scan angles.

Finally the Transmission Line Model, as described in [Van de Capelle, 1988] was chosen as theoretical model. This seemed to be a good compromise between accuracy, simple implementation and CPU-time.

2.1.3 Experiments

After implementation of the Transmission Line Model, several patch-antennae (as microstrip antennae are usually called) were made and measured. The agreement between calculations and measurements were varying. When the coaxial feed probe was connected to the edge of the upper conductor, the agreement in resonance-frequency and -impedance was quite well (see fig 2.1.1).

Repeated measurements with identical antennae showed a variation of 15 Ohm (= 5%) in resonance-impedance. The difference between calculation and measurements is in the same order. Other antennae were made with the feedpoint located more to the centre of the patch. This technique was used to get a better matching to the 50 Ohm feedline but a shift in resonance-frequency (up to 120 MHz = 2.3%) was observed (see fig. 2.1.2).

TNO report

NLR ——————— TNO ——————— TUDelft

Feed–point at the edge

[Ohm]

Resistance

[GHz]

Frequency

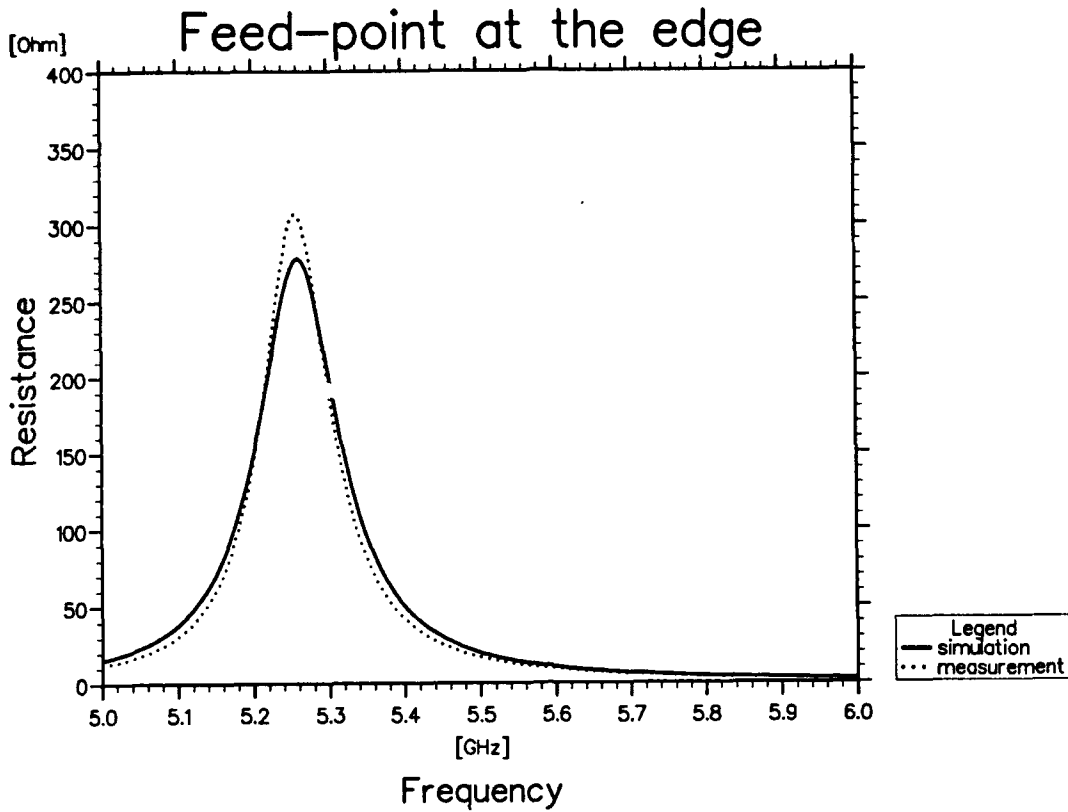Legend
— simulation
··· measurement

Fig. 2.1.1:   Comparison of the calculated and measured impedances of a square microstripantenna.
The feed point is at the edge. Substrate thickness is 0.79 mm

Influence of the feed position

[Ohm]

Resistance

[GHz]
Frequency

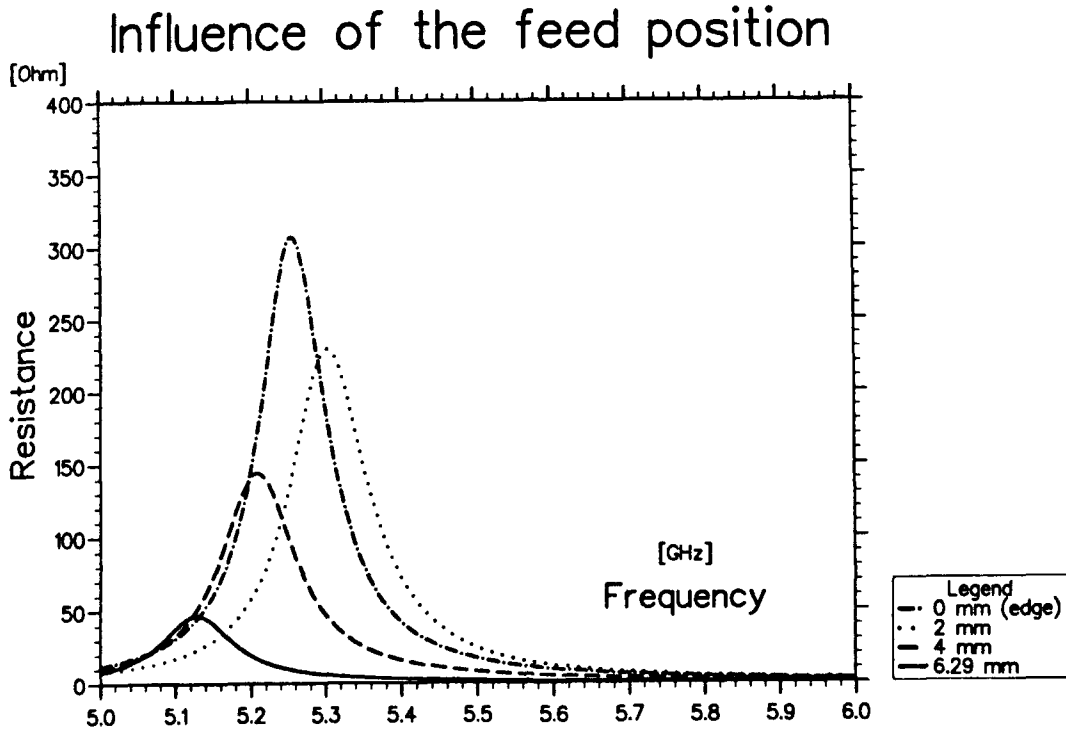Legend
—· 0 mm (edge)
·· 2 mm
— 4 mm
— 6.29 mm

Fig. 2.1.2:   Comparison of the impedance measurements for various feed positions

This strange phenomenon was not predicted by the model. A good explanation has not been found yet. It is expected that the feed probe influences the field between the conductors. This field was probably not a pure TM_{01}-mode anymore, as assumed in the models. The radius of the inner coaxial conductor (1.27 mm) was at these frequencies 7% of the size of the upper conductor (17.89 mm). At lower frequencies, this ratio was less. The radiation patterns showed that the cross-polarisation levels increased while moving the feedpoint from the edge to the centre of the patch. The radiation patterns were not well predicted by the model, especially the cross-polarisation patterns.

Many different configurations were made, with 1, 2 and even 4 feed points, feed points in the middle of the edges and at the corner of the upper conductor, single and dual polarised elements. The best single polarised element appeared to be the element with one feed-point at the edge. The best dual polarised element was the one with two feedpointes at the orthogonal edges, fed by a rat-race (see fig. 2.1.3)

$\bullet$ = feed point

Single
Polarised
Element

Dual Polarised Element
fed by a ratrace
behind the patch
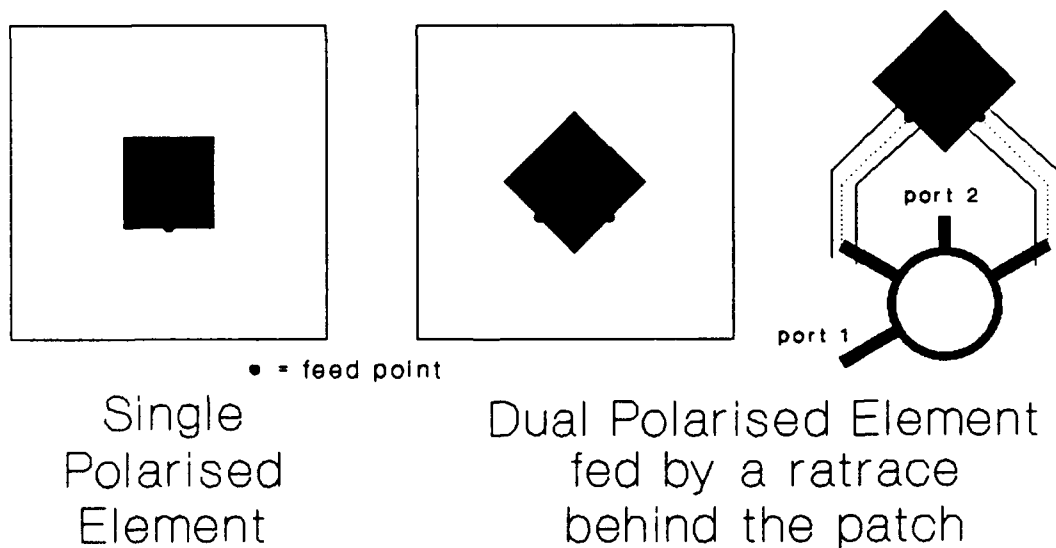
Fig. 2.1.3:   Lay-out of the final patch configurations

The 2 inputs of the rat-race gave the 2 (linear) orthogonal polarisations. In both cases both connectors were excited. For one polarisation, two orthogonal modes of the patch were excited in phase, for the other polarisation anti-phase. The cross-polarisation level of this dual polarised patch was comparable to the single polarised configuration, so the dual polarised one is preferable

above two single polarised patches. The cross-polarisation level was -25 dB or less between the bearing angles of ± 60 degrees, towards greater angles the cross-polarisation level became more. Figure 2.1.4 shows the radiation pattern in the diagonal plane, which is the intermediate between E- and H-plane. This was the worst case for the cross-polarisation.
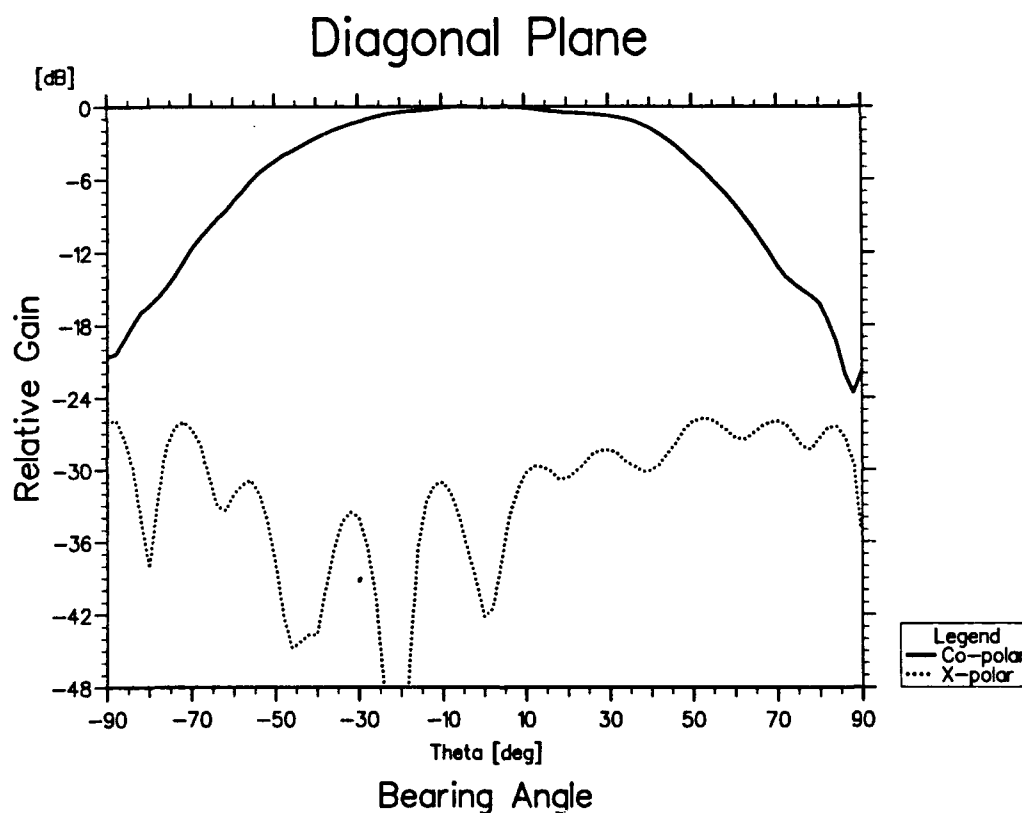
Fig. 2.1.4:   Radiation pattern of the dual polarised element.
The diagonal plane is the intermediate between the E- and H-plane

The measurements were done while the patch antenna was mounted on an aluminum ground plane of 30x30 cm. In the cross-polarisation patterns diffraction effects from the edges of the aluminum groundplane appeared. Covering the edges with absorbing material resulted in an improvement of about 5 dB. The remaining cross-polarisation was quite irregular which means that there were several disturbances like diffraction from the edges of the aluminum ground plane and the finite dielectric substrate, spurious radiation from the feed probe etc. Pozar discussed several of these effects in a recent article [Pozar, Kaufman, 1990]. He needed a metal ground

plane extending 5 λ (=28 cm) from the patches on all edges to keep the diffraction effects below -40 dB. Here we had hardly half of the metal ground plane, therefore -25 dB seems to be reasonable.

Although this isolated single patch element has very promising characteristics, the diffraction effects of the surroundings can disturb the cross polarisation. This aspect has to be studied further for the PHARUS project.

The described dual polarised patch, fed by a rat-race, will serve as basic element for the array development. Its -3dB beamwidth-points are + en - 45 degrees and in this range the polarisation decoupling is better than 22 dB.

More details about the antenna study can be found in [Paquay, 1990].

2.2   Microwave switches

Early on in the design of the PHARUS system it became apparent that PIN diodes were the most appropriate switching elements available. In this work a new large signal, wideband (DC-10 GHz) PIN diode model for use in switches is proposed. The model has been implemented in a harmonic balance simulator (HP's MDS).

2.2.1   Available PIN diode models

PIN diodes are applied in a wide variety of microwave control circuits: in switches, phase-shifters, limiters, modulators and samplers.

Although PIN diodes are relatively simple semiconductor devices, their behaviour is far more complex than that of simple diodes.

In a PIN diode, the semiconductor wafer has a heavily doped p and n region, separated by a layer of high resistivity material that is nearly intrinsic. This intrinsic region has almost negligible doping and consequently a very high resistance. This high resistance and a relatively large I-layer width result in an extremely low junction capacitance and a high breakdown voltage. When forward bias is applied across the diode, it is found that at high frequencies, the diode acts essentially as a resistance. This RF resistance is controllable by adjusting the forward bias on the diode. Below the lowest frequency of operation, PIN diode performance resembles that of a conventional rectifier diode. When the PIN diode is reverse biased, the diode appears as a capacitor shunted by a high parallel resistance.

There is a transition region between the DC and high frequency ranges. In this region, reactive effects are introduced by the semiconductor junctions that may by significant enough to dominate the overall device impedance. This means that at low frequencies the diode impedance may have a dominant capacitive or inductive component, depending on the applied bias [Caverly, R.H. and G.Miller].

There is NO SINGLE MODEL which can describe the PIN diode for both low- and high-frequencies. For low frequencies a simple diode model can be used. In switching circuits for RF signals, the PIN diode is approximated with two separate linear circuits, one for the forward bias and one for the reverse bias state. These two circuits can be joined to form a high-frequency linear PIN diode model having bias dependent elements.

One method of joining the low- and high-frequency models is based on the assumption that the high-frequency resistance is proportional to the stored-charge in the diode. Another more realistic solution is to solve the transport, continuity and space-charge balance equations: the result yields the impedance of the device. This method is, however, difficult to integrate into existing CAD systems, since the required computations are very complex. Furthermore device geometry and semiconductor parameters are normally not available.

In the following we present an equivalent circuit model of the PIN diode. The device is considered as a "black box"; the most important device properties being determined by measurement.

2.2.2 Model development

Model evaluation was performed using the Hewlett-Packard HP85150B Microwave Design System (MDS) CAD package.

DC, low frequency and microwave measurements form 1 to 10 GHz were carried out. Use was made of HP's parameter extractor TECAP as well as in-house instrument control-programs.

The equivalent circuit model of the PIN diode was constructed using built in MDS component models where appropriate. These components are based on widely used and accepted models.

A universal tool for component generation in MDS is the SDD element (Symbolically Defined Device). In this element the port currents can be defined as a function of port voltages or other port currents. It is possible to either explicitly or implicitly define these currents. The possibility of introducing frequency dependence is limited. Frequency dependence can only be incorporated as a multiplicative factor termed a weighting function.

As each new component was added to the pin model, its influence on the model performance was assessed.

To begin, small-signal simulations were made to show the impedance versus frequency characteristics of the device at different bias levels.

Next large signal Harmonic Balance simulations were carried out. Since the diode impedance depends on three different parameters: the *frequency*, the *bias* and the *signal amplitude*, six different parametric curve sets were computed for each model.

The PIN diode was biased using a series 100 ohm resistance. Using this method the same DC voltage source can be used both in forward and reverse bias states.

2.2.3 New PIN diode model

The new model consists of a diode model, an intrinsic-layer model and a frequency-dependent network for joining the two models.

The intrinsic-layer model was implemented as a two-port SDD element, using a *new* idea: the measured small-signal RF resistance of the diode is considered to be the derivative of the "real" current vs. voltage curve, which cannot be measured, but can be calculated as the primitive function of the small-signal RF current vs voltage characteristics. (This principle is well-known in the case of normal diodes.)

The most critical part of model construction is the matching of the low- and high-frequency models. A serial arrangement was used with a frequency-dependent diode model using the same equations employed for the internal diode model of MDS. This was implemented in an SDD element with a frequency-dependent weighting function. This solution ensured the convergence of computations in all test situations.

2.2.4 Measurements

Three different PIN diodes were measured: a Telefunken type BA479G (glass encapsulated) and two HP types: a HPND4038 (beam-lead) and a 5082-0030 (chip).

The measurements were made under computer control between 1kHz and 10 GHz. The results were transferred to MDS where direct comparison of the simulated and measured diode impedance results is possible. Diode parameters were extracted using TECAP.

2.2.5 Results

This work has resulted in a new, "full-band" (DC-10GHz) model of a PIN diode. The model is implemented in the HP8515OB Microwave Design System (MDS). The measured and simulated impedance data (BA479G) show good agreement as shown in fig. 2.2.1 and 2.2.2.

The model is a large signal model. It should prove useful for limiter and switching-pulse circuit design and for distortion calculation.

As an example a simple switch was simulated. The results shown demonstrate the usefulness of the model (fig. 2.2.3 and 2.2.4).
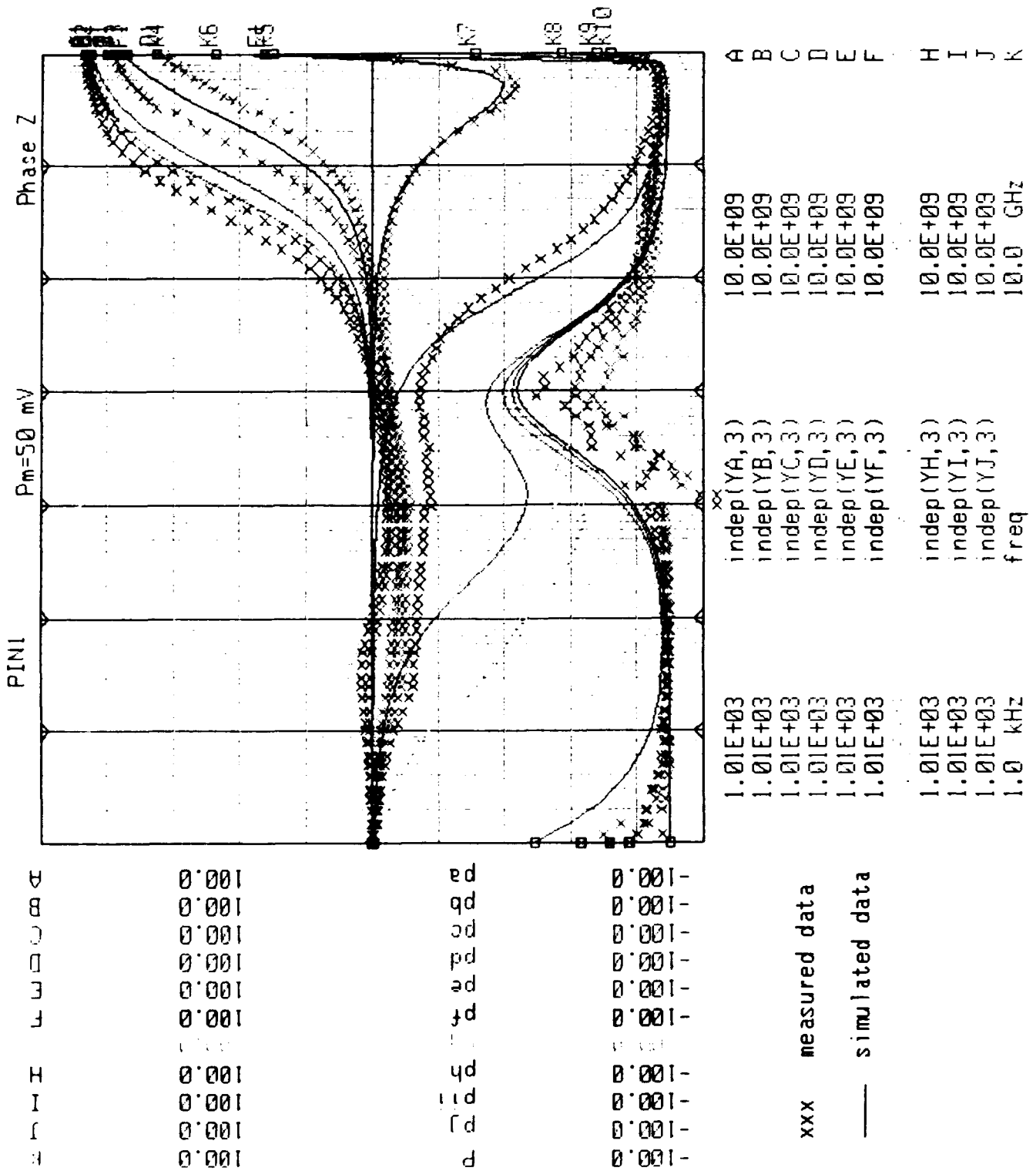
Fig. 2.2.1:   Measured and simulated data of the magnitude of the diode impedance

TUDelft

Magnitude Z   Pm=50 mV   PIN1

A	indep(YA,3)	10.0E+09	1.0E+03	
B	indep(YB,3)	10.0E+09	1.0E+03	
C	indep(YC,3)	10.0E+09	1.0E+03	
D	indep(YD,3)	10.0E+09	1.0E+03	
E	indep(YE,3)	10.0E+09	1.0E+03	
F	indep(YF,3)	10.0E+09	1.0E+03	
H	indep(YH,3)	10.0E+09	1.0E+03	
I	indep(YI,3)	10.0E+09	1.0E+03	
J	indep(YJ,3)	10.0E+09	1.0E+03	
K	freq	10.0 GHz	1.0 kHz	

A	1000000000.0	ma	1.0	
B	1000000000.0	mb	1.0	
C	1000000000.0	mc	1.0	
D	1000000000.0	md	1.0	
E	1000000000.0	me	1.0	
F	1000000000.0	mf	1.0	
H	1000000000.0	mh	1.0	
I	1000000000.0	mi	1.0	
J	1000000000.0	mj	1.0	
K	1000000000.0	M	1.0	

xxx measured data

——— simulated data

Fig. 2.2.2:   Measured and simulated data of the phase of the diode impedance

NLR

TNO

TUDelft

STIMULUS

CMP51
STRSTPPTS

STIMGROUP=STIMGROUP
START=0
STOP=3
LINEAR PTS=4
REVERSE=NO

CMP21
CPROBE

PORTNUM=2
R=50.0 OH
JX=0.0 OH

CMP22
VPROBE

CMP2
PORT_SPAR

AGROUND

CMP30
C

C=cs

CMP43
VPROBE

$L = lp$

AGROUND

CMP28
L

EQUATION v0=0

EQUATION vd=0

EQUATION cs=1000 pF
EQUATION lp=100 nH

AGROUND

CMP41
CPROBE

CMP50
nSQUARE

VDC=vd V
VPEAK=v0 V
FUND=1

CMP44
VPROBE

PIN34

CMP59
node134

CRF=0.3pF
CP=0.4pF
Cjo=0.7pF
Vj=0.4V
m=0.75
FC=0.86
tau=1e-9

FTR=0.1MHZ
TR=0.5
IS=0.85nA
N=1.92
K=0.87
A=0.0638
RL=10MOH
RS=1.60H
LS=0.15nH

CMP8
R

R=100 OH

CMP48
VPROBE

CMP39
CPROBE

CMP27
L

$L = lp$

CMP12
VPROBE

CMP29
C

C=cs

* OPTIONS *

CMP49
OPTIONS

MNS.dataset=DATAneusub

WARN=yes
MAXWARNS=10
VRELTOL=1e-5
IRELTOL=1e-5
TOPCHECK=YES

* CONTROLLER *

CMP1
CT

SWEPT_VAR=v0
STIMGROUP=STIMGROUP
ANALYSIS1=cmp26
OUTPUT_VARS=

CMP23
VPROBE

PORTNUM=1
R=50.0 OH
JX=0.0 OH
PAC=0 dBm
PHASEAC=
P=-40 dBm
PHASE=0.0
FUND=2
HARM=1

CMP26
RLS

AGROUND

CMP24
CPROBE

Fig. 2.2.3: A simple switch circuit

Output voltage

Driving current / voltage

Input voltage
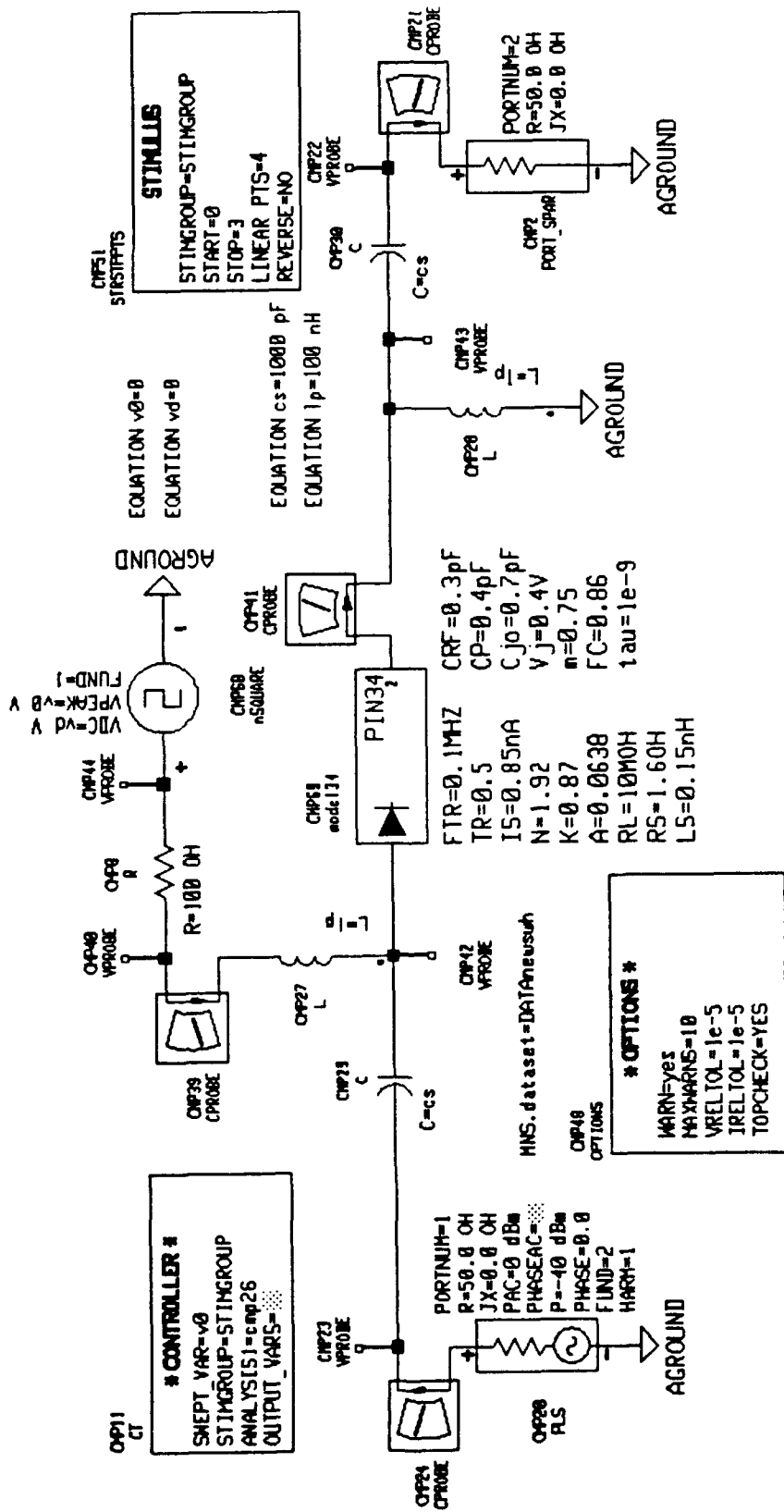
Diode current / voltage

Driving current spectrum
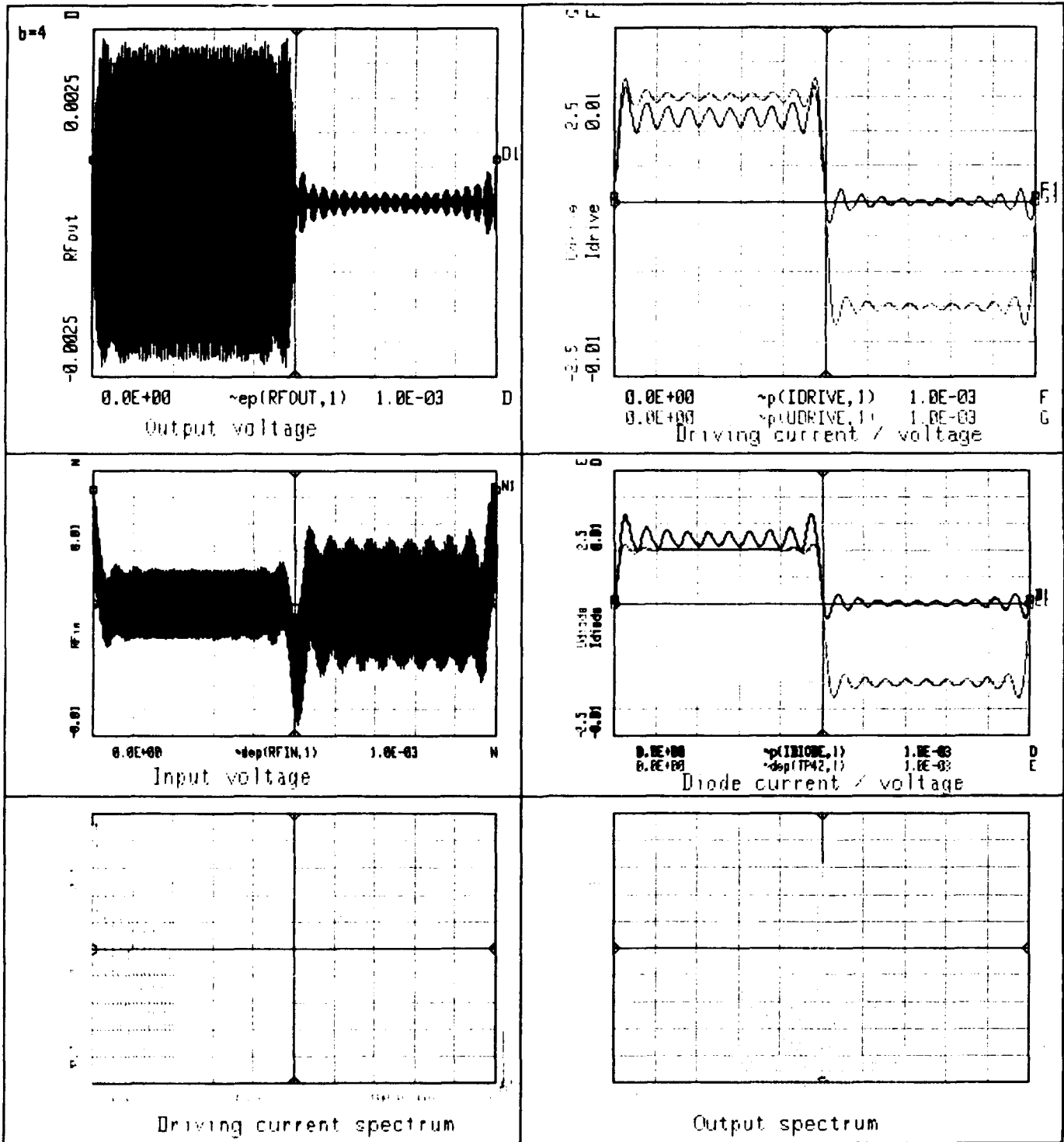
Output spectrum

Fig. 2.2.4:   Voltages in a simple switch

2.3   Microwave components

2.3.1   Introduction

The microwave circuits developed for the PHARS T/R module, such as the power amplifier, low noise amplifier, phase shifter and T/R switch can be regarded as state-of-the-art devices characterized by excellent performance.

At the start of WP 1.2, early 1989, it was likely that these components also would be used for the PHARUS T/R modules. The development of new or alternative devices was therefore discarded also because there were no fixed specifications available for the PHARUS phased array antenna at that time. The only development activity performed during WP 1.2 was the redesign of the PHARS phase shifter. This redesign concerns the replacement of the PIN diode chips by beam lead types. By doing this the assembling cost of the phase shifter can be substantially lowered. Another advantage is the greater circuit reliability provided by the use of beam lead diodes.

2.3.2   Beam lead PIN diode

Fig. 2.3.1 depicts the planar structure of a beam lead PIN diode. Connection of the diode terminals to the circuit is made through the two beam leads. The beam lead diode provides a number of advantages over the chip diode type which are

-     more reliable connection
-     lower assembling costs due to simpler circuit mounting
-     very low packaging parasitics
-     better reproducibility
·   reduced drive power consumption because of low drive currents

All these advantages except the last one are attributed to the absence of bond wires. The bonding of thin fragile wires to diode chips is a critical process. The wires introduce parasitic inductances and exact control of their lengths is difficult to obtain with manual bonding.

The major disadvantage of the beam lead diode is the substantial higher device cost. However, this cost disadvantage is more than compensated by the lower mounting and assembling costs. The beam lead diode is ideally suited for series mounting in a microstrip circuit. Using a parallel gap welder, bonding to the microstrip circuit can be done in one operation. Chip diodes require at least two assembly operations. A die attachment (connecting the base of the chip to the circuit) followed by a wire bonding.(connecting the chip top contact to the circuit). This results in much higher assembling costs for chips.

2.3.3 Beam lead diode phase shifter

The beam lead diode phase shifter was constructed in Al_2O_3 microstrip and consists of four cells giving phase shifts of 180, 90, 45 and 22.5 degrees, respectively. The 90 and 180 deg bits each consist of a 3 dB rat-race coupler loaded with two PIN diodes. The 45 and 22.5 deg bits are configured as loaded line sections anu are also equipped with 2 PIN diodes. The configuration of the phase shifter is identical to that of PHARS phase shifter except that the originally applied PIN diode chip HP 5082-0047 from Hewlet* Packard has been replaced by the beam lead type HPND-4038 also from Hewlett Packard.

2.3.4 Experimental evaluation

In order to evaluate the performance of the beam lead diode in a phase shift configuration two phase shift sections, a 180 deg bit and a 45 deg bit have been developed and realized. The design of the two circuits was done with the microwave circuit simulation program LIBRA from EEsof. The RF parameters for the diode model used during the simulation w.re derived from measured diode S-parameters for both bias states of the diode. The measured S-parameters were obtained with the test circuit depicted in Fig. 2.3.2. This circuit involves a 50 ohm microstrip in which the diode is series connected.

The schematic circuit diagram of the 45 deg bit is shown in Fig. 2.3.3. It consists of two identical stubs each provided with a PIN diode spaced approximately a quarter wavelength apart on the main transmission line. A phase shift results from changing the loading susceptances across the main transmission line by switching the diodes from one bias state to the other. The measured phase shift data of this circuit are given in Fig. 2.3.4 in combination with the simulated results. A good agreement can be noted between calculations and measurements. The maximum average insertion loss was about 0.5 dB over the frequency band 5.2 - 5.6 GHz. The maximum return loss did not exceed -15 dB. All measured results were very close to the theoretical predictions.

Fig. 2.3.5 shows the schematic circuit diagram of the 180 deg bit. The microstrip RF circuit consists of a 3 dB rat-race coupler, two PIN diodes and two open-ended transmission lines. The diodes are series mounted between the open-ended line sections and the 3 dB coupling arms of the rat-race coupler. The required phase shift is obtained by switching in and out the transmission lines behind the diodes. The electrical lengths of these lines are responsible for the desired phase shift.

The measured phase shift of the realized circuit was about 10 degrees higher than the design value as can be seen in Fig. 2.3.6. No reasonable explanation can be given for this discrepancy. However the required nominal phase shift can be obtained by reducing the lengths of the two open-ended line sections. This line adjustment affects only the phase shift, the other RF circuit parameters like VSWR and insertion loss are hardly influenced. The maximum measured return loss was better than -18 dB over the frequency band 5.2 -5.6 GHz. The maximum average insertion loss was less than 0.75 dB.

The performance of these two phase shift sections is comparable to that obtained with PIN diode chips.

A complete description of the results is given in [De Hek].
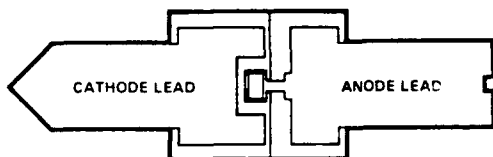

Fig. 2.3.1:   Beam Lead Mesa PIN Diode Structure

Fig. 2.3.2:   Test circuit for measuring S-parameters of the PIN beam lead diode
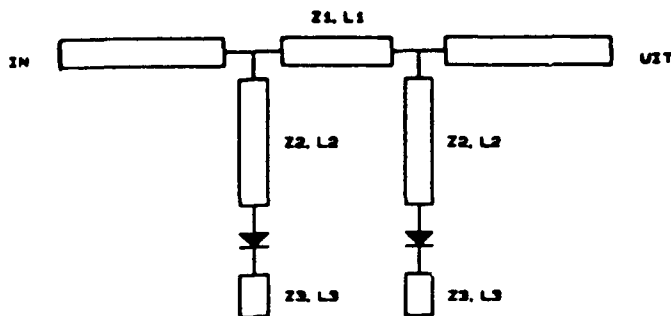

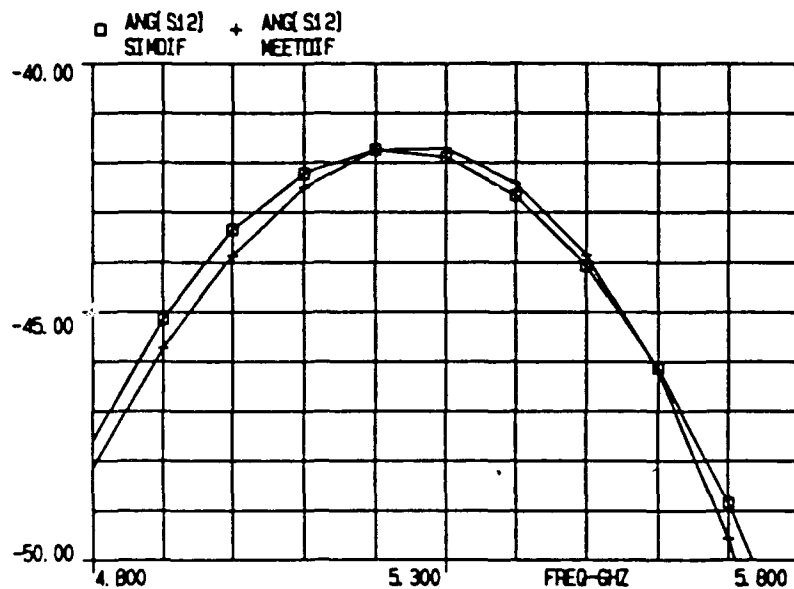Fig. 2.3.3:   Schematic circuit diagram of the loaded line phase shift section

Fig. 2.3.4:   Experimental and simulated phase shift results for loaded line 45 deg bit
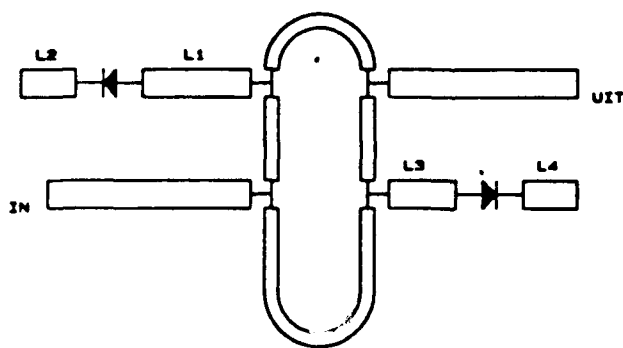

Fig. 2.3.5:   Schematic circuit diagram rat-race coupler phase shift section
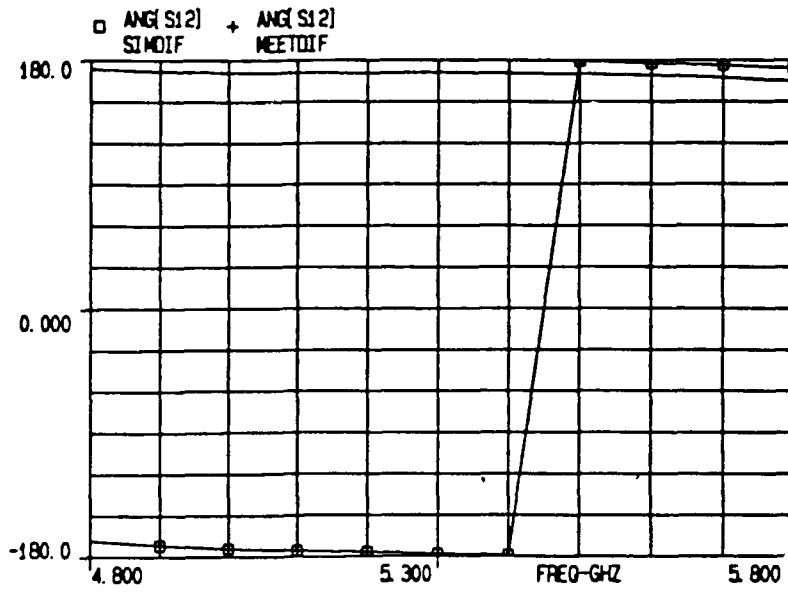
Fig. 2.3.6:   Experimental and measured phase shift results for 180 deg rat-race coupler bit

TNO report

Page
30

2.4   Internal calibration

2.4.1   Introduction

The purpose of calibration is to get an accurate and precise instrument. The precision of the instrument can be determined using internal calibration, while the accuracy is denoted with absolute calibration. With internal calibration only the instrument is considered. Because of practical considerations the antenna is usually discarded in this type of calibration. When a phased array antenna is used, this decoupling is no longer possible, because the antenna is now part of the whole system. Internal calibration becomes quite difficult to perform in the case of a phased array antenna with distributed transmitters and receivers.

In the following table the items to be calibrated in a SAR-system like PHARUS are given.

Internal	External
Phased array antenna pattern + Gain	
pulse amplitude/energy	Antenna pattern, Gain (other
pulse shape (τ)	then phased array)
PRF	reference-reflectors
phase	- size
system transfer function	- place
bandwidth	- orientation angle
depression angle	- response
range	
yaw, pitch, roll, drift.	
aircraft speed	
height	
calibration signals	
processing parameters	
propagation losses.	
wavelength	

Table 2.4.1:   Items to be calibrated

There are two different methods for internal calibration:

1.   Separate subsystem calibration: every subsystem is fully characterized and calibrated.
2.   Ratio calibration: overall calibration of the total system.

The ratio method is superior to the separate method but the actual method to be used depends a lot on the technological possibilities and the measuring time involved. Figure 2.4.1 gives a summary
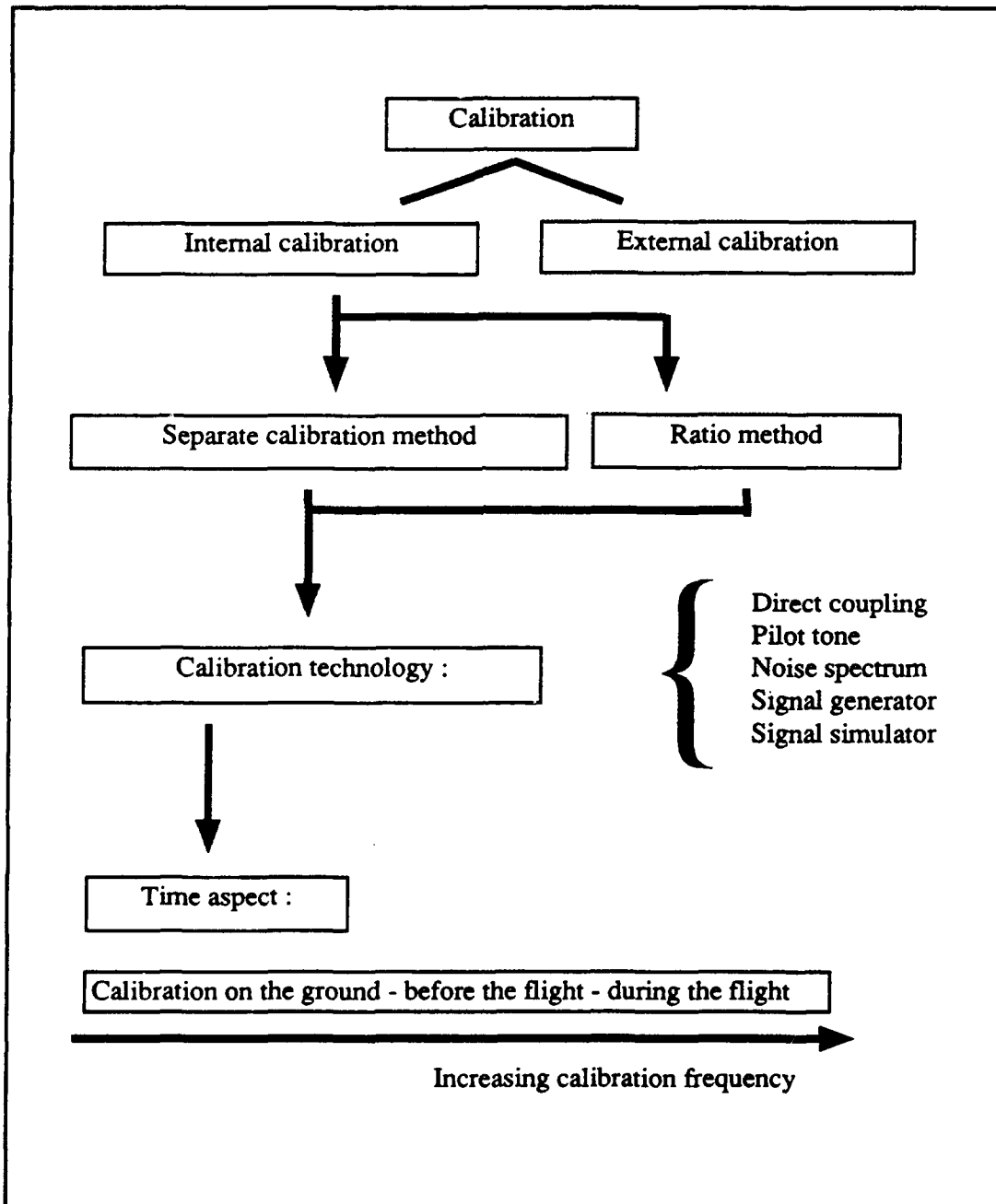

Fig. 2.4.1: Summary of different calibration aspects

2.4.2   PHARUS internal calibration

The internal calibration of the PHARUS system can be accomplished for example by using an attenuated replica of the transmit signal and feeding this into the receiver. There are however some restrictions concerning this simple solution. Both the power amplifier (PA) and the low-noise amplifier (LNA) have to be turned on during an internal calibration measurement. The minimum isolation between the output of the PA and the input of the LNA has to be 80 dB. For dynamic range measurements an additional 50 dB is needed, so the isolation between PA and LNA has to be at least 130 dB. In practice this can not be realized.

An other possibility is to use a delay line to produce additional isolation between transmitter and receiver. In the case of distributed transmitters and receivers the number of delay lines has to be the same as the number of T/R modules, so this method is also impractical and an active calibration system with a separate calibration T/R module has to be used.

As already mentioned in section 2.1 the antenna configuration includes a rat-race for power distribution to the patch. Using an additional well selected output port of the rat-race a fraction of the output power will be coupled through a combiner to the calibration module. The same module can be used to inject a signal into a receiver. The configuration shown in figure 2.4.2 gives the chosen layout of the ratrace by using a high impedance probe with a coupling of 40 dB.
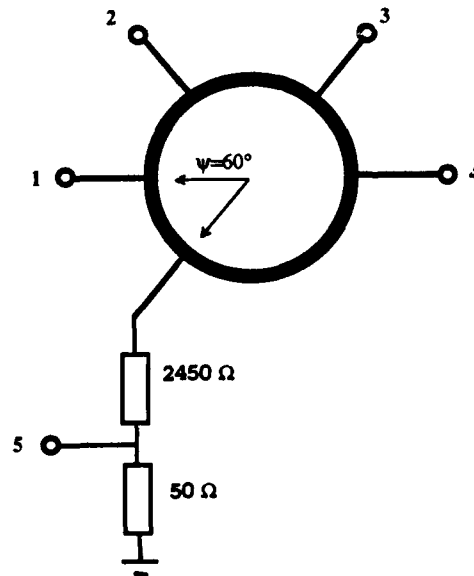
Fig. 2.4.2:   Coupling using a direct high impedance probe

Simulation of this configuration using Hewlett Packard's Microwave Design System (MDS) software results in the S-parameters shown in figure 2.4.3. From the figure it can be seen that the probe has no influence on the response of the rat-race. The input signal from port 1 is equally divided over port 2 and 4 (-3 dB top row responses). The decoupling of port 3 is around the central frequency of 5.3 GHz good (bottom left). The coupling of the probe with port 1 and 3 is identical and has a very broadband behaviour (bottom right).
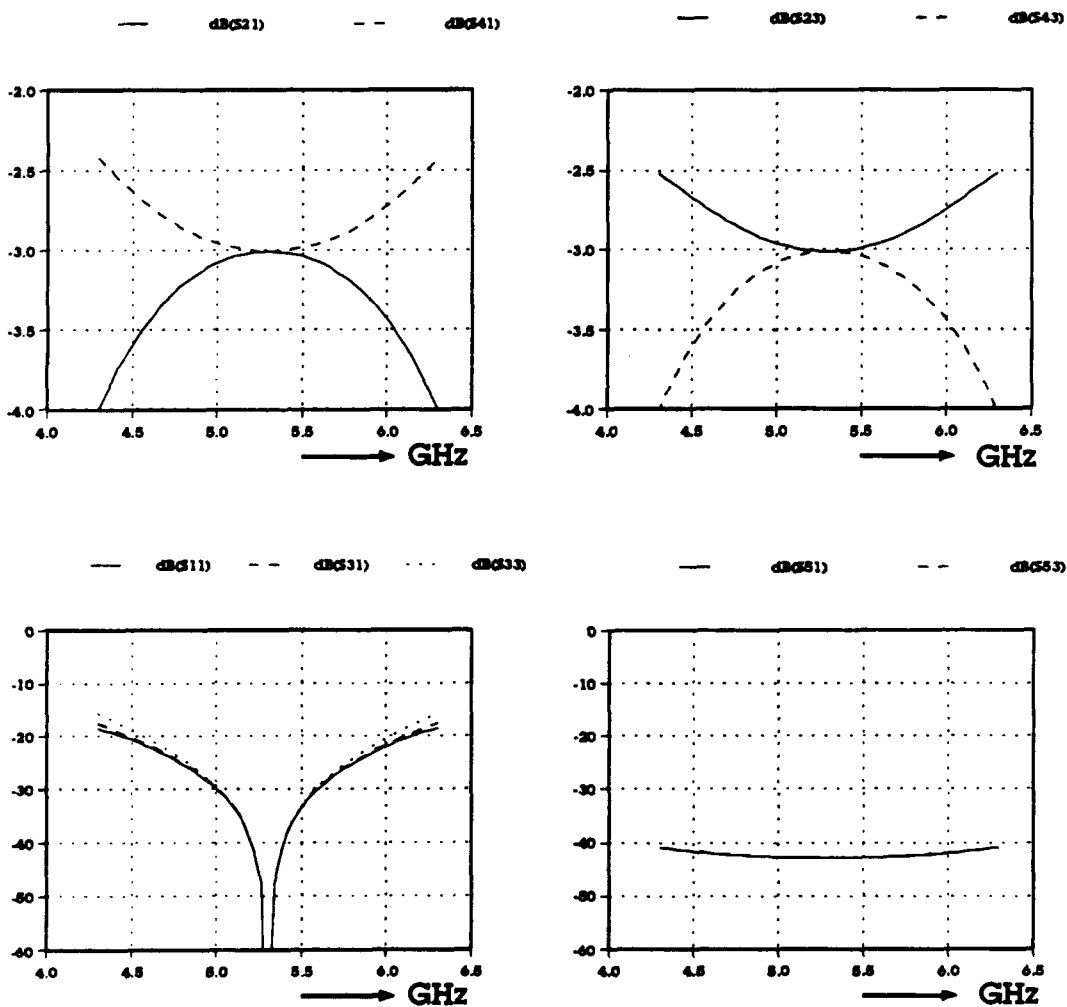
Fig. 2.4.3:   Simulated S-parameters of the configuration shown in fig. 2.4.2

This configuration seems to meet the requirements. The realization of the proposed calibration method needs to give the final answer.

TUDelft

More details about internal calibration and the influence of errors on the antenna pattern can be found in (Vellekoop, Snoeij and Tian, 1991).

The proposed configuration for the radar front end is given in figure 2.4.4

Fig. 2.4.4:   Block diagram of the proposed system

2.5   Antenna measurements (near field, pulsed conditions)

The PHARUS active phased array antenna will be, when constructed, measured in the FEL-TNO planar near-field measurement facility. The reason for near-field measurement instead of far-field measurement is threefold:

- A complete characterization of the antenna radiation pattern is necessary (not only principal plane radiation patterns);
- lots of radiation patterns, e.g. for different scan-angles, need to be measured;
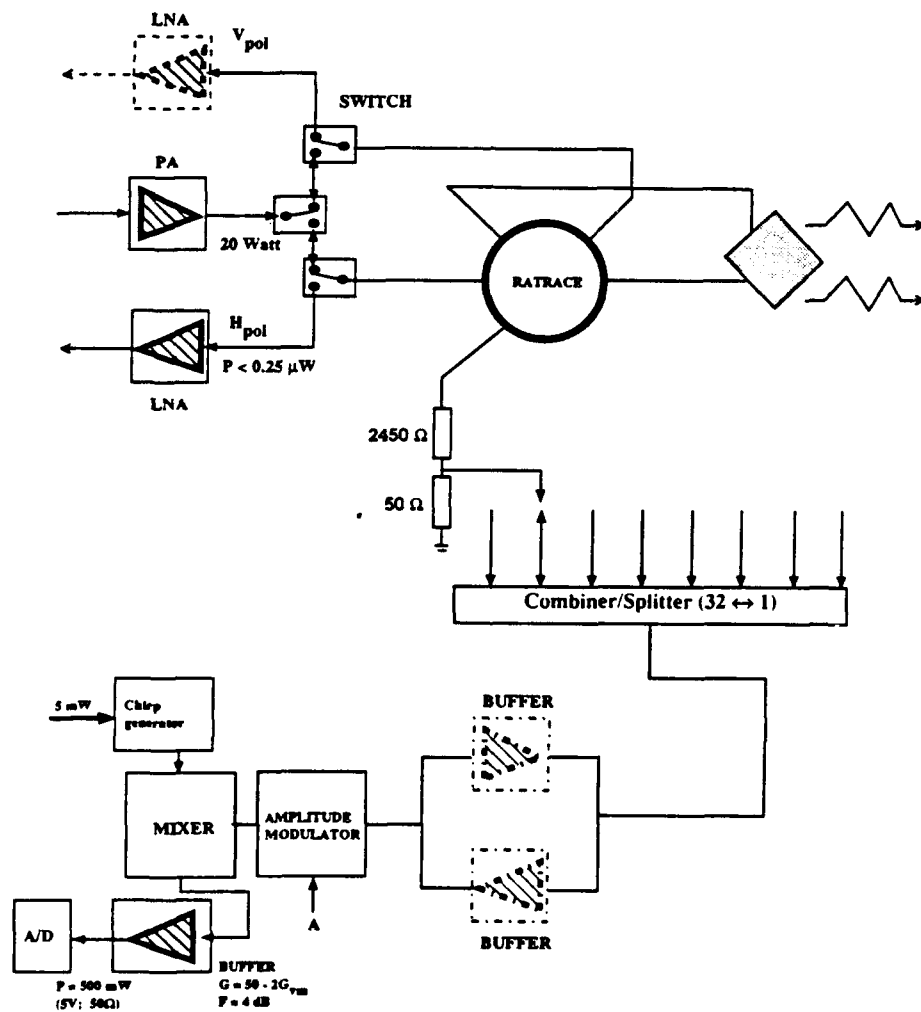- the measurement time must be minimized; in one near-field measurement session, several complete patterns can be obtained simultaneously.

In the FEL-TNO planar near-field measurement facility, it is possible to measure sidelobes down to -30 dB with an accuracy of about 0.5 to 1 dB. The PHARUS antenna must be characterized in send and receive mode. With little effort, both can be done in the near-field measurement facility [Visser, FEL-90-B092].

It is also necessary to characterize the PHARUS antenna on transmitting under pulsed-RF conditions, because:

- In that way, the antenna on transmitting will be characterized under operational conditions;
- the active components will behave differently under CW conditions;
- CW operation increases considerably the heat dissipation of the active devices. Destruction is then not unlikely.

The low pulse repetition frequency used for PHARS and probably will be used for PHARUS (about 3.5 kHz, pulsewidth 12.8 μs) causes problems in performing pulsed-RF measurements. Existing measurement equipment is not designed for measuring such signals. It appears, however, that it is possible to perform pulsed-RF measurements with a standard (CW) HP 8510B vector network analyzer with the use of one frequency synthesizer. The measurement configuration is shown in figure 2.5.1 [Visser, FEL-90-B238].
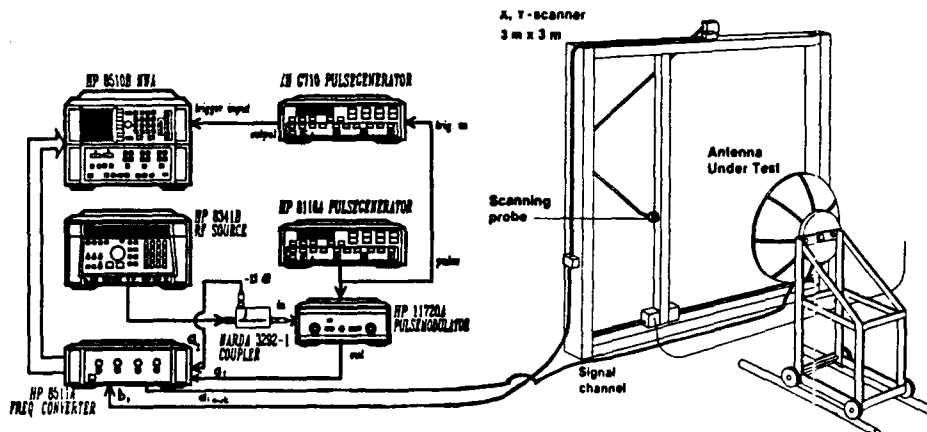
Fig. 2.5.1·   Low-PRF measurement configuration

Using the external triggering possibility of the network analyzer, low-PRF pulsed-RF signals can be measured as if they are CW signals [Visser, FEL-90-B238]. The trigger signal is extracted from the pulse signal, thus providing a good synchronization. Measurements are carried out for multiples of the pulse period. With a delay, the trigger pulse can be shifted into the RF pulse to maximize the received power. Attained specifications are:

- Dynamic range : 50 dB;
- amplitude accuracy : ± 0.10 dB;
- phase accuracy : ± 1.0°;
- minimum measurement time : 1.14 ms.

First tests of pulsed-RF near-field measurements indicate that the same accuracy in antenna far-field characteristics are obtained as with CW measurements [Visser, FEL-90-B262]. This is shown in the following.

Tests were performed on a 1 m diameter C-band parabolic antenna with a Geyerhorn as feedhorn (F/D = 0.4). Figure 2.5.2 shows a 3D impression of the far-field amplitude, calculated from near-field data, measured in a CW measurement configuration. In the CW measurement configuration, the external trigger connection with the NWA in figure 2.5.1 is removed; instead internal triggering is used. Both pulse generators are turned off, but the pulse modulator remains, though inactive, in order to maintain the same RF-path as used with pulsed measurements.

PHYSICS AND ELECTRONICS LABORATORY TNO   NEAR FIELD ANTENNA MEASUREMENT SYSTEM

amplitude

Tue 1 Oct 1991
19:46:17
height angle 40 deg
rotation   40 deg

-0.0 dB

—— -10.0 dB

-20.0 dB

-30.0 dB

—— -40.0 dB

- -50.0 dB
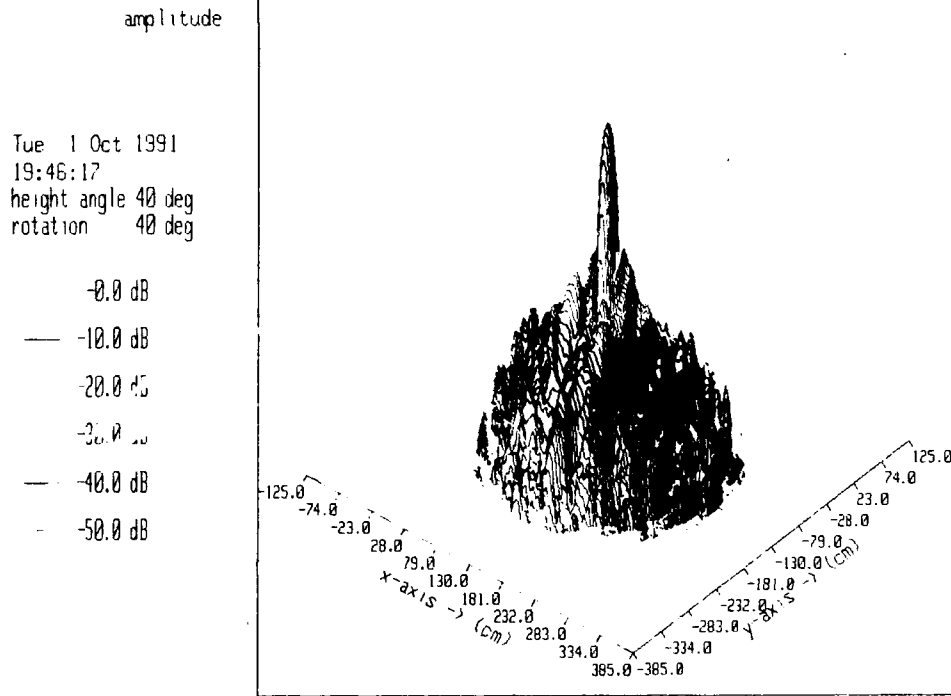
NF-DATAFILE   .   .   .   exttrff3
DATE .   .   .   .   .   .   11 Jul 1990
TESTANTENNA (AUT).   .   .   par1
FREQUENCY (MHz).   .   .   5300
NUMBER of COLUMNS   .   .   256
SPACING IN X-DIRECTION(cm) 2.00

TIME 12:41:14
PROBE .   .   .   .   .   .   -
DISTANCE PROBE (-) AUT (mm)74.70
NUMBER of ROWS   .   .   .   256
SPACING IN Y-DIRECTION(cm) 2.00

Fig. 2.5.2:   Far-field amplitude of a C-band parabolic test antenna; calculated from CW measurement

Figure 2.5.3 and 2.5.4 give the principal plane radiation patterns for CW and pulsed-RF measurements. Figure 2.5.3 gives the vertical cross section of figure 2.5.2; figure 2.5.4 gives the horizontal cross section of figure 2.5.2.

PHYSICS AND ELECTRONICS LABORATORY TNO   NEAR FIELD ANTENNA MEASUREMENT SYSTEM
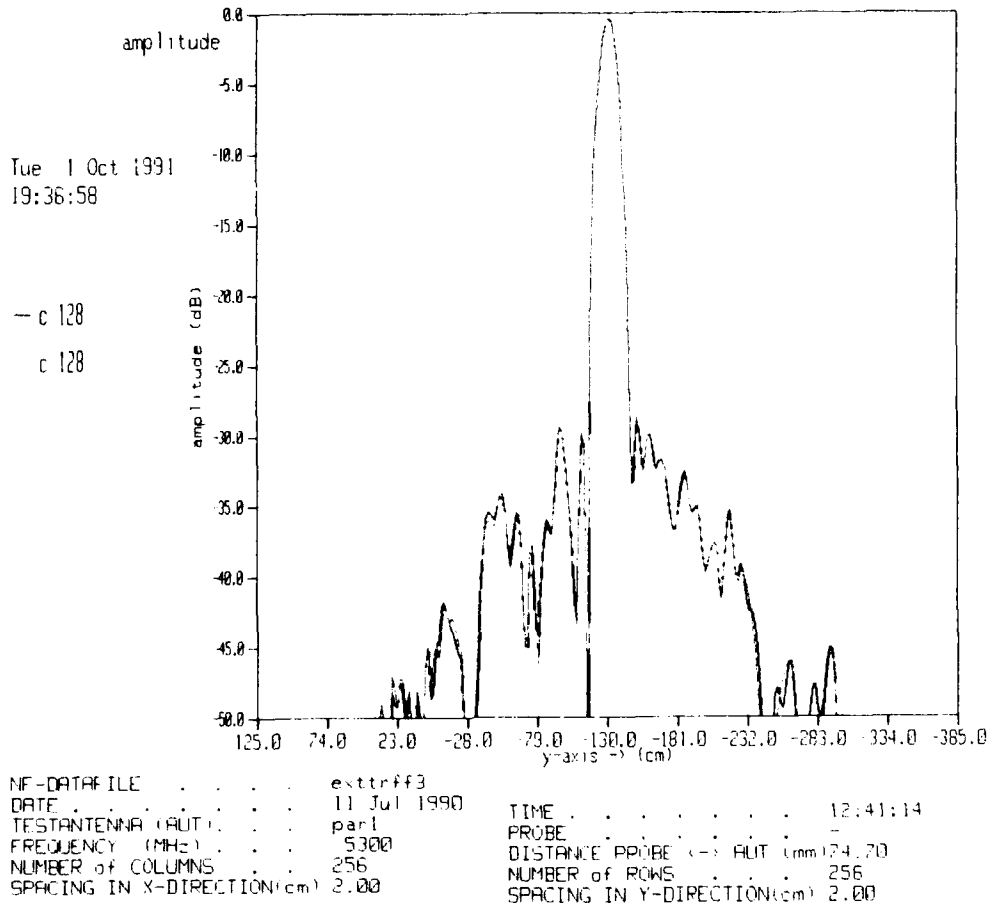
Fig. 2.5.3:   Principle plane radiation pattern of a C-band parabolic test antenna; vertical cross section

PHYSICS AND ELECTRONICS LABORATORY TNO   NEAR FIELD ANTENNA MEASUREMENT SYSTEM

NF-DATAFILE inttrff3
DATE . . . . 11 Jul 1990
TESTANTENNA (AUT). . . part
FREQUENCY (MHz) . . . 5300
NUMBER of COLUMNS . . 256
SPACING IN X-DIRECTION(cm) 2.00

TIME 13:13:22
PROBE . . . . -
DISTANCE PROBE (-) AUT (mm)74.70
NUMBER of ROWS . . . 256
SPACING IN Y-DIRECTION(cm) 2.00
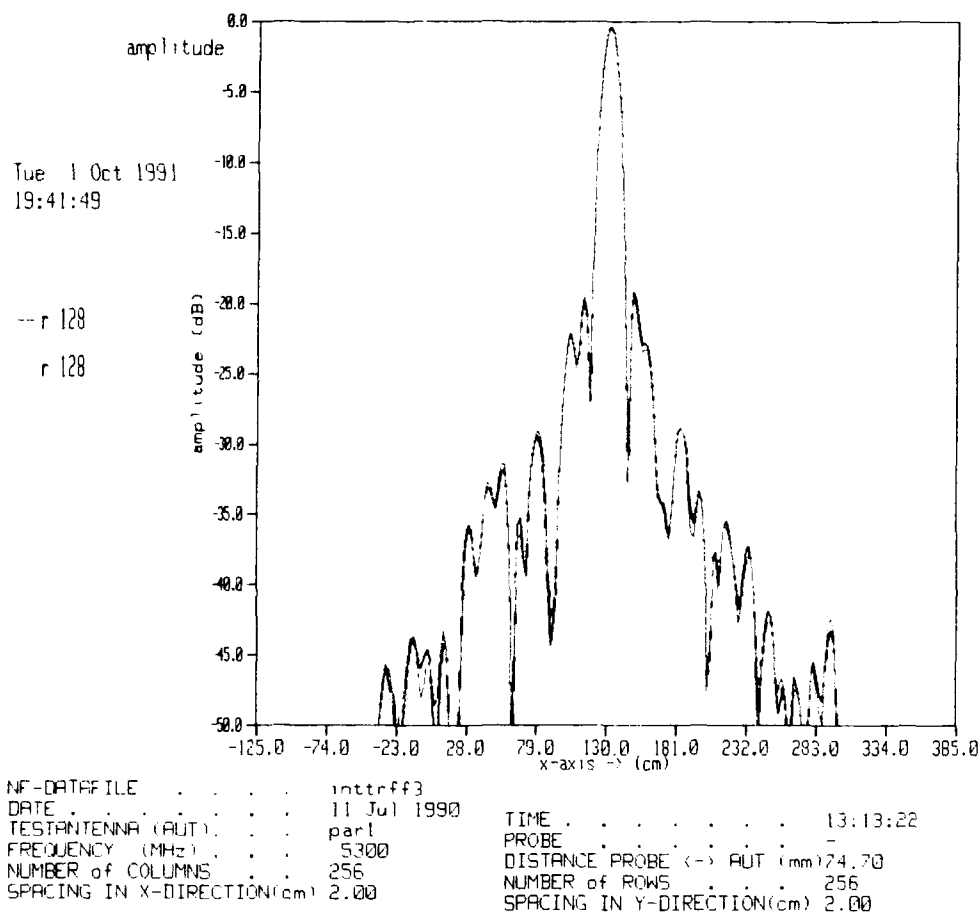
Fig. 2.5.4:   Principle plane radiation pattern of a C-band parabolic test antenna; horizontal cross section

The patterns agree very well. Comparison of pulsed-RF patterns with patterns obtained with a completely different CW measurement configuration give the same good agreement.

In order to perform PHARUS near-field measurements, the following items need attention:
-     control of heat production;
-     protection of measurement equipment when switching between send and receive mode;
-     measurement automatization.

2.6   Conclusions

The antenna design study has increased our knowledge of and experience with patch antenna technology sufficiently to enable the design of the PHARUS antenna.

The usefulness of theoretical models is very limited in patch radiator cross polarisation optimizing. In the definition study an experimental approach was followed.

The best patch configuration for PHARUS is the double feedpoint structure in combination with a rate race for powerdistribution. The cross polarisation of this configuration is less than -22 dB for the specified 90 degree angular range.

Pin diode modeling has led to a better understanding of the behaviour of these devices under (high RF-power) pulsed conditions. The results of this model shows good agreement with the measurements and can be used in the design of the PHARUS modules.

The results of the 45 and 180 deg phase shift sections have demonstrated that in a phase shifter circuit the PIN diode chips can be replaced by beam lead types without any degradation in RF performance.

The best calibration method is the ratio method. This method can however not be used in the case of a phased array with distributed transmitters and receivers. Every T/R module has to be calibrated separately. The direct coupling using a high impedance probe on an otherwise unused port of the rat-race is very promising.

To characterize the PHARUS antenna under pulsed-RF conditions a special low-PRF measurement configuration is realised at the FEL-TNO planar near-field measurement facility with standard equipment. The measured antenna patterns under pulse and CW condition agree very well. Comparison of pulsed-RF patterns with patterns obtained with a completely different CW measurement configuration give the same good agreement.

3   RESULTS FROM THE MOTION COMPENSATION STUDY

3.1   SAR data simulation

3.1.1   General description of SARGEN 1.0

SAR data simulation can be done at many levels, and with various degrees of sophistication. The software package SARGEN was developed at FEL-TNO to investigate the effects of undesired aircraft motion on SAR images: this main objective has determined the basic set-up of SARGEN. It was developed and run on a Cyber 840A Mainframe.

SARGEN 1.0 simulates the raw video signal from an airborne SAR, arising from reflections from a collection of point targets on the ground, plus thermal noise. This signal is determined by all major system parameters, and of course, by aircraft motion. Not included are: the actual range response function after range compression, which is assumed ideally rectangular, range migration effects, or any radar imperfections. The aircraft motion must be specified by 'time stamped' sequences of 3 position- and 3 attitude parameters, pertaining to a point on the airframe relative to the position of the antenna phase centre.

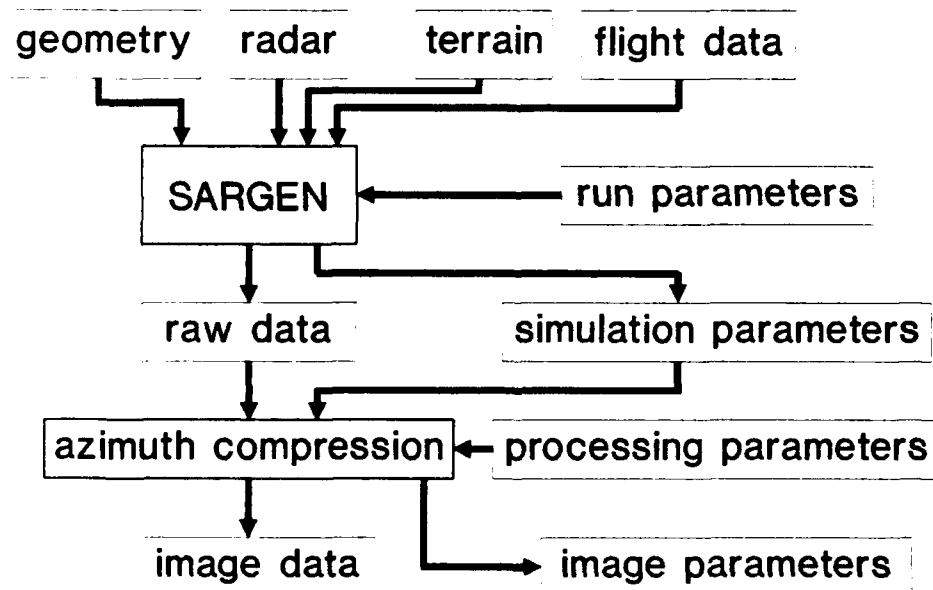Figure 3.1.1 shows the set-up of SARGEN 1.0.

Fig. 3.1.1:   Basic simulation set-up with SARGEN

The in- and output blocks correspond to parameter or data files. The contents of these files are as follows:

'FLIGHT DATA'   : contains the aircraft trajectory

'RADAR'   : contains radar system parameters like wavelength, bandwidth, antenna dimensions, receiver noise factor, PRF, and presumming factor.

'GEOMETRY'   : contains parameters describing the mapping geometry, like (nominal) altitude, slant range, ground velocity, but also the relative position of the antenna with respect to the motion reference point.

'TERRAIN'   : contains an array of point targets, given by their position, and complex reflection coefficient.

'RUN PARAMETERS'   : contains parameters controlling the simulation run.

The result of a simulation run is a simulated raw data file, and a simulation log file, summarizing the parameters, and some run time messages which may have occurred. The raw data must be azimuth compressed to form the SAR image.

SARGEN 1.0 was validated by some simulations using simple idealized motions, for which the effects could be analytically determined and compared with simulations, and by simulations using actual motion data of the Metro II aircraft, for which the effects could be partly quantitatively and partly qualitatively predicted. Details of SARGEN 1.0 can be found in [Otten, 1989].

SARGEN 1.0 has been used at NLR for the motion compensation study, reported further in this chapter.

3.1.2   Extensions of SARGEN 1.0

It was soon recognized that a SAR simulation package could serve more purposes than the one described above. SARGEN 1.0 was also used, for instance, to determine azimuth ambiguities under various processing conditions, and to generate test data to verify SAR processing implementations. However, some extensions were necessary, in particular to be able to test autofocus algorithms.

The current version is SARGEN 2.1, which runs on the CONVEX 230 computer at FEL. The most important extensions are:

-    general FIR prefiltering instead of just presumming
-    simulation of speckle, for a given semi-homogeneous background, including aircraft motion effects
-    a more realistic range response simulation (sinc-type compressed pulse)

This extended simulation was used in the autofocus study, see also paragraph 4.7.3.

3.2   SAR Image degradation by motion induced phase errors

One of the main problems to overcome in order to obtain high quality (i.e. high resolution, reliable amplitudes, high accuracy and low geometrical distortion) imagery from airborne synthetic aperture radar is the accurate measurement of and correction for (undesired) motions of the antenna phase centre.

A great deal of effort is spent on this subject, and various forms of motion compensation methods are being developed, ranging from the use of data acquired by (possibly a combination of) motion measuring units to the estimation of the correction for undesired motions on the basis of the measured SAR data themselves.

In the framework of one of the preparatory studies performed before the actual PHARUS system is designed, NLR carried out a study called 'Error Analysis'. This study was dedicated to SAR image degradation due to various forms of antenna motions, with special emphasis on the actual flight circumstances which will be encountered during operation of the PHARS and PHARUS systems. The results of this study, given in the NLR report 'SAR image degradation by motion induced phase errors' [van der Burg, 1990: CR 90164 L] are summarized here. They include an estimation of the maximum amount of residual, non-compensated motions of the PHAR(U)S antenna which can be tolerated accounting for image quality constraints. This estimate was obtained by using two different approaches, the results of which will be briefly outlined here.

3.2.1   Indicative upper limits to (residual) SAR antenna motions

Indicative upper limits to the amplitude of line-of-sight velocity variations of the PHAR(U)S antenna are calculated from some strictly defined criteria concerning the maximum permitted image degradation (i.e. a maximum azimuth shift of one resolution element, a maximum resolution loss of 10 % in the along track direction and a minimum peak sidelobe ratio of 30 dB).

The basic assumption is that phase errors are due to pure sinusoidal, high and low frequency line-of-sight motions of the antenna. From the resulting upper limits the maximum permitted amplitudes of motions in the cross track and vertical direction are inferred for a specific viewing geometry. Moreover, it is specified what maximum sinusoidal variations of aircraft roll, pitch and yaw are allowed, accounting for the presence of a lever arm.

For the present study two cases were considered:

a)   PHARS case   : 6 m azimuth resolution; 6 km altitude; 13 km ground range,

b)   PHARUS case : 1 m azimuth resolution; 6 km altitude; 30 km ground range.

An example of the resulting upper limits in case of pure sinusoidal cross track motions is reproduced in figure 3.2.1, whereas the results for roll motions are shown in figure 3.2.2. In these figures the maximum permitted motion amplitudes are compared with actually measured motions of NLR's Metro II laboratory aircraft shown by a 'reference spectrum' (labelled '25'). This spectrum was derived from attitude and position data measured during a flight made under flight conditions which can be considered representative for the circumstances which will be met during operation of the PHAR(U)S system.

In addition, a worst case spectrum is plotted which is the envelope of the collection of Metro II spectra (a total of 8) which were available for this study.

CROSS TRACK
VELOCITY

(m s−1)

PHARS, PHARUS

25 ●

WORST CASE SPECTRUM

AZIMUTH SHIFT

PHARS

REFERENCE
SPECTRUM

RESOLUTION
LOSS

−30 dB
SIDELOBES

AZIMUTH SHIFT

RESOLUTION
LOSS

PHARUS

FREQUENCY (Hz)

Fig. 3.2.1:   Indicative upper limits to the amplitude of sinusoidal disturbances of the cross track velocity
component as a function of frequency.

3.2.1.1   Linear motions

Figure 3.2.1 indicates that in the case of PHARS the actual measured cross track velocity components of the Metro II exceed the indicative upper limits only for motion frequencies less than about 0.8 Hz. As a consequence, image degradation effects due to cross track motions (i.e. azimuth shift and resolution loss) can be expected in this frequency range. A similar conclusion can be drawn for the vertical motions of the Metro II. In the case of PHARUS conditions the constraints are much tighter: the actual measured motions exceed the indicative upper limits for virtually all frequencies up to about 2 Hz.
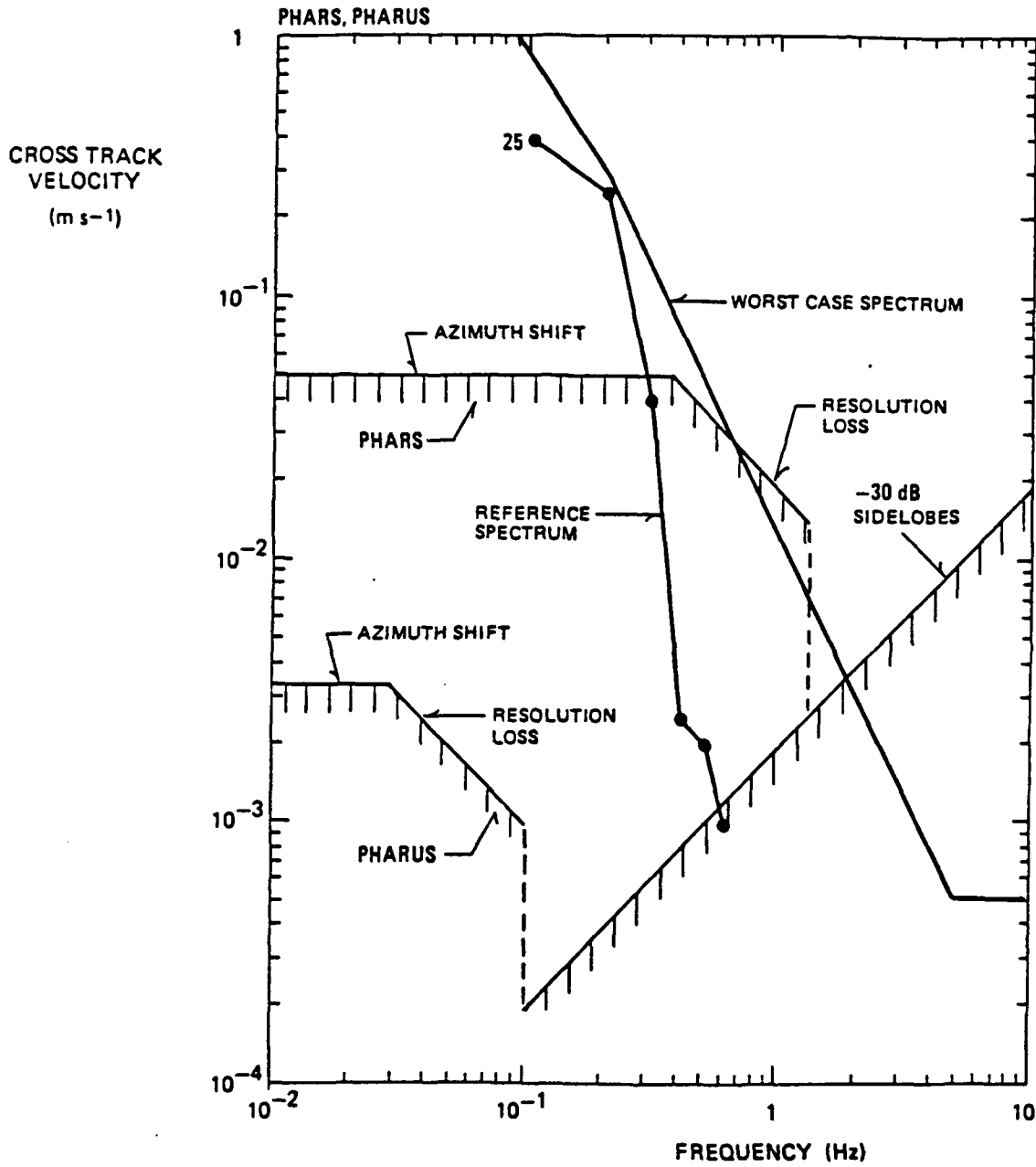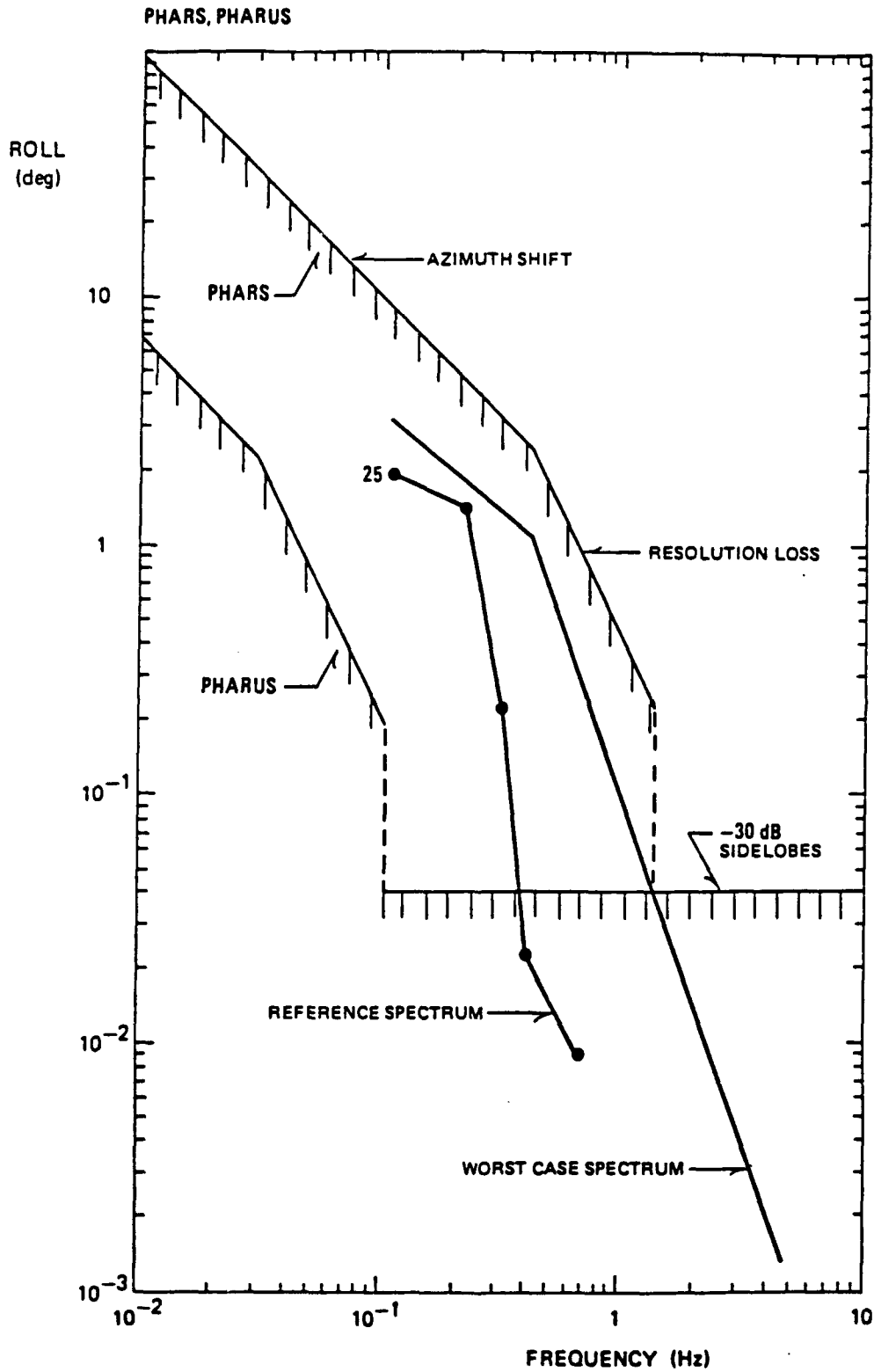
Fig. 3.2.2:   Indicative upper limits to the amplitude of sinusoidal disturbances of the roll as a function of frequency.

3.2.1.2   Roll, pitch and yaw motions

For roll (figure 3.2.2), pitch and yaw motions, the amplitudes indicated by the worst case spectrum are consistently smaller than the upper limits for all frequencies in case of PHARS conditions. This implies that no substantial image degradation due to Metro II attitude variations alone is to be expected during operation of PHARS. Again, for PHARUS conditions a substantial image degradation can be expected due to (low frequency) attitude variations of the Metro II.

3.2.1.3   Discussion

From this analysis it can be concluded that, pertaining to azimuth shift, resolution loss and peak sidelobe ratio, attitude variations of the Metro II are of minor importance in the case of PHARS conditions; the required motion cancellation factor for cross track and vertical motions is about 10 (for low frequencies). However, PHARUS image constraints require a cancellation up to a factor of about 100 for low frequency motions in case of cross track and vertical velocity components, whereas a factor of about 10 is required in case of attitude variations (frequency dependant).

From a motion compensation point of view an optimum starting point to achieve high quality SAR imagery is to make use of a platform which is as stable as possible against disturbances caused for instance by air turbulence. Therefore, the Metro II motions are compared with those of another type of aircraft, in this case the Fokker 50. Based on theoretical grounds, and confirmed by Fokker 50 flight data, it is concluded that using a Fokker 50 as a SAR platform would not lead to any significant improvement in turbulence induced motion variations.

The present discussion completely relies on sinusoidal phase variations. For real flight data this assumption is not valid. In addition, image degradation was considered due to variations of only one single motion component at a time, whereas in practice the individual motion components will interfere, resulting in cancellation or intensification of the motions of the SAR antenna. One way of accounting for these restrictions is to carry out a series of computer simulations using real (Metro II) flight data. Such simulations were carried out; along with the results they will be summarized next.

3.2.2 Aircraft SAR imaging simulation

The simulation software 'SARGEN' developed by FEL-TNO provides a simple tool to generate raw SAR data under user-defined flight conditions.

Subsequent data processing of these raw data results in a simulated SAR 'image' which can then be analysed (using the software program SAR_ANAL) to obtain the amount of degradation for a particular set of input parameters.

The purpose of these simulations is to monitor image quality degradation due to non-ideal aircraft motions encountered during a 'remote sensing flight'.

To support communications of the user with 'SARGEN' a user interface was developed based on the NLR COmmand LAnguage System (COLAS).
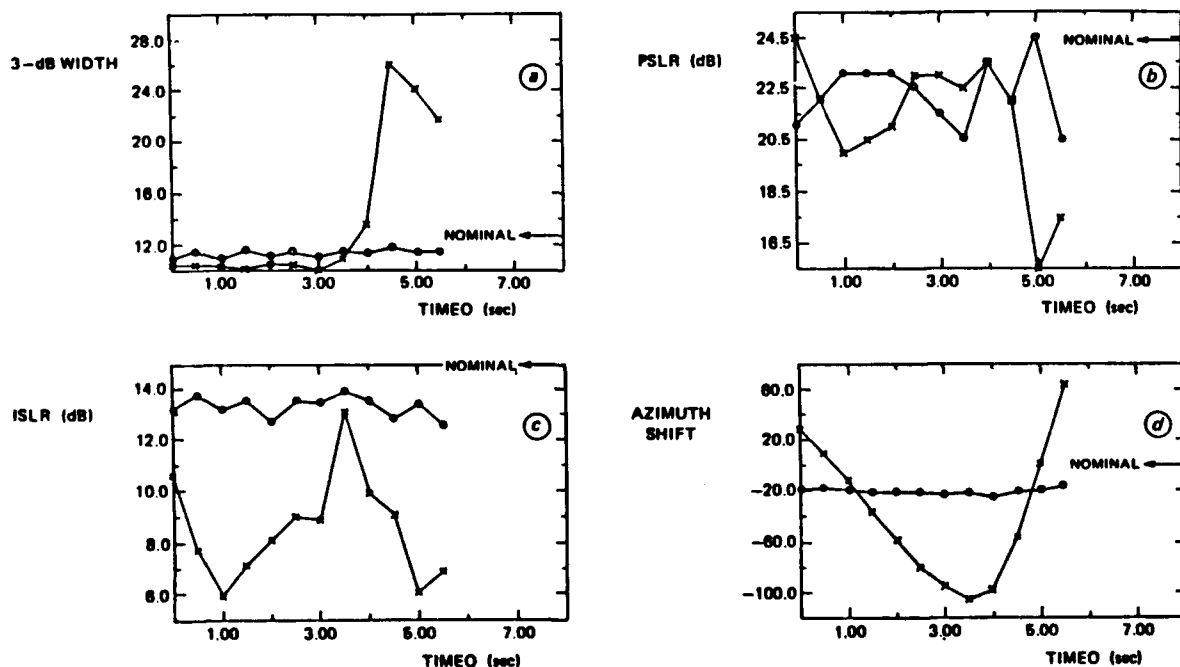

Fig. 3.2.3:   Image quality degradation (PHARS conditions) as a function of flight time
(x: real Metro fight data, o: components below 1 Hertz removed)

3.2.2.1   Joint non-ideal motion components

The plots in figure 3.2.3 show the effect of the joint non-ideal motion components of the Metro II on the various image quality parameters under PHARS conditions (altitude: 6000 m, ground range: 7500 m, nominal resolution: 6 m). The results using real Metro II flight data are indicated with crosses.

Removal of low frequency (i.e. less than about 1 Hz) motion components from the flight data yields the results indicated by circles. Figure 3.2.3 indicates that in the latter case a reasonable image quality can be achieved. However, the same flight data set used for simulations under PHARUS conditions results in large image imperfections (resolution loss and increased side lobes). These conclusions confirm the findings inferred from the indicative upper limits.

3.2.2.2   Vibrations

Note that it is assumed that the antenna is rigidly mounted to the aircraft fuselage. In case of vibrations the Metro II motions introduced in the 'SARGEN' software are no longer representative for motions of the antenna phase centre.

The effect of transverse sinusoidal vibrations of the SAR antenna have also been simulated. It is concluded that a reasonable design constraint is that the maximum amplitude of the transverse vibrations of the antenna pod are restricted preferably to less than 0.5 mm. If vibrations cannot be damped down to this level image quality constraints are required to measure these vibrations and correct for them afterwards.

3.3 Aircraft motion sensor package

This chapter describes the work performed during the study "Inventarization of compensation and flight path reconstruction methods", carried out in the framework of the "Preparatory study antenna motion and compensation".

The objective of this study was to specify a system configuration that enables the flight path of the SAR antenna to be determined accurately.

This study builds on the results of a previous study ("Error analysis": see chapter 3.2) giving an indication of the operational accuracy requirements to be achieved by the proposed motion measuring configuration.

3.3.1 Inertial measurement systems

The calculation of position and attitude of the SAR antenna with the accuracy specified in chapter 3.2 is not possible using purely inertial systems.

Even the best inertial systems need external position updates to keep the error within the specified bounds.

The most convenient absolute position reference available today is the Global Positioning System, which uses radio signals transmitted by a number of satellites to determine positions with an accuracy of about 10 metres anywhere on earth. When such an absolute reference is available, the accuracy of the inertial system itself is not too critical.

The main requirement is that the sensor signals have the accuracy, resolution and threshold sufficient to keep the error within bounds over the integration time of the SAR.

IRS performance summary

PERFORMANCE	
Attitude angles	0.1 degree
Heading	0.4 degree
Velocity (radial 4 hours)	6 m/s
Position	2 nmph
Accelerations	0.1 m/s^2
Angular rates	0.1 degree/s
Bandwidth	8 Hz

PHYSICAL CHARACTERISTICS	
Size	0.320x0.327x0.188 m
Weight	20 kg
Electrical power	96 W
Reliability	4700 MTBF

ENVIRONMENT	
Temperature (operating)	0 deg C to 70 deg C

ARA performance summary

GYRO CHANNEL	
Full scale rate	175 degree/s
Scale factor error	0.2 %
Drift g-insensitive	7 degree/hr
Drift g-sensitive	8 degree/hr/g
Drift g-squared	0.07 degree/hr/g^2
Alignment	2 mrad
Digital resolution	0.007 degree/pulse
Random drift	0.15 degree/hr

ACCELEROMETER CHANNEL	
Full scale acceleration	120 m/s^2
Scale factor error	0.2 %
Bias	0.04 m/s^2
Drift g-squared	70 μg/g^2
Alignment	2 mrad
Digital resolution	0.00476 m/s/pulse
Bandwidth	100 Hz

PHYSICAL CHARACTERISTICS	
Size	0.209x0.243x0.096 m
Electrical power	25 W

ENVIRONMENT	
Temperature (operating)	-12 deg C to + 71 deg C
Random vibration	12 g

Table 3.3.1: Main performance characteristics of IRS and ARA

NLR operates two different types of inertial systems that comply with this requirement.

The first is the Honeywell Inertial Reference System (IRS), a strapdown inertial navigation system based on laser gyroscopes.

The second system is the Lear Siegler Attitude Reference Assembly (ARA), a strapdown inertial sensor package designed for use in short range (Firebrand) missiles.

3.3.1.1 Performance

The main performance characteristics of the Honeywell IRS system and the Lear Siegler ARA system are shown in Table 3.3.1.

This table clearly shows that the IRS is much more accurate than the ARA.

But the ARA has the significant advantage that it is small enough to be mounted in the antenna pod close to the SAR. Another significant advantage of the ARA is its large measurement bandwidth, whereas the 8 Hz bandwidth of the IRS means that potentially important vibration components cannot be compensated.

3.3.2 Error modelling and simulation

A simplified model for the inertial system errors was derived, which is valid for periods in the order of the SAR integration time (1 to 10 seconds) and for approximately horizontal steady flight. This model consists of three (almost) independent submodels.

The most important submodel for the SAR application contains the roll angle and the cross-track displacement as error states.

The error sources in this submodel are the Y accelerometer and its A/D converter and the X gyroscope and its A/D converter.

The variances of the sensor errors in this model were determined from manufacturer data sheets and from laboratory test data.
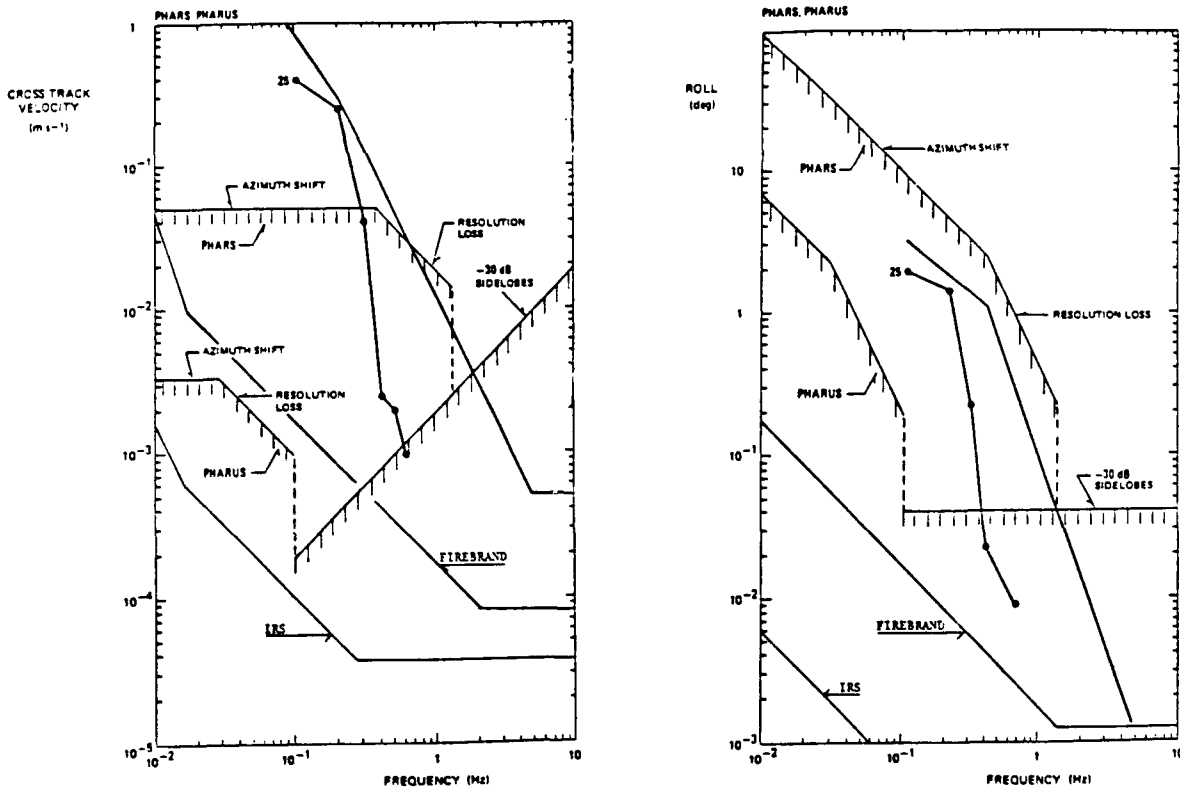

Fig. 3.3.1: Comparison of error model results with Metro II spectra and indicative upper limits

3.3.2.2   Simulation

The error variances of the error model can be converted to effective RMS spectra like those used in the analysis described in chapter 3.2.

Typical results are shown in Figure 3.3.1. The error model was simulated over a period of 100 seconds, and time histories of the errors in the three attitude angles and the three position components were generated.

The time histories were subsequently used by the SARGEN package (see chapter 3.2.2) to obtain an indication of the degradation of the SAR image due to the simulated sensor errors.

A result from this analysis is shown in Figure 3.3.2, where the resulting SAR impulse response function is shown (resulting 3-dB resolution: 1.1 m; peak to sidelobe ratio: 20 dB; see chapter 3.2.2 for a description of input parameters for simulations under PHARUS conditions).
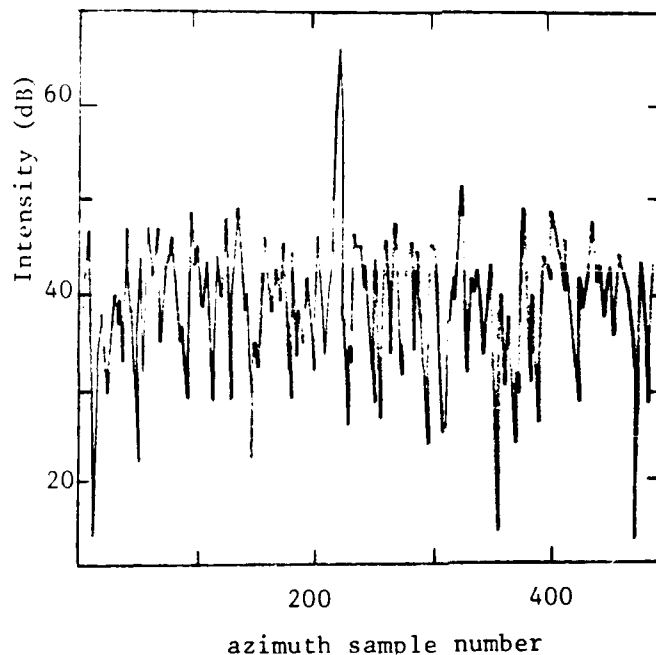

Fig. 3.3.2:   Azimuth impulse response function derived from simulated flight data
(azimuth spacing: 0.35 m)

3.3.3 Implementation for PHARS

Based on the previous error analysis it was decided to use the instrumentation set-up shown in Figure 3.3.3.

The ARA is used to determine the position and the attitude of the SAR over a short time period. Therefore it is mounted in close proximity to the SAR in the antenna pod.

The IRS is mounted in the aircraft cabin, and is used to estimate and correct for the errors in the ARA signals.

The signals of the two inertial systems were recorded in ARINC serial format on a separate track of the flight recorder.

In order to evaluate in the future the level of accuracy achievable with GPS it was decided to add a GPS antenna and a simple GPS receiver to the measurement system.
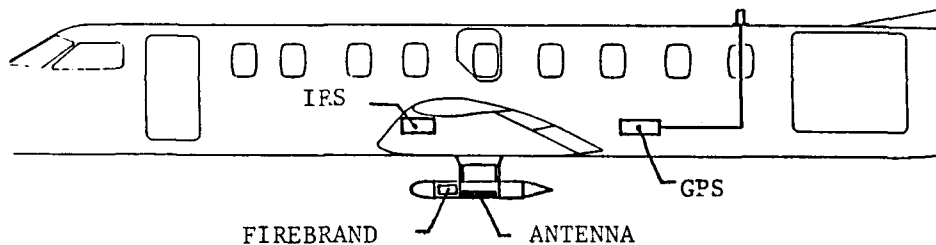
Fig. 3.3.3:   Proposed motion measuring configuration

3.3.4 Results of the data processing

The inertial measurement data require a processing sequence which is completely separated from the SAR data (see chapter 4.3). The inertial data is recorded on a separate track and has to be converted to computer compatible format. The standard calibration procedure of the NLR is applied to the inertial data and the data is transmitted to NLR's Mainframe computer. Here the data is stored in NLR's Post-Processing (NPP) database.

3.3.4.1 Correction

The first step in the NPP processing is the correction of the data for time shifts, misalignments and other effects. One error source that has a large effect on the final accuracy is the dead-band of the A/D converters of the ARA package, and a special algorithm was developed that compensates most of this effect.
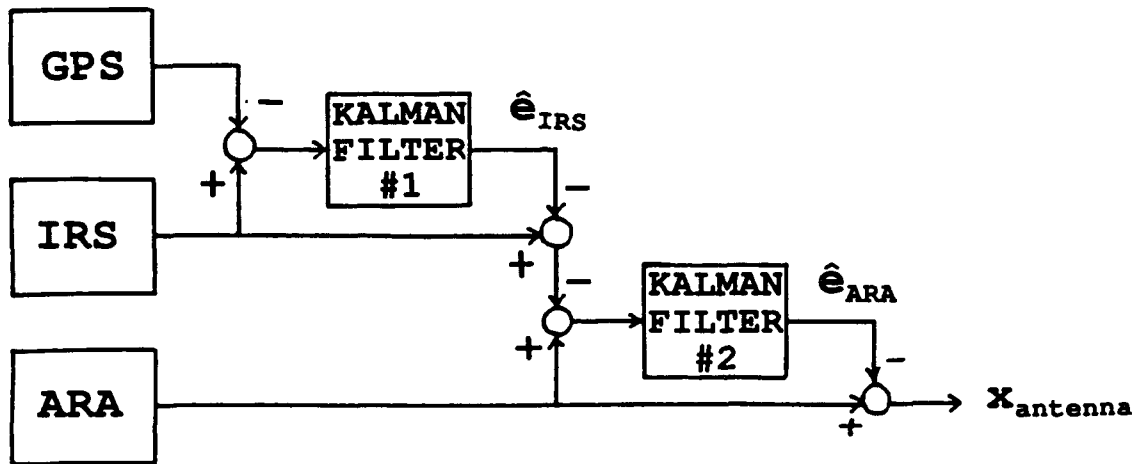
Fig. 3.3.4: State estimation process

3.3.4.2 Kalman filter procedure

The next step is the precise reconstruction of the flight path and attitude angles of the IRS using the barometric altitude and GPS measurements (when available) for updates in a Kalman filter procedure. Subsequently the antenna position is derived from the IRS position.

The ARA output signals are integrated and compared with the IRS-derived antenna position for updating in a Kalman filtering procedure.

Finally the antenna position and attitude are converted to a standard format and axis system, and copied to computer tape for transfer.

Figure 3.3.4 shows the complete state estimation process.

3.3.4.3   Propeller

During the processing of the inertial measurements of the first PHARS flight it was noted that a 3 Hz component was quite prominent in the IRS signals.

Analysis of this component revealed that it was the result of insufficient aliasing suppression in the IRS.

The three-blade propeller of the Metro rotates at 32.3 Hz, which results in a 97 Hz component due to the passage of the wake of each propeller over the aircraft. The IRS samples at 50 Hz and due to insufficient anti-aliasing suppression this results in a 3 Hz component in the output.

The 97 Hz component can be clearly seen in the ARA outputs (see Figure 3.3.5), because the ARA has a 100 Hz measurement bandwidth, so that the ARA signals do not suffer from the same aliasing error.

The processing of the inertial data effectively uses only the ARA data for frequencies above 0.1 Hz which means that the aliasing errors at 3 Hz do not show up in the final results.
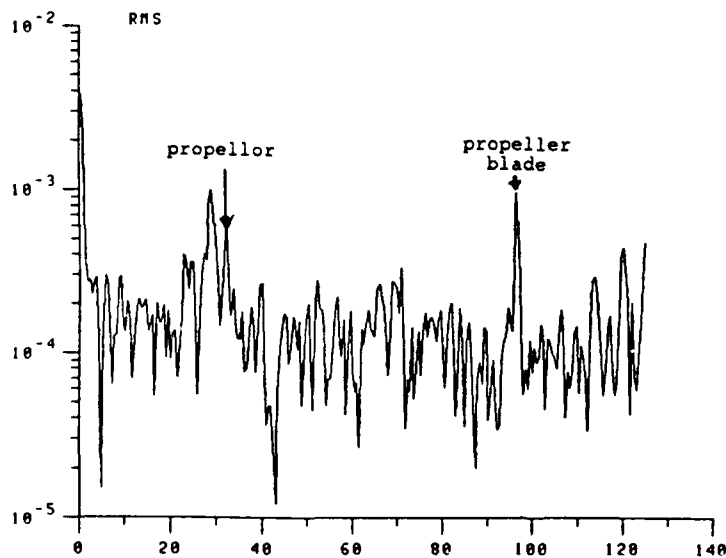
Fig. 3.3.5:   ARA output showing the 97 Hz component

3.4 Conclusions

A SAR raw data simulator is developed to study aircraft motion and motioncompensation. The simulator proved to be useful for a wide range of analysis.

The aircraft motions of Metro II and Fokker F50 have similar properties and can be corrected by INS systems to a level needed for PHARS and PHARUS.

A motion measurement system is realised, consisting of an ARA close to the antenna and an IRS in the cabin, eventually coupled to a GPS system. This combination performed to satisfaction.

4 RESULTS FROM THE PHARS SAR TESTBED

4.1 System specification

In the PHARUS definition study a SAR testbed is designed and constructed to meet the following specifications:

Radar type	Coherent pulse radar
RF frequency	5.25 GHz (C-band)
first IF frequency	350 MHz
second IF frequency	21.875 MHz
PRF	3500 Hz
Waveform type	linear FM (no amplitude weighting)
Pulse length	12.8 μs before pulsecompression
	32 ns after pulsecompression
Pulsecompression ratio	400
Pulsebandwidth	31 MHz (fixed)
Generation technique	I/Q memory read-out
DAC frequency	87.5 MHz, 8 bit
Total memory cap.	4096 bytes
Total peak transmit power	160 Watt
Module peak transmit power	20 Watt
Number of modules	8 (transmit and receive)
Range	3 - 14 km
Antenna	8 elements antenna with 4 patches each, uniform, no
tapering	
One way antenna gain	21 dBi
Antenna sidelobes	13 dB
Polarisation	vertical
Azimuth beamwidth	7.5 degree (two way)
Antenna length	0.40 metres
Doppler bandwidth	460 Hz (@ antenna)
After Azimuth filter	218 Hz
Azimuth processing BW	100 Hz (1 meter resolution)
Azimuth presuming factor	16
Azimuth filter	32 points FIR
Azimuth weighting	uniform
Azimuth scan angle	-12 to +12 degree (1 degree step)
Elevation beamwidth	24 degree (two way)
Elevation pointing angle	fixed
Mech. elevation angle	20, 35 and 60 degree (depression angle)

Resolution	4.8 m in range
	1.2 m single look in azimuth
Receiver:	
Total system noise factor	2.5 - 3 dB
Receiver bandwidth	40 MHz
Receiver output type	offset IF
IF gain	+6 dB to +57 dB (1 dB step)
Total system gain	95 dB max.
Sampling freq. in range	87.5 MHz (A/D conversion)
	4096 * 8 bit
Datastorage	8.4 Mbit/s
Airplane	NLR Metro II
altitude	3 - 6 km
speed	100 m/s
position and motion registration	IRS, ARA
Mains voltage	115 Volt, 400 Hz
Mains current	3.5 A (operational)

4.2   Radar airborne instrumentation

The airborne instrumentation for PHARS is based on an existing recording chain for remote sensing.

4.2.1   NLR's remote sensing recording chain

Since 1979 the laboratory aircraft of NLR have flown several remote sensing systems.

For the recording of the remotely sensed data and the data related to the trajectory and altitude of the aircraft a suitable instrumentation system was designed for different remote sensors. The system was designed with a maximum use of hardware components already available and shared existing routines and procedures as much as possible. The general diagram of the NLR recording chain for remote sensing is shown, consisting of an airborne component (figure 4.2.1) and a groundbased component (figure 4.2.2).
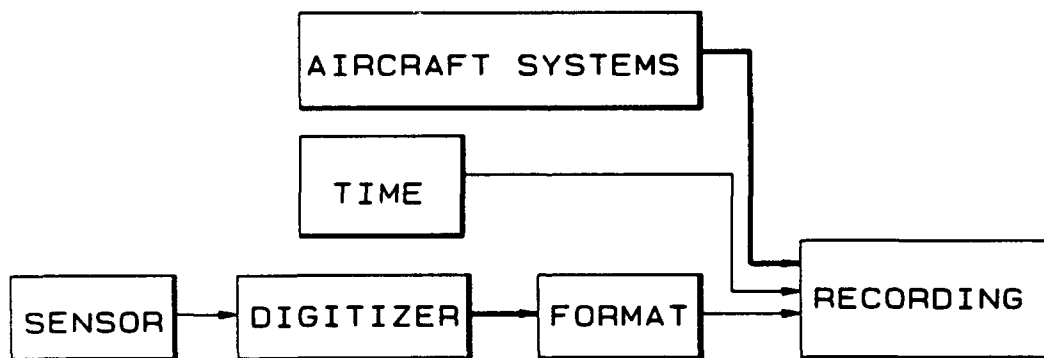
Fig. 4.2.1:   General diagram of the airborne recording for remote sensing

4.2.1.1   Airborne remote sensing recording

Each new remote sensor requires a dedicated digitizer. At this moment NLR operates a SLAR with SPEEDIG, an optical scanner CAESAR with CEDIG and the PHARS with PHAREDIG. There used to be a Thermal Infrared Scanner with TIRDIG and a TV-camera with BEELDIG, but these sensors are not supported anymore.

The digitized remote sensing data is organized in a telemetry-like serial format by the Data Formatter DAF. DAF is programmable to accommodate different data structures (bitrate; number of bits, words and channels).

The serial data of DAF, mostly at 8.4 Mbit/s, is encoded by an Ampex High Bit Rate system (HBR) into signals for seven tape tracks of an Ampex AR700 instrumentation recorder, running at 60 Inch Per Second (IPS).

At the same time up to six tracks of the recorder are usable for the recording of aircraft data generated by instruments like an Inertial Reference System (IRS) and a Digital Air Data Computer (DADC).

One track is committed to the recording of a Greenwich Mean Time (GMT) signal with a resolution of 0.1 ms.
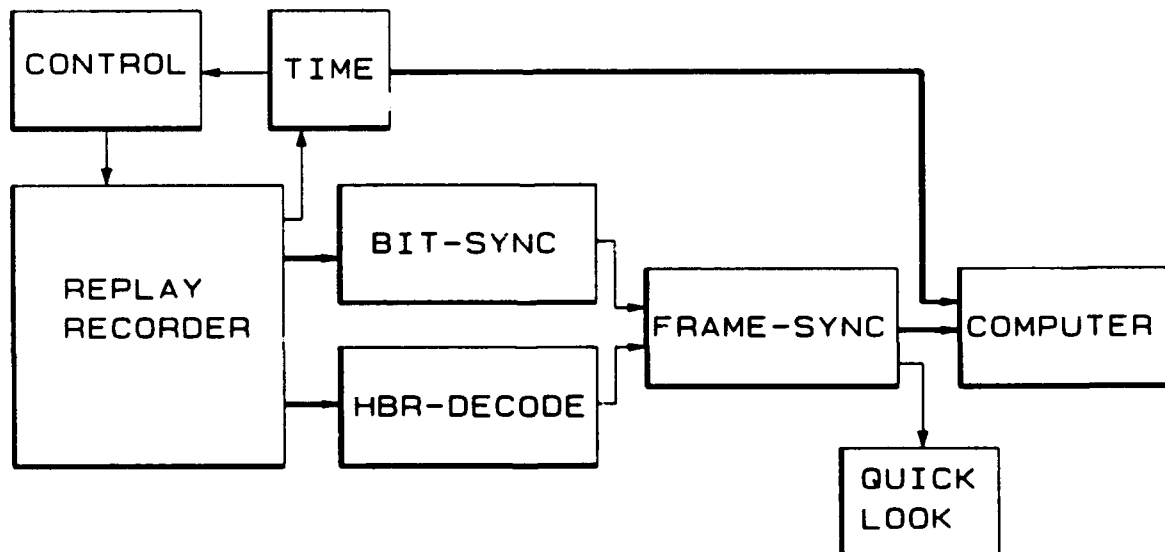

Fig. 4.2.2:   General diagram of the groundbased replay facility for remote sensing

4.2.1.2   Remote sensing replay

At the groundbased replay facility the tape is replayed and a selection of the data gathered is made, based on the recorded GMT-signal.

Selected data from the remote sensor is decoded and transformed into a bit-serial datastream. From input to output the HBR recording for remote sensing can be considered as a single telemetry channel. The frame synchronizer transforms the serial data into parallel words which are, in combination with End of Channel marks and timetags, transferred to a computer. The computer checks the validity of the data, reorganizes it and writes selected data to a Computer Compatible Tape (CCT) for further processing.

Aircraft data is replayed track by track, using the same facility. Each one-track signal is decoded into a serial bitstream by a bitsynchronizer, the bitstream is decomposed into parallel words by the same framesynchronizer (with different settings). Frame synchronizer words, in combination with marks and timetags, are transferred to the same computer which decodes the words into time histories of raw parameter values. Raw aircraft data is routed to a Central Data Base (CDB) for calibration and becomes available as a file in the main computer system. Correlation of remotely sensed data and calibrated aircraft data is based on the recorded time.

4.2.2   Instrumentation of PHARS

Design criterion of the PHARS SAR testbed was the use of the above described recording chain, which limited the bitrate to 8.4 Mbit/s.

Figure 4.2.3 shows the instrumentation for the operation of the PHARS SAR testbed in more detail. The main blocks of the general diagram of the airborne component as described above are recognizable. No alterations were necessary at the replay facility.
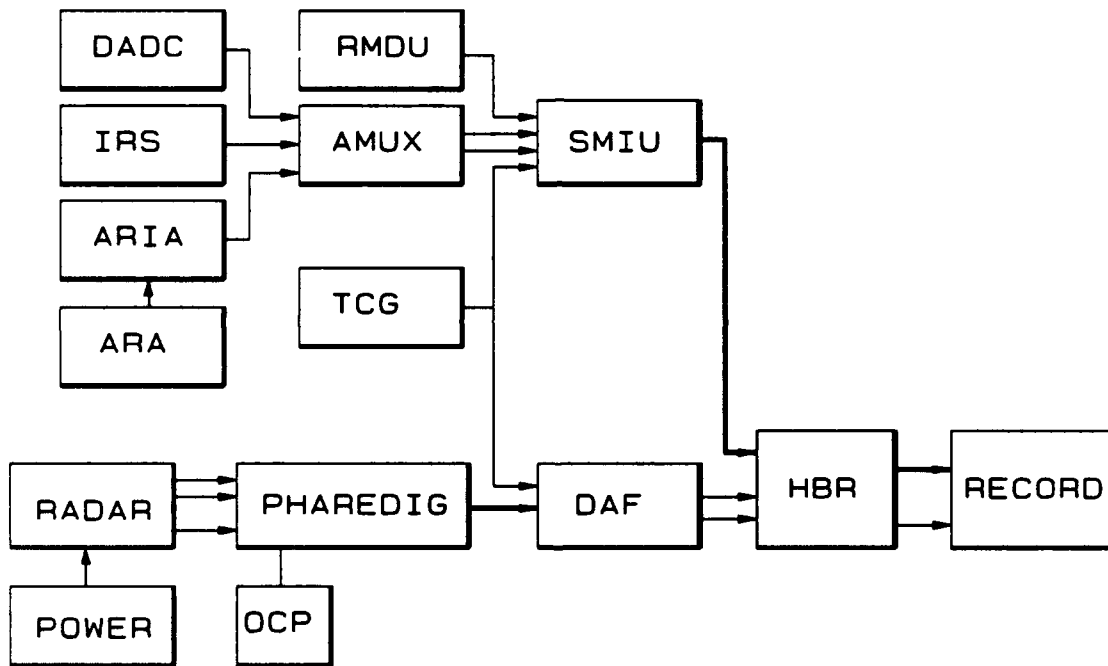

Fig. 4.2.3:   General diagram of the airborne instrumentation for the PHARS SAR testbed

4.2.2.1   Short description

The remote sensor component consists of the radar and its power unit, designed by FEL-TNO and housed in the external pod designed by NLR.

The Digitizer of the PHARS SAR testbed is called PHAREDIG, which is connected to the Operators Control Panel OCP to control and monitor both the radar and the digitizer.

DAF, HBR and RECORD are the DataFormatter, the High Bitrate Encoder and the tape recorder as described before.

ARA is the Attitude Reference Assembly, mounted in the pod, next to the PHARS antenna. It is considered as a part of the Aircraft Data system. ARIA is the ARA interface which contains the control electronics for ARA.

IRS is the Inertial Reference System; the data of this system is combined, off line, with ARA data to calculate the trajectory and attitude of the antenna.

DADC is a Digital Air Data Computer.

TCG is the Time Code Generator which produces a time signal suited for taperecording (Greenwich Mean Time).

RMDU, AMUX and SMIU are interfaces which are used by NLR to transform signals with different types of coding into signals that are recordable on magnetic tape.

All instrumentation is placed inside the aircraft except for the radar, its Power Unit and ARA which are accommodated to the external instrumentation pod.

4.3   Phars Pod

NLR's Metro II laboratory aircraft is equipped with four "hardpoints" in the bottom of the fuselage close to the intersection of the longitudinal axis and the lateral axis. An interface rack is used to accommodate various external pods with instrumentation.

4.3.1   Construction

The PHARS radar with its Power Supply Unit is housed in a dedicated pod which fits into the interface rack. The pod is designed with emphasis on rigidity and lack of vibration.

It is of a triple box structure made of machined aircraft aluminum (Dural) walls, with farings of glasfibre reinforced epoxy.

The equipment can be mounted in its box from the frontside, and so being part of the construction and contributing to the stiffness. The main measures are given in figure 4.3.1.

DIRECTION OF FLIGHT

DIMENSIONS IN MILLIMETRES
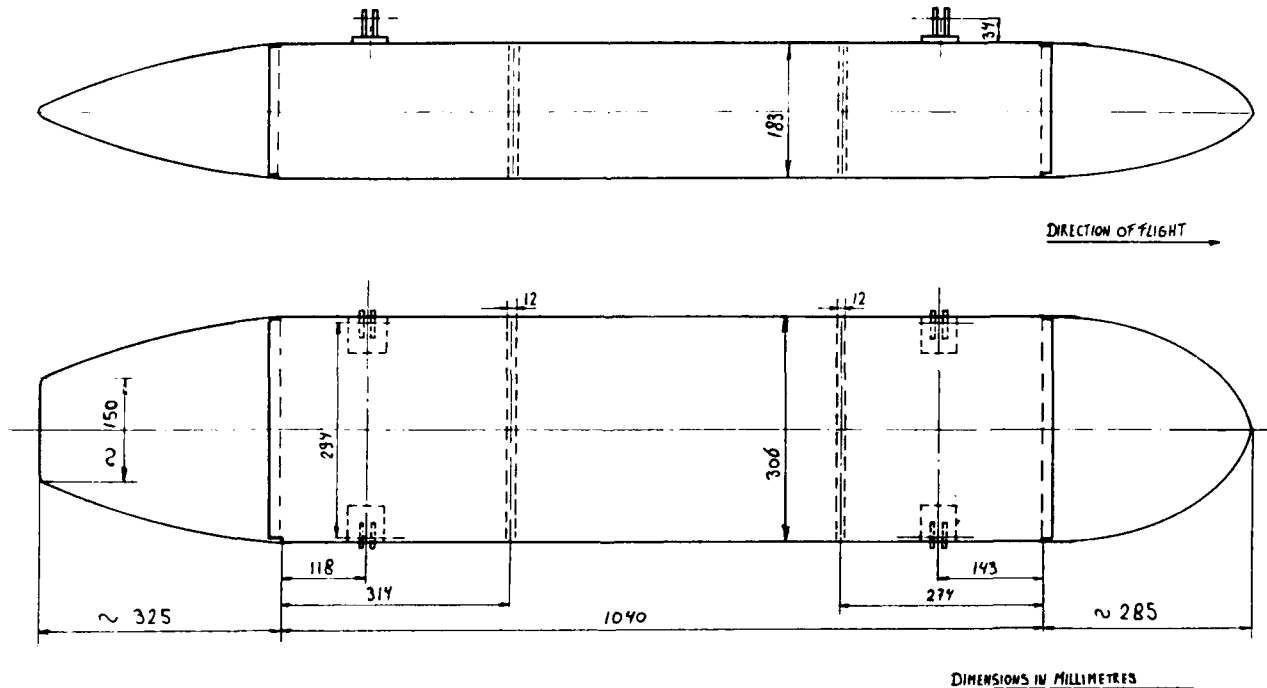
Fig. 4.3.1:   Outlines of the external instrumentation pod for the PHARS SAR testbed

The centre box contains the PHARS radar; the lid is a flat radome of C-band transparent material.

The rear box contains the PHARS Radar Power Supply Unit which transforms the 115V 400Hz aircraft power into several DC voltages.

The front box is equipped with a strapdown inertial measurement sensor comprising three accelerometers and three rate gyros (ARA).

4.3.2   Electrical interface

The wiring running from the pod to the aircraft is kept to a minimum:

-       a 40 wire cable for the operation of the inertial sensor,

-       one 115V 400Hz shielded twisted pair power line,

-       two tri-axial 50Ω signal lines,

-       a data link consisting of two shielded twisted pairs.

4.4   Radar hardware

The system configuration of the SAR testbed PHARS is shown in figure 4.4.1.

Fig. 4.4.1:   Block diagram of the radarsystem

For a functional description of the configuration we distinguish two situations; the transmit and the receive mode.

In the transmit mode a SYNC signal generated by the Timing & Control circuit starts the Chirpgenerator, producing a 31 MHz bandwidth chirp. A modulator, fed by the DRO-PLL signal, is used to convert the IF chirp signal to the microwave frequency band. After filtering and amplifying the combiner/splitter distributes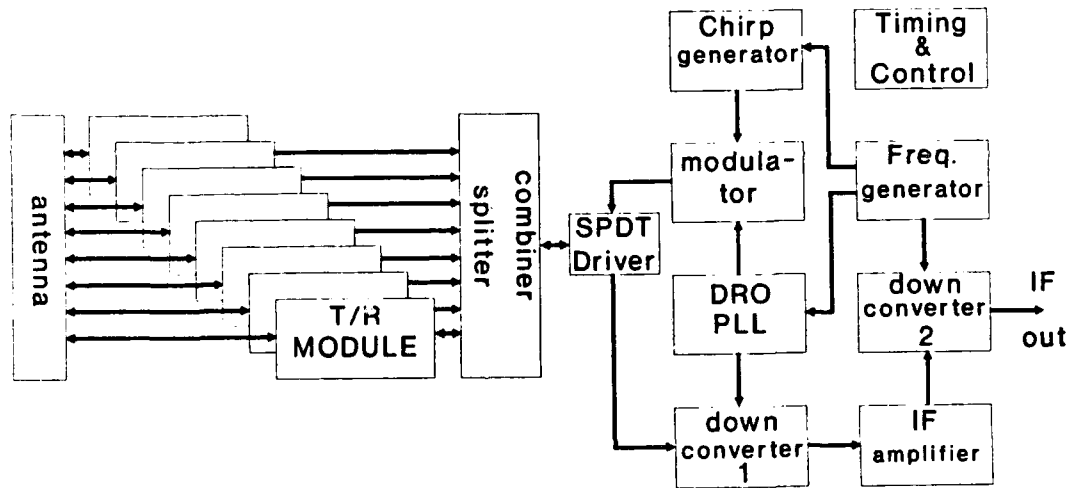 this microwave signal over the eight T/R modules. After amplification in each T/R module the microwave signal is fed to the antenna elements. Each module contains a four bit phaseshifter for antenna beamforming in azimuth direction.

In the receive mode the received signals are amplified by LNA's in the modules. Again the phaseshifters in the modules is used for antenna beamforming. Summation of the received signals takes place in the combiner/ splitter circuit. The output of the combiner/splitter is connected with the first downconverter, where it is converted in the first IF frequency by using the signal of the DRO-PLL as local oscillator signal. An IF amplifier with digital gain control amplifies the IF signal to obtain a usable output power level. The second downconverter gives an output signal with an offset frequency of 21.875 MHz. This output signal of the radar is fed to the digitization unit inside the airplane.

The Timing & control unit consists of a microcontroller and several Programmable Logic Array's (PLA's) to create the control functions and timing signals for the SAR system.

A description of the most important blocks in the diagram of figure 4.4.1 is given in the next paragraphs.

4.4.1   Antenna

The antenna consists of eight elements and each element has four patch radiators (see figure 4.4.1.1). The patch radiators are serially feed by interconnecting the patches with transmission lines. The feedpoint of each antenna element is located at the edge of each first patch.
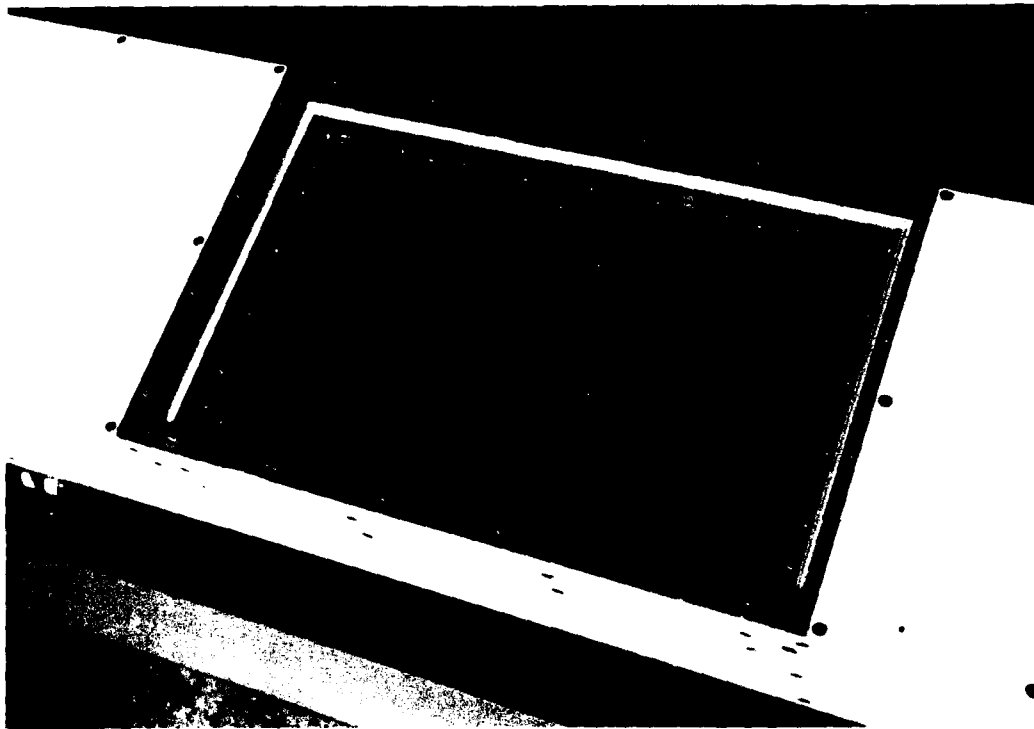
Fig. 4.4.1.1: Antenna configuration used in the PHARUS testbed

The impedance of the antenna at the feedpoint is about 50 Ohms and the polarisation is vertical. The vertical antenna beamwidth is approximately 24 degrees as is required for this SAR application.

The antenna is built on Duroid substrate with an aluminum groundplane. With phototechniques the patches are etched from the copper topplate of the Duroid substrate. This technique can be applied for mass production because it is cheap and has a good reproducibility.

The resonance frequency of the patch resonators is at 5.25 GHz with a frequency bandwidth of about 250 MHz. The resonance frequency of the patches are temperature independent. The dimension of the complete antenna on Duroid substrate is about 50 * 25 cm. Each element has a length of 15 cm and between the elements there is a mutual spacing of 42 mm. The gain of each element is about 12 dB and for the complete antenna the gain is about 21 dB.

To obtain a high integration level for this radar system snap-on connectors for the antenna - T/R module connection have been used.

4.4.2   T/R module

Each element of the antenna is connected with one T/R module. The eight T/R modules are mounted on the aluminum groundplane of the antenna to enable a short connection between the T/R module and the antenna element. The physical dimensions of the module are 13 * 4 * 4 cm. Each of the modules consists of a two stage FET power amplifier, a two stage low-noise amplifier with a limiter at the input, two SPDT switches and a four bit phase shifter (see figure 4.4.2.1).
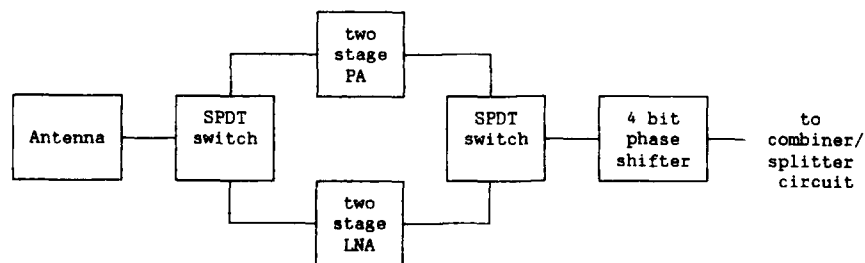

Fig. 4.4.2.1: T/R module

TNO report
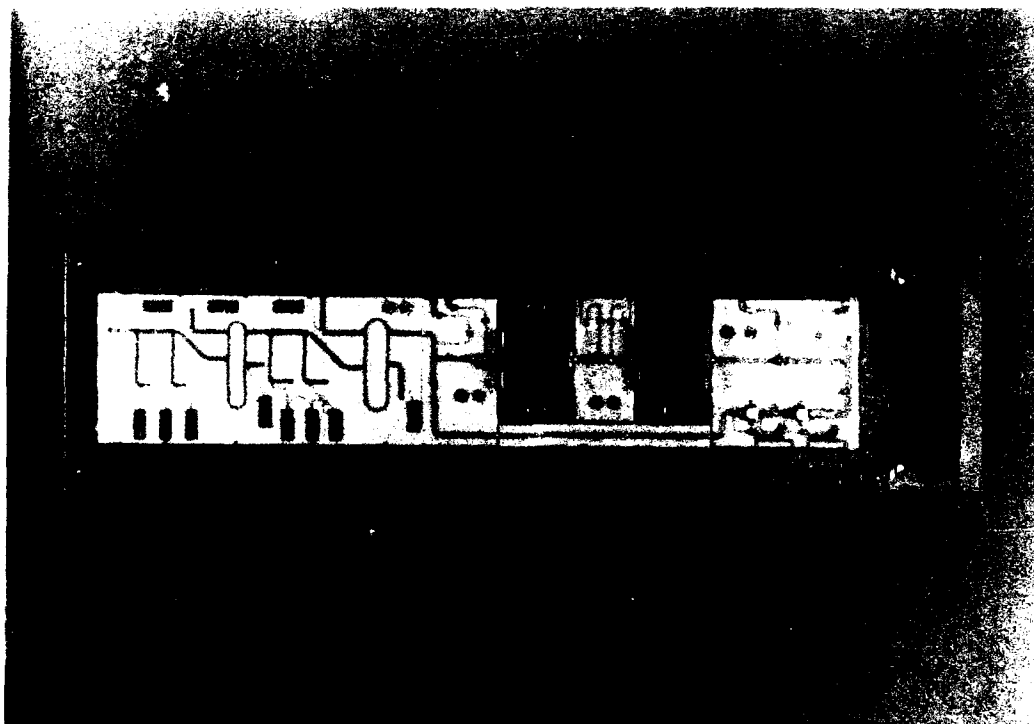
4.4.3   Frequency generation circuit

The frequency generation is based on a low phase noise temperature stabilized crystal oscillator (see figure 4.4.3.1). By using multipliers for the higher frequencies and dividers for the lower frequencies all necessary frequencies can be generated without loosing coherency.

```
              ┌──────────┐
              │ multi-   │ 700 MHz
              │ stages   ├──────── to DRO-PLL
              │multiplier│
              │ circuit  │ 350 MHz
              │          ├──────── to first IF mixer
              │          │
              │          │ 328.375 MHz
              │          ├──────── to second IF mixer
              │          │
    ┌─────────┤          │  87.5 MHz
    │         │          ├──────── clock chirpgenerator
    │         │          │
    │         │          │ 21.875 MHz
    │         │          ├──────── to I/O circuit
    │         └──────────┘
┌───┴──────┐
│reference │
│crystal   │
│oscillator│
│10.9375   │
│  MHz     │
└───┬──────┘
    │      ┌──────────┐
    │      │ divider  │ 3500 Hz
    └──────┤ circuit  ├──────── prf
           └──────────┘
```
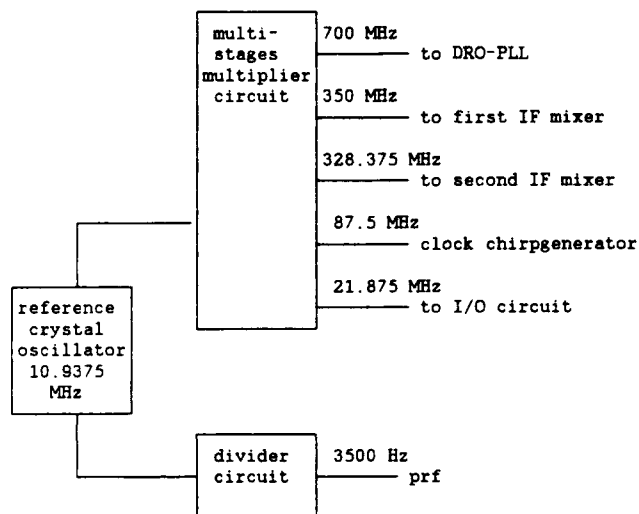
Fig. 4.4.3.1: Frequency generation circuit used in the PHARUS testbed

The microwave generator is a highly stabilized oscillator using a dielectric resonatoi (DRO). This dielectric resonator is mounted on a dielectric disk with a low permittivity in a metal cavity (see figure 4.4.3.2). The loaded Q of the total resonator is more than 20.000 at a frequency of 5.6 GHz. The active device in this oscillator is a two stage bipolar transistor amplifier to obtain a very low noise factor. The DRO is made tuneable with a varactordiode which is coupled with the resonator circuit.

TUDelft
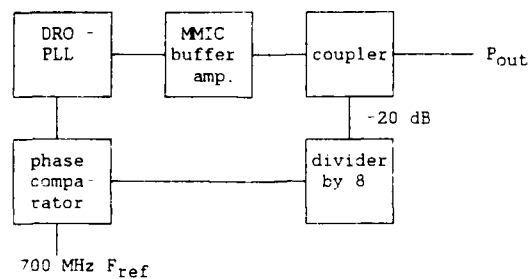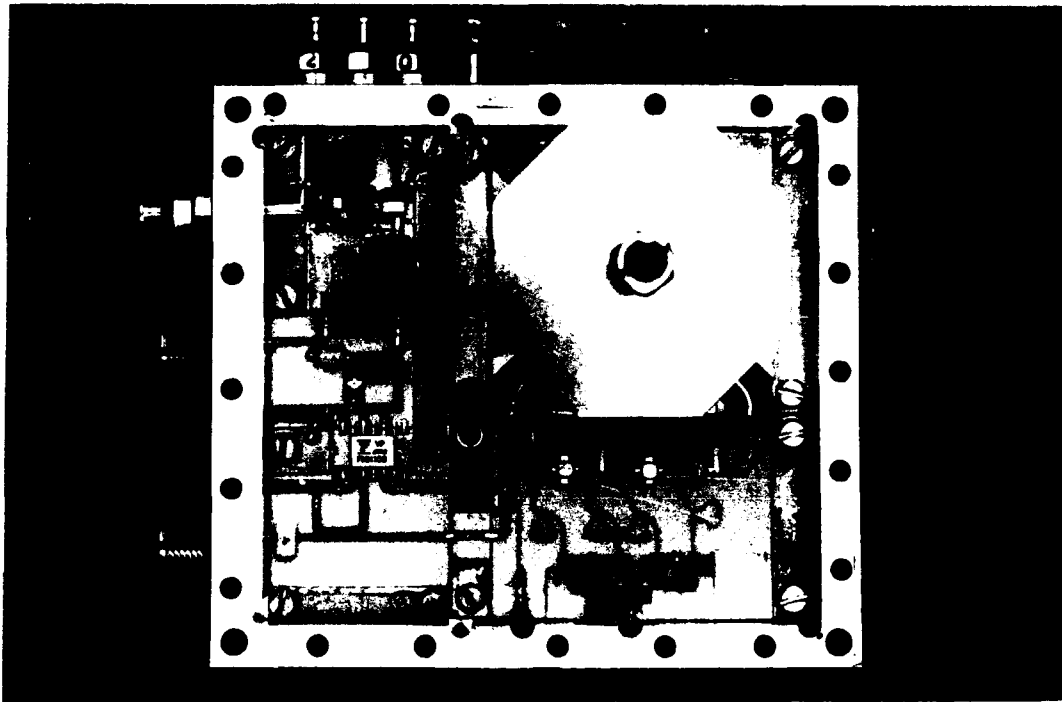
Fig. 4.4.3.2: Microwave phased locked loop dielectric resonator oscillator (DRO-PLL)

The added noise of the DRO-PLL is less than 2 dB at the microwave outputsignal measured from 1 Hz to 1 kHz near the carrierfrequency of the DRO-PLL.

4.4.4   Digital chirpgenerator

To generate a frequency sweep signal with coherence to the crystal oscillator the concept of a digital generator was chosen. The digital generator consists of an addressgenerator, two static RAM memories and two Digital to Analog Converters (DAC's) (see figure 4.4.8.1).
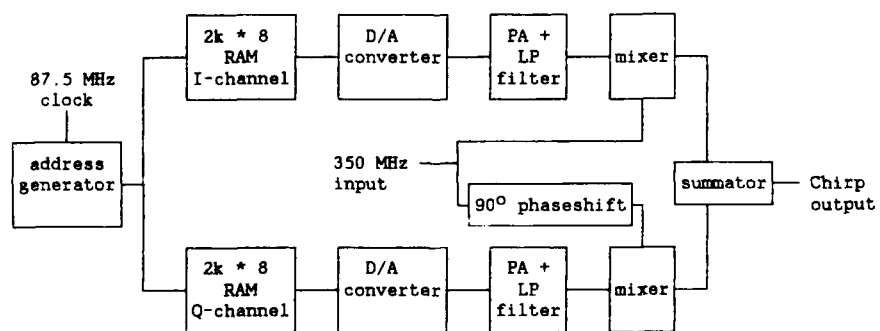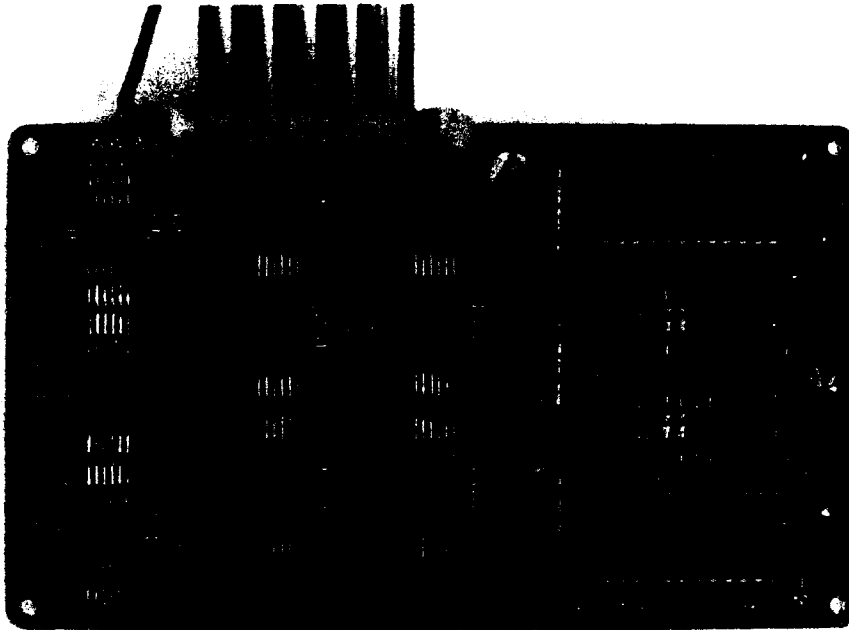
Fig. 4.4.4.1: Chirp generator using I&Q method

The (arbitrary) chirp pattern is downloaded from an Eprom to the static RAM memories. After this loading the chirp generator is ready to be used in the radarsystem. The I and Q output signals are fed to a single side band modulator to convert these signals in a chirpsignal with a central frequency of 350 MHz.

4.4.5 Timing & control

On Deck1 of the radarconstruction, shown in figure 4.4.6.1, a microcontroller board is mounted for the digital timing and control. The microcontroller controls the phasesetting data for the T/R modules, the temperature etc. (see figure 4.4.5.1).

To synchronise the digitalization unit in the airplane a 21.875 MHz clock signal is sent to this unit. At the beginning of each transmit pulse one period of the 21.875 MHz signal is suppressed to trigger the digitalization unit.

```
        RADARSYSTEM          |    AIRPLANE

                 +----------+ |
                 | micro-   |--------- RS422 data &
                 | controller| |        communication link
                 +----------+ |
 +------+ +------+ +------+ +--------+|
 |phase | |temp. | |timing| |control |
 |setting| |sensor| |&    | |IF-amp  |-------- 21.875 MHz
 |T/R module| |   | |control| |      ||         offset freq.
 +------+ +------+ +------+ +--------+|
                                ----------- 21.875 MHz
                              |            timingsignal
                              |
                              |  Powersupply
                              --------- 115 Volt / 400 Hz
                              |
```
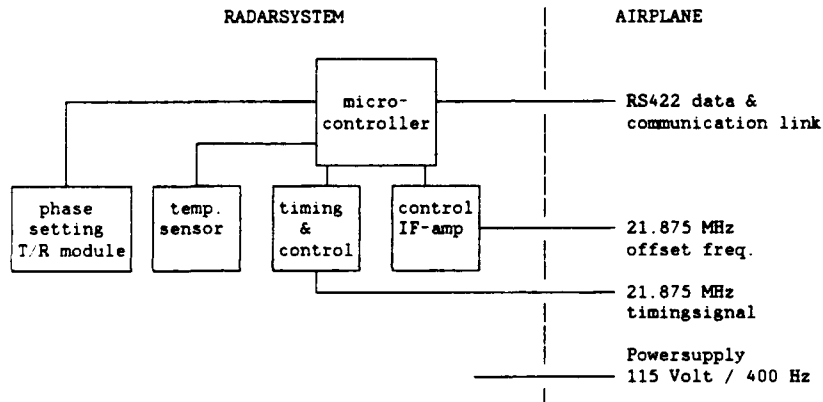
Fig. 4.4.5.1: Timing and control with RADAR-AIRPLANE interface

There are four links from the radarsystem to the digitalization unit: a RS422 datalink, a 21.875 MHz timing signal, the IF output signal and a powersupply link.

4.4.6   Mechanical considerations and construction

Mechanically three decks can be distinguished (see figure 4.4.6.1): one deck with the T/R modules and the antenna, one deck with the high frequency generation and conversion circuits, and one deck with the timing & control and the low frequency generation circuits.
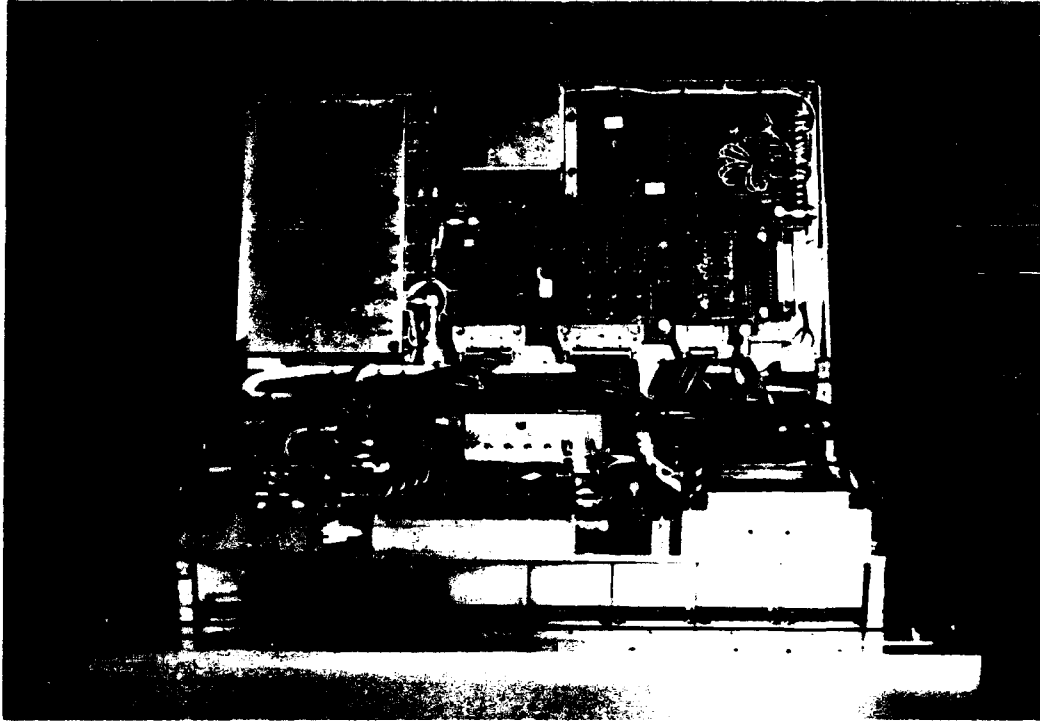
DECK 1	frequency generation	Timing & Control	I/O		Power Supply module
DECK 2	DRO-PLL IF amp.	Driver up & down converters		Chirp generator	
DECK 3	T/R modules & antenna				

Fig. 4.4.6.1: View of the inner side of the radarsystem

Deck 1 provides for the communication to the digitalization circuits on board of the airplane.

With the aid of CAD/CAM programs and equipment we were able to achieve a high level of integration. The total dimensions of the radarsystem is about 50 * 25 * 25 cm without the powersupply.

4.5   PHARS data handling

The PHARS data handling makes use of the existing recording chain for remote sensing data described in chapter 4.2 of this report.

This chapter deals with the DIGITIZER/PREPROCESSOR unit dedicated to the PHARS SAR testbed. The unit, designed and manufactured by NLR, is called PHAREDIG: PHARs Experimental DIGitizer.

The Operators Control Panel (OCP) will be described in chapter 4.6.

The position of PHAREDIG as part of the PHARS SAR testbed is indicated in figure 4.5.1.
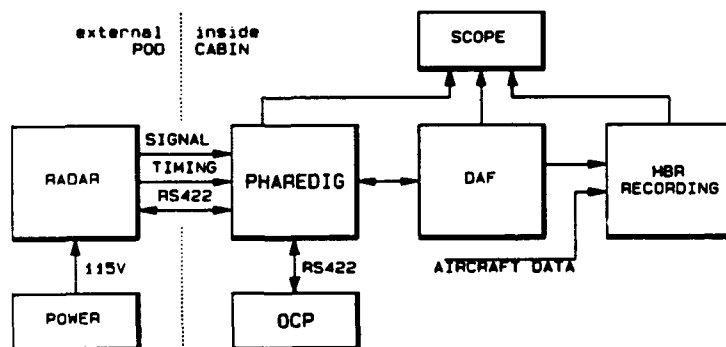
Fig. 4.5.1:   PHAREDIG as part of the instrumentation for the PHARS

4.5.1   Functions of PHAREDIG

The functions of PHAREDIG are:

-    digitizing the IF backscattersignal as provided by the radar,
-    synchronizing PHAREDIG sampling frequency and sampling schedule to the complex timing signal of the radar
-    presumming the signals of several lines with a digital FIR filter
-    preparing presummed lines for delivery to DAF, the frontend of the recording system
-    processing presummed lines for Monitoring, Gain Control and Range Gate Control
-    providing the communication with the radar and with the OCP.

4.5.2 Functional Description of PHAREDIG

The block diagram of PHAREDIG is given in figure 4.5.2. The different functions will be described in more detail below.
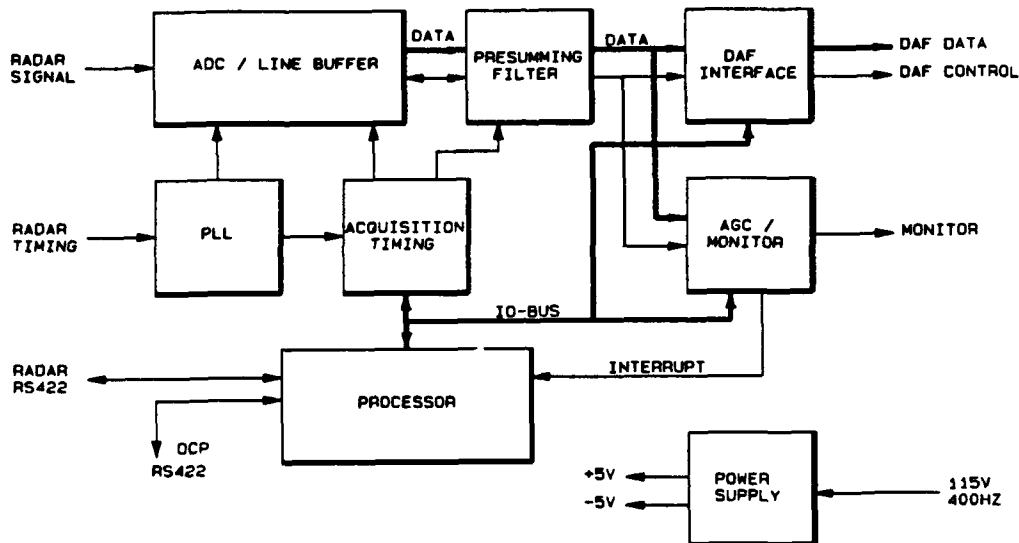
Fig. 4.5.2.1: Schematic diagram of the PHARS Digitizer PHAREDIG.

The radar generates two signals:

- an analog signal representing the received radarsignal, demodulated to an offset frequency of 21.875 MHz,

- a timing signal consisting of a square wave of 21.875 MHz, which is isochronous with the unmodulated carrier signal; from this square wave, single positive pulses are suppressed marking the start of the transmission of a chirped pulse by the radar: Pulse Repetition Frequency (PRF) of 3500 Hz.

The Phase Locked Loop (PLL) generates the sampling frequency of 87.5 MHz which is the quadruple of the carrier frequency of 21.875 MHz. The PLL detects the missing pulse which triggers the Acquisition Timing.

The Analog to Digital Converter (ADC) is a flash converter, digitizing to 8 bits. A selection of samples is stored in a high speed Line Buffer: 4096 samples at 87.5 MHz.

The selection of the samples is dictated by the Acquisition Timing.

Small groups of samples are selected to measure parts of the transmitted pulse, another group is taken to measure the noise level and the main group of samples is taken in the fixed Range Gate after a delay to compensate for the altitude of the aircraft. The Range Gate can be controlled by the Processor.

The contents of the line buffer are transferred to the Presumming Filter. This filter consists of two FIR filters running in parallel. Each filter calculates the response over 32 input lines together producing one filtered line per 16 input lines.

The DAF INTERFACE takes each filtered line, adds administration data such as the value of the gain and the range gate, and triggers the recording interface DAF. DAF takes the line word for word by handshaking and assures the recording of the data at a maximum bitrate of 8.4 Mbps.

The AGC/MONITOR receives the same filtered line as the DAF interface. A partial pulse compression is performed by correlation. The correlation process is again a parallel FIR filter, now over 64 values in the same line, producing a result per 32 input values. Each compressed line contains 128 output values which are converted into an analog signal to be viewed with an oscilloscope. A digital circuit detects the position of the first trespassing of a controllable threshold (ground echo) and the position and value of the maximum value in each line. These values are transferred to the processor which can perform automatic gain control and range gate control. The processor returns filtered values of these positions which are used to locate two markers in the analog monitor signal.

The PROCESSOR is connected to the PHAREDIG boards by a simple bidirectional serial data/command bus. Via this bus the range gate in the acquisition timing is controlled, the additional information for the DAF interface is transferred and the communication with the AGC/MONITOR is realized. Via two RS422 datalinks the PHAREDIG processor communicates with the radar processor and with the OCP (which is a portable PC).

From the OCP commands can be given to PHAREDIG and via PHAREDIG to the radar. Each second a complete overview of the status of the radar and PHAREDIG is transmitted to OCP. The PHAREDIG embedded software is written in assembler.

4.6   Operators control panel

The PHARS SAR testbed is monitored and controlled by an Operators Control Panel (OCP), for which a portable Personal Computer was chosen.

4.6.1   OCP configuration

The Personal Computer used is a TOSHIBA 3100E with a RS422 interface.

A Plasma type of display was selected, since Liquid Crystal Displays suffer from mechanical distortion at low cabin pressure, which deteriorates the readability.

To cope with the demanding aircraft environment, a RS422 serial datalink was chosen instead of a standard RS232 link.

The software for the OCP was written in Turbo Pascal 5.1, although some routines were implemented as assembler calls.

4.6.2   Functions

The functions of the OCP during the operation of PHARS are:
-        Controlling the Operation Modes and Parameter Settings of PHARS,
-        Displaying the current status of PHARS,
-        Recording the history of the status,
-        Recording a logbook of reported errors and of operator actions.

OCP receives the status of the radar in a 64-byte binary message each second. This message can be saved in a status file which can be replayed afterwards. The bytes in the message are decoded; the status information is displayed in readable and understandable form.

Records of operator actions and system errors are written in the logbook file as text lines, including time of occurrence. Several types of error can be reported by the OCP, varying from hardware errors (e.g. datalink parity error) to protocol errors (e.g. NAK-ACK error). The logbook cannot be switched off. Each logbook line starts with the date, the OCP time and the PHAREDIG time, followed by the record. The operator can write comments by typing a # sign, followed by the comment.
As an example the first few lines of the logbook of the second PHARS flight are given in figure 4.6.1.

```
901108 11:58:36 00:00:00 session log file for "vlucht2" opened
901108 11:58:36 00:00:00 operator = johan
901108 11:58:49 00:00:27 "DEF \ocp\tbl\default.def" and "ST" executed after PHAREDIG wake up
901108 11:58:49 11:58:49 re 2
901108 11:58:53 11:58:54 rg 0
901108 11:58:56 11:58:57 gc 40
901108 11:59:12 11:59:12 st 115915
901108 11:59:44 11:59:44 st 115945
901108 12:00:13 12:00:14 nop
901108 12:07:53 12:07:54 log on
901108 12:10:46 12:10:47 #take off
901108 12:12:22 12:12:23 tx 1
```

Fig. 4.6.1:   Example of the first few lines of a PHARS logbook file

4.6.3   Screen lay out

The screen normally used in the OCP mode is the STATUS screen.

It is a text display of 25 lines by 80 characters, divided into four sections:

-      Header section,

-      PHARS information section,

-      System section,

-      Communication section.

```
Session: WISHFUL          PHARS FLYING TESTBED           900401  13:30:00

  ANTENNE                   RADAR                    PHAREDIG

                        Transmitter      ON      Mode             PRE
Elevation       30 °                            Range gate cmd   3510 m
Azimuth         -2 °    Chirptype         0      Range gate       3510 m
                        PRF           3400 Hz    Echo threshold    140
                                                 First echo at    4610 m
                        Gain         +50.0 dB    Gain cmd        +50.0 dB
                                                 Maximum           180
Temp. 1         35 °C   Temp. 3          21 °C   Maximum at       4720 m
Temp. 2         21 °C   Temp. 4          21 °C

                                                 PLL               OK
                        HF modules       OK      Comm. operator    OK
                        Power supply     OK      Comm. radar       OK
                        Overheating      OK      Time          13:30:00

Directory: C:\LOG                  Log file:    WISHFUL.mlg   Size:   6400
                                   Replay file: <none>
DA    live           log  1 on   error: OK                           35
>> GC 50
>> DA +
>>
>>
```

Fig. 4.6.2:   A typical STATUS screen of the PHARS SAR testbed

An example of a STATUS screen is shown in figure 4.6.2.

The header section shows Session Name, Date and Time, among other things. In a NoGo situation a flashing NoGo sign is added and an acoustic signal is activated.

The information section contains three sets of information. For example, in the PHAREDIG block, Gain cmd is the commanded value and in the radar block, Gain gives the actual setting reported by the radar via PHAREDIG.

In the system section the directory, name and size of the log file is displayed. If replay is selected, the replay filename is showed. On the third system line the OCP status is displayed: the parameter under command and its commanded value if applicable, the "LIVE" or "REPLAY" mode, Status Logging ON/OFF, System OK/ERROR, System activity indicator.

The bottom four lines are used to communicate with OCP.

4.6.4 Commanding

OCP control commands are used to switch ON/OFF logging, to change the screen, to see FREE disk space and to QUIT the program. A HELP function is available. With Ctrl-R a time mark is placed in the logbook.

PHARS control commands are used to change parameter settings, such as GAIN, Range Gate and Drift Angle correction, or to select operation modes, such as Transmitter ON/OFF, FIXate all parameters at current values. Parameters can be set by a number, can be increased or decreased step by step, and can be set to AUTomatic or FIXed. A special command is DEF [filename], which causes the use of a file for DEFault settings. With this tool a number of PHARS-modes can be prepared in advance, reducing the chance of errors occurring.

4.6.5 Replay

A logbook file has the format of an ASCII text file ready for printing.

A Status file can be replayed with a special mode of the OCP program. With the command REPLAY [filename] the indicated file is used as input for the OCP. The screen looks just like the screen during the flight, except for the indication "REPLAY". During replay the "speed" can be set to FAST (x10), NORMAL, SLOW (/5) and HOLD. Also available is a STEP mode and a SKIP mode.

4.7 SAR processing

4.7.1 General description of PHARS processing

The development of SAR processing software for PHARS was started using raw SAR data supplied by RSRE in the UK, while the SARGEN simulation package was being developed simultaneously. Using real and simulated data, a comparison of basic approaches to azimuth compression was carried out [Otten, FEL-89-131], resulting in a preference for a time domain correlation processor for PHARS. Range compression was implemented later, using a frequency domain approach. This was followed by a study and implementation of autofocus algorithms, and by the incorporation of motion correction in the processing.

The current SAR processor for PHARS, running on the CONVEX 230 at FEL, consists of three main modules:

- the first module performs range compression, real-to-complex conversion (image band filtering), frequency offset removal, synchronization and merging of radar data with motion data and corner turning. Compression, image band filtering and offset removal are combined in the frequency domain, as described in [Otten, FEL-89-C226], and more concisely in [Otten, 1990].

- the second module performs azimuth compression with the option of multilooking, line-of-sight correction using INS/ARA data or autofocus estimates, and along-track resampling. The output is complex or real, in floating point representation, thus preserving full dynamic range.

- the third module performs post-processing, i.e. scaling, slant- to ground range conversion by resampling, and logarithmic compression. The output consists of 1-byte pixel values.

This 3-module set-up is a compromise between modularity and efficiency, especially with regard to I/O operations.

Additionally, there are two autonomous autofocus modules, generating a phase correction curve which may be used in the azimuth compression.

Figure 4.7.1 shows the overall set-up.

PHARS PROCESSING
on CONVEX 230

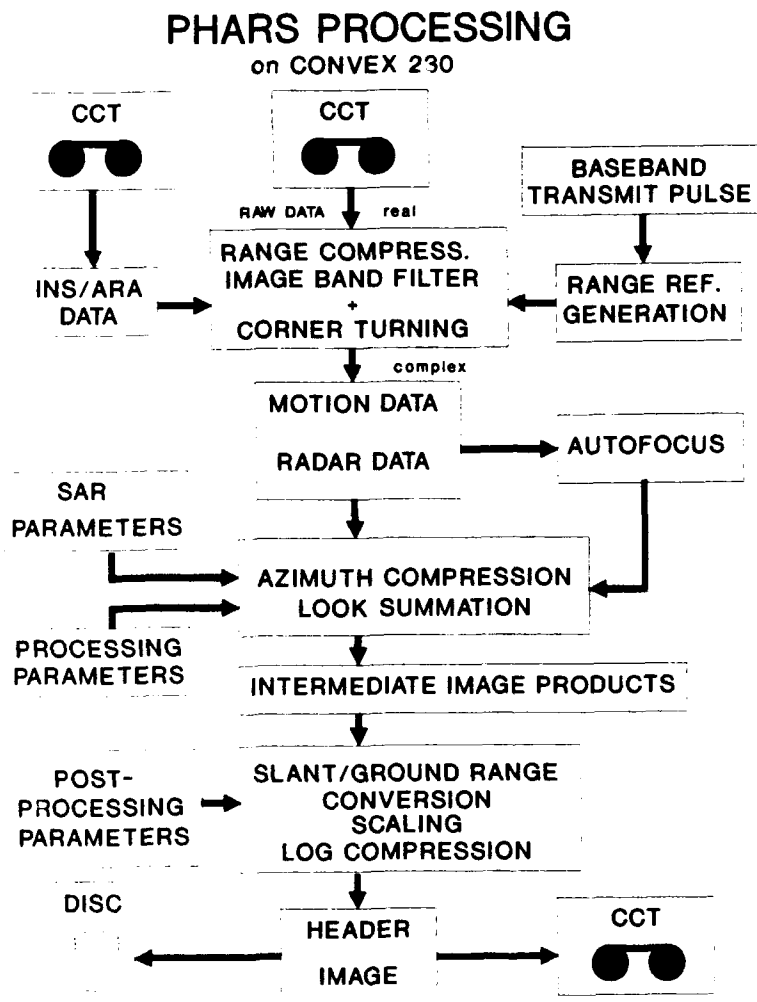Fig. 4.7.1:   PHARS processing set-up

All image files contain headers, which are formed by the first few 'image' lines, containing the main SAR and processing parameters, and some further identification data like data type, processing date, and an optional text.

Finally, there is a Doppler Centroid Estimation module [Madsen, 1989]-not shown in figure 4.7.1-which has been used in some processing experiments.

4.7.2   The motion correction scheme

There are several ways of approaching the problem of correcting undesired aircraft motion; ideally, the SAR image must be well focused, geometrically correct, and radiometrically correct. The current processor performs motion correction by applying phase shifts, corresponding to the line-of-sight motion, directly to the range compressed data[1]. This has the advantage that it achieves good focusing and geometric correction in azimuth at the same time [Wood, 1988], not considering along track velocity variation. It also has a disadvantage, with regard to radiometric correction, which will be discussed in the paragraph on flight test results.

Variation of along track velocity is corrected by azimuth resampling of the range compressed data. A cubic spline interpolator is used, which does not affect the signal spectrum over the Doppler band of interest seriously.

A radiometric correction is calculated for each pixel value, consisting of three intensity correction factors: the first factor compensates for range dependence; the second factor compensates for the influence of the antenna elevation pattern, and includes grazing angle, range, and roll of the aircraft; the third factor compensates for azimuth beam pointing errors, and for the radiometric effects of line-of-sight phase correction. It includes yaw and pitch angles, grazing angle, and the line-of-sight velocity component of the phase corrections.

---

[1]   They could also be applied to the azimuth reference functions

4.7.3 Autofocus

Two autofocus modules have been implemented, after an extensive survey [Otten, FEL-89-C243], and tested on simulated and real data.

The map drift method [Brown, Ghiglia, 1988] works as follows: N subapertures are separately processed to form N looks, the drift between these looks, caused by focusing errors, are estimated by crosscorrelation. The crosscorrelation functions are averaged over range. The drift estimates are used to form an Nth-degree phase correction polynomial. This process is repeated until the estimated drifts all equal zero.

The Least Squares Shift (LSS) method [Eichel, Ghiglia, Jakowatz, 1989] is based on the assumption that the imaged terrain, even if it is fairly homogeneous, can be thought of as a collection of point targets: one aperture is initially focused and Fourier transformed. In the frequency (or image-) domain, the strongest response is located, and the whole image line is shifted so that this maximum response corresponds to zero Doppler. This is done in each range gate. From the inverse transforms of the shifted image lines the phase error derivative is estimated by a least squares type of estimator, involving weighted averaging over range. This provides an estimate of the phase error derivative for every sample across the aperture.

Tests on simulated data and real data from a British SAR system (RSRE) indicated that the LSS method was the most powerful, mainly because of its ability to correct relatively high frequency errors [Otten, 1990]. The results with PHARS data are described in the next section.

The autofocus modules generate aperture-length phase error curves. By having them overlap, these curves are fitted together to form the total estimated trajectory. By comparing the overlapping parts, an error parameter is calculated, which mainly serves as an indicator of possible autofocus failures.

4.8   Flight test results

4.8.1   Radar performance

The analysed images from the November 1990 test flight include images of Scheveningen (urban area, sea, dunes), Wassenaar (urban area, wooded and open area), and the 'Flevo polder' (agricultural area). In the Flevo polder corner reflectors were set up. These few images contain a wide range of scene types, and a wide range of backscatter levels, providing quite an extensive test set for performance evaluation.

From visual inspection of the first PHARS images it could be concluded that:

a)   the images were reasonably clear and focused, indicating that, on the whole, the radar was operating correctly.

b)   a distinct light and dark pattern in the range direction could be observed, shifting back and forth with the rolling of the aircraft. This indicated the occurrence of an interfering echo signal via a second propagation path including some part of the aircraft, most likely the wing. A theoretical explanation of this effect taking into account the precise measurements of the aircraft wing and pod mounting was successful in that it did show the possibility of this interference effect occurring, confirming also the observed periodicity. The intensity of the interference was larger than initially expected; it was found later that the antenna had been set at a smaller depression angle than first intended, which explained how the interference could be so strong.

      By estimating the perturbed elevation antenna pattern, the images could be corrected well enough to remove the visible error.

c)   dark patches in the image showed stripes along the azimuth direction, obviously not coupled to aircraft motion, indicating a small error signal from the radar or recording hardware. This could be traced to cross talk of digital clock signals into the radar signal, mentioned in 4.5.5. Since these cross talk components were found to be very constant, they could be removed during processing.

d)   some artefacts occurred in the images: some could be attributed to an occasional faulty line in the raw data, and to raw data overflow, mainly caused by strong reflections from nadir.

      A more detailed analysis of image data revealed that:

e)   The point target response in range showed a peak sidelobe far from the main lobe, approximately 35 dB down. This might be attributed to a small amplitude ripple in the

received pulse. This sidelobe does not exceed reasonable image quality criteria. Furthermore, the range response was not symmetrical, see figure 4.8.1 It appeared that the range spectrum of the recorded data was not quite flat over the signal bandwidth. The irregular sidelobes indicate phase distortion of the received pulse, the spectrum indicates amplitude drop. The latter effects may by due to thermal effects during transmission of a pulse. Phase distortion can be compensated, though this has not been done as yet. The observed drop in the amplitude spectrum cannot be undone; it causes a loss in signal-to-noise ratio between 1 and 2 dB.

f) a sensitivity analysis, using corner reflector responses, indicated a lower sensitivity than might be expected on the basis of theory. Since the corner reflector signal level can only be derived from the image data, the observed loss includes all possible losses, including those in the processing, which, however, are thought to be 2 dB at most. Part of the loss can be attributed to the interference effect; how much exactly is unknown. An estimate of integration losses is 8 dB. The observed sensitivity at the optimum point was about -38 dB. With the intended 30 degree depression angle this would have been -45 dB.

Figures 4.8.2 and 4.8.3 show fully processed images of Scheveningen, showing a bit of the North Sea, and of Wassenaar, and part of Leiden. The subjective image quality is quite good, although there is some visible evidence of radiometric error. These images are processed in 4 look, 3 m resolution mode.

RANGE IMPULSE RESPONSE
UNWEIGHTED
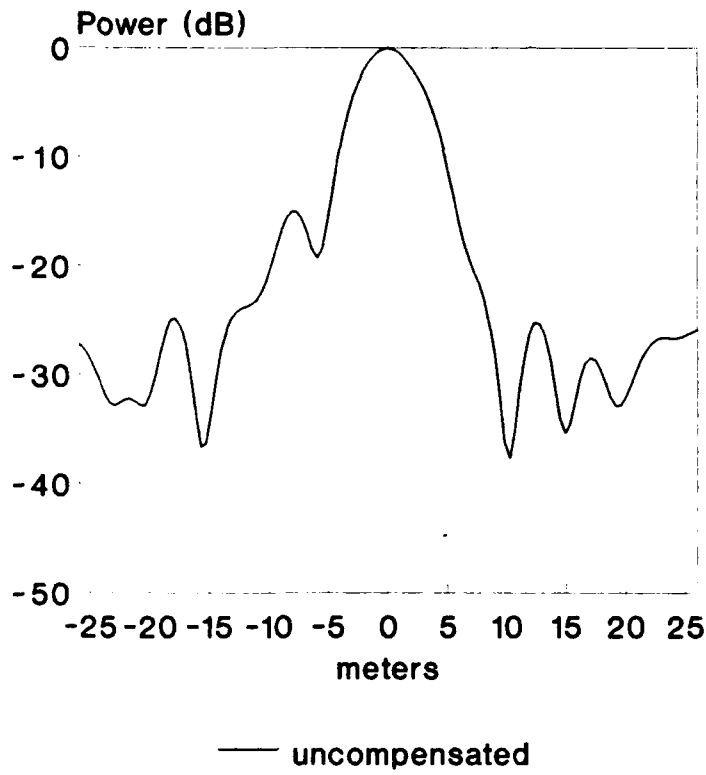
—— uncompensated

PHARS

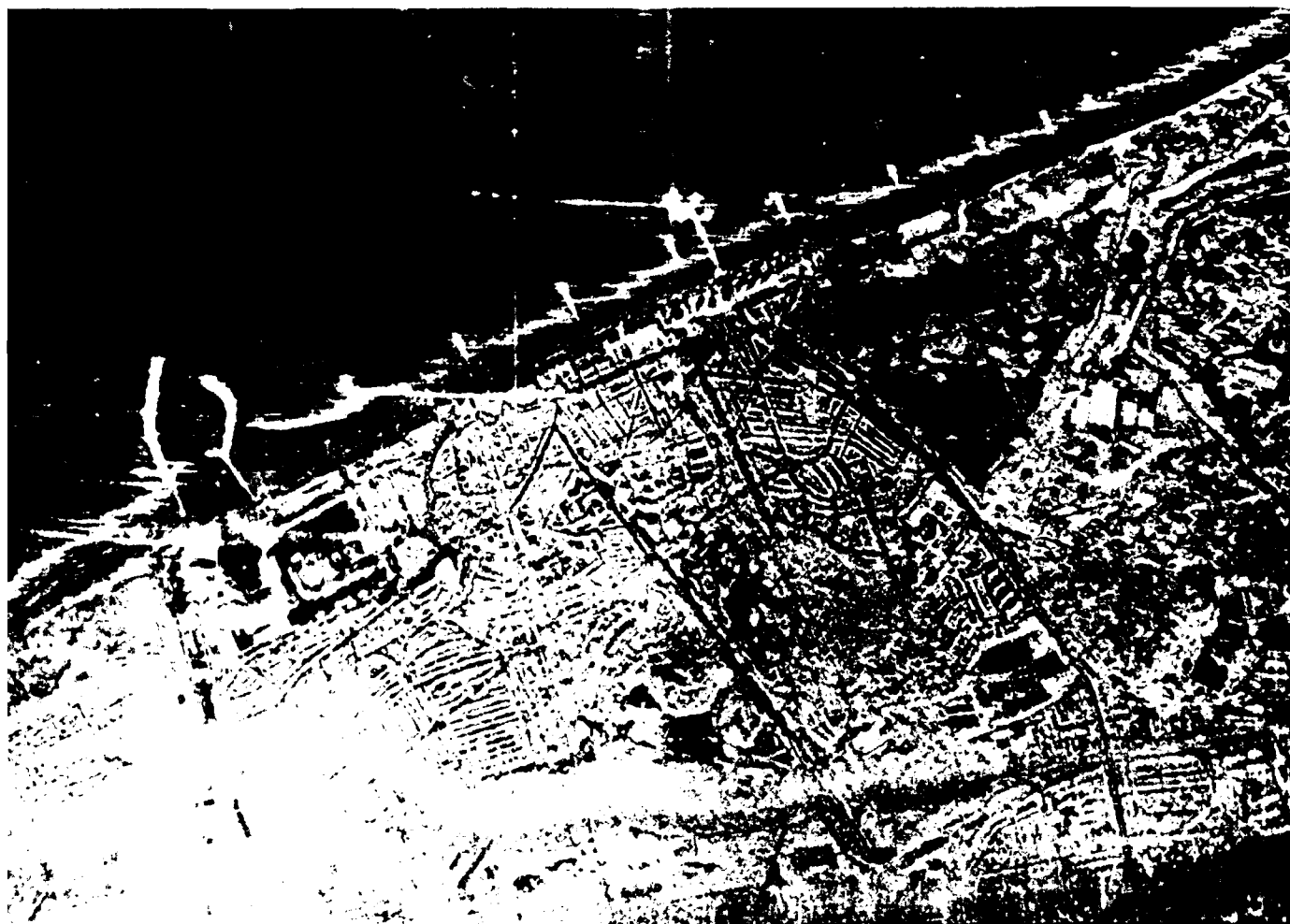Fig. 4.8.1:   Range impulse response

Fig. 4.8.2:   PHARS image of Scheveningen and part of the North Sea

Fig. 4.8.3:   PHARS image of Wassenaar and part of Leiden

4.8.2   Motion compensation

Two aspects of motion compensation will be briefly discussed here:

1)   The quality of the trajectory data

2)   The image quality with the current compensation scheme

As for 1), the INS/ARA motion data were found to be quite reliable. Applying phase corrections derived from them visibly improved image quality, and from the corner reflector responses it could be derived that azimuth resolution and sidelobe levels were practically ideal. Only in the 1 meter resolution, single-look mode, a slight resolution loss was observed (10%, at 6.3 km range), and some further main lobe widening into the first sidelobes, apparently due to a small low frequency error. Figure 4.8.4 shows 3 m/4 look (50% overlap) and 1 m/single look point target responses in azimuth.

AZIMUTH IMPULSE RESPONSE WEIGHTED, 4 LOOKS

AZIMUTH IMPULSE RESPONSES WEIGHTED, SINGLE LOOK
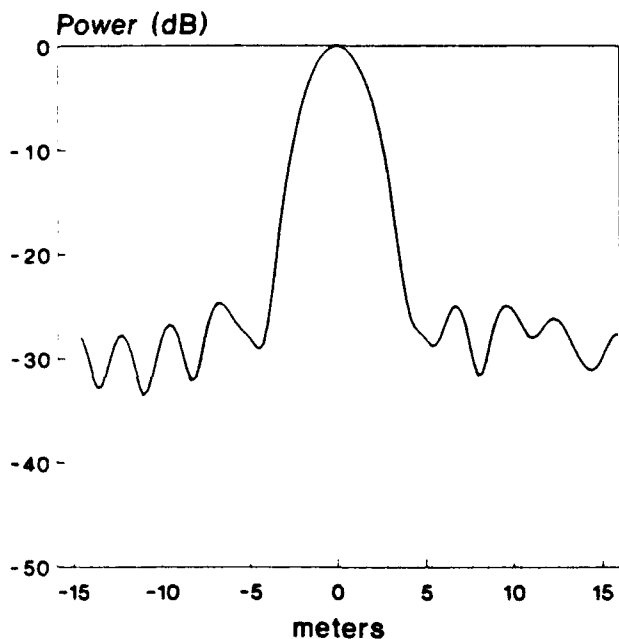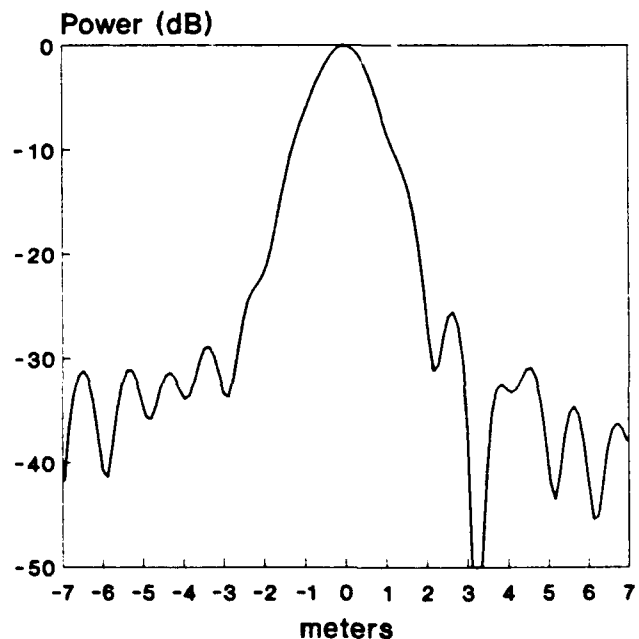
Fig. 4.8.4:   Motion compensated azimuth impulse responses
left: 3 m resolution, 4 looks with 50% overlap
right: 1 m resolution, single look

The success of the antenna elevation pattern correction also proves the basic validity of roll measurements, although little can be said about accuracy. The yaw and pitch measurements could not be so explicitly verified, but seem to be realistic. Further validation of these will be derived from Doppler centroid estimations, and a more detailed radiometric analysis.

Autofocus was also applied to the data, using both the map drift and LSS methods. The success of these methods varied considerably: the map drift method works reasonably well within its limitations. On the PHARS data it worked satisfactorily up to about a 1 second synthetic aperture (giving 2 m single look resolution at 6 km), on most scenes except sea, and those parts of the Flevo polder data that contained no other features than large agricultural fields. These fields provide insufficient support for cross correlation of looks. An additional problem with this short range system is that averaging over range is limited, due to the significant variation of depression angle over the swath. The LSS method was found to be somewhat unpredictable: its performance ranges from very bad -this occurs mostly when a very dominant, complex scatterer[2] is present- to very good -this occurred on the corner reflectors, where the full 1 m resolution was achieved without difficulty. The range averaging problem also affects the usefulness of this type of estimation for PHARS data, see [Otten, FEL-91-C185] for detailed information.

From the very accurate trajectory estimation on the corner reflectors, the approximate error in the INS/ARA data could be determined. This error was in accordance with the observed focusing quality, but was more than figure 3.3.2 suggests: It was found that error was due to an error in the aircraft velocity measurements. An improved velocity estimate using GPS data eliminated the remaining error.

The second item of this paragraph concerns the quality of the SAR image, after the trajectory data have been incorporated.

Firstly, focusing is good, as was already mentioned. Azimuth resolution up to about 1 m is actually achieved. Secondly, it can be estimated from the observed trajectory data quality that the azimuth geometric distortion due to LOS less than 0.1% per kilometer range, meaning that for every 100 m in azimuth, the absolute azimuth error is less than 1 m at 10 kilometer range. In practice, this error will not always accumulate, so that the largest absolute error in a given scene depends on the actual flight path. The already mentioned velocity error causes a fixed azimuth scaling error of 0.3%. In range, significant deviations from the ideal track appear to occur (several tens of meters), when the track is long enough (several kilometers). This range migration is too slow to affect the focusing, but causes image pixel migration in large scenes. This is not

---

[2]   i.e. consisting of more than one 'point target'

accounted for in the current processor. Image resampling in range will be required to eliminate this effect.

Thirdly, the quality of radiometric correction could not be reliably assessed, mainly due to uncertainties in the antenna elevation pattern, which is deformed by interference. Because of aircraft roll, this also precludes accurate assessment of yaw banding and Line Of Sight (LOS) velocity correction. One problem could be observed, however: when a long track is processed, the absolute LOS velocities, which are contained in the phase corrections, become quite large. These corrections then introduce a very large Doppler centroid shift, which makes it impossible to unambiguously correct the image radiometrically with the current set-up. This can only be avoided by transferring part of the phase corrections from the data to the azimuth reference, and taking further measures to eliminate the resulting geometric distortion.

4.9   Conclusions

A compact radarsystem with a high level of mechanical and electrical integration is realized.
For the mechanical construction CAD/CAM programs have been used, resulting in a radarsystem
with small dimensions.
For the design of the electrical circuits CAD programs in combination with modern components
like MMIC's, digital chips, power FET's, etc. and thin film technology are used.

From the results of the November 1990 PHARS test flight, it can be concluded that:

-     The radarsystem has functioned well electrically and mechanically during the testflight and
      an amount of usable data is available to verify the results of the other studies in this
      definition study.
-     the radar is operating correctly, and providing clear imagery. The desired resolutions have
      been achieved.
-     Measures have to be taken to prevent interfering reflections from the aircraft wing.
-     The range response could be slightly improved. To do this it has to be determined why the
      received pulse spectrum is not quite flat.
-     The azimuth impulse response closely approaches the ideal response, when motion
      compensation is applied. This, and the fact that focusing is not very good without motion
      compensation, proves that the motion compensation system is working satisfactorily.
-     In the case of PHARS, direct compensation is more reliable than autofocus. Autofocus using
      the map drift method works well on most scenes, except on very low contrast scenes, like
      agricultural fields without any smaller scale features. The LSS method cannot be
      indiscriminately applied to an arbitrary scene. It is easily upset by complex dominant targets;
      on the other hand, it works even better than direct compensation on actual point targets.
      Both autofocus algorithms are useful tools, particularly for research, where some human
      intervention is possible: a more sophisticated strategy would have to be devised in order to
      make autofocus into a fully automatic procedure. At longer ranges it would also become
      more advantageous to use autofocus.
-     Geometric accuracy in azimuth is good, in range it is reasonable but needs some
      improvement, especially for large scenes. This requires range resampling in the image to be
      implemented in the processor.

- Radiometric accuracy still needs to be determined. Uncertainty in the antenna elevation pattern, including the interference effect, have prevented an accurate assessment of radiometric accuracy so far. It has been found, however, that with the current processor good geometric and radiometric accuracy cannot be simultaneously obtained when the deviations from the ideal flight path are relatively large. This is most likely to occur if the processed scene is large. To overcome this, the processor will have to be modified, and will become more complex.

- Sensitivity of the radar is lower than expected. This is partly due to the interference effect. A best value of -38 dB was obtained (i.e. noise equivalent gamma at 6 kilometer range). The outcome of a next test flight, using a interference screening plate, gain measurements on a new antenna, and noise- and amplifier gain measurements on the radar hardware should lead to a better evaluation of the actual losses.

- The data recording system needs minor adjustments but is otherwise OK. Some cross talk, most likely from a system clock, has been found in the radar signal: this can be removed during processing.

A more detailed account of the PHARS data evaluation is given in (Otten, FEL-91-C101)..

5   PHARUS PREDESIGN STUDY

5.1   Introduction

In this chapter the predesign of the PHARUS system is described. The predesign will serve as a starting point for the development of the PHARUS system in the realisation phase of the project. The technical properties of the proposed system should be regarded as design goals. The predesign is based on the knowledge and the expertise that was built up in the preparatory studies as reported in the previous chapters. It is therefore expected that the PHARUS system will be in close agreement with the design goals without experiencing important difficulties or delays.

During the definition study the predesign was heavily influenced by financial restrictions on the PHARUS realisation phase. Initially the design was directed towards a high resolution SAR system (to comply with defence studies) with operational capabilities. This implied a high power antenna design: a resolution of 1.5 meter should be maintained over a sufficiently long range for operational applications. Apart from the powerful radar and its associated high speed, high capacity, digital processing and recording equipment, the ground segment and the documentation should be well developed, in order to enable reasonable success scores and short turn-around times in campaigns.
Soon it turned out that such a system could not be afforded under the available financial budgets. Alternatives were then developed. The original plan however is described in chapter 5.2.

The alternative designs that were consecutively developed returned more or less to earlier views on the design goals for a polarimetric SAR [Krul, 1986]. By reducing the maximum resolution, both in range and in azimuth, and by limiting the maximum range, the radar design became less demanding. As a consequence the digital sampling frequency, the real time processing speed and the storage data rate could be reduced.
Another aspect of the first high resolution design, the operational capability, was also reconsidered and finally dropped from the plan. In this way the radar development received as much priority as possible, enabling a state of the art design, cost-effective and worthwhile developing. Consequently the current design should be marked as a medium to high resolution polarimetric SAR for research studies, with a limited ground segment structure and limited documentation. This design is presented in chapter 5.3.

5.2   The preliminary high resolution design

5.2.1   general

In an active phased array SAR system as considered in this study, the number of microwave modules determines both the transmitted power and the antennagain. Each module can be connected to only one patch antenna, if the low cross polarisation design of the antenna study is followed (outcome of chapter 2.1). The system thus has to be realised with a limited number of high power modules. In this design a number of 128 modules was chosen, rendering 2.5 kW transmitted power when the individual modules deliver 20 Watt, like the PHARS modules. The antenna is most likely configured as 8 x 16 elements (elevation x azimuth), though 4 x 32 is also a possibility. The first option results in a better definition of the elevation diagram.

The selected configuration will be capable of realizing high resolutions over long ranges in the single polarisation mode. In dual and quad pol (polarimetric) mode, the range is reduced. Alternatively, the resolution in range and in azimuth can be reduced in any of the modes, while maintaining the maximum range. Internally this is translated in terms of lowering the sampling frequencies in azimuth (Doppler bandwidth) or in range (signal bandwidth). Some unconventional modes are the widescan mode, where the full range is scanned in two steps, a MTI (Moving Target Indication) mode and a Spotlight mode, where the antenna is aimed during a longer time at an area of interest, with the purpose of increasing the resolution in that area to very high values.
A summary of the properties of the high resolution system is given in table 5.1.

PHARUS performance for high resolution SAR	
1,5 m range resolution 0,75 m single look azimuth resolution 4 polarisations 2500 W transmit power 60 km maximum range 100 Mb/s data rate	recording mode: 1 or 2 polarisations polarimetric dual swath long range MTI spotlight selectable resolution

Table 5.1:   Key features of the high resolution design

5.2.2   The radar

The microwave modules form the most important part of the radar. They are more complex than the PHARS modules, because the PHARUS is a polarimetric SAR, necessitating a dual receive path, and the possibility to transmit either Horizontal or Vertical polarisation. Further extensions are the internal calibration path and two separate vector modulators as opposed to a single phase shifter in the PHARS. The design of one or more MMIC's for these functions is foreseen.

The central node of the PHARUS system is similar to that of the PHARS testbed. The development of a high bandwidth chirp generator was studied already, and is not a serious problem.

The thermal control of the radar, especially the modules needs a proper thermal design. The amount of heat produced is considerable. From the point of view of radar stability, temperature control is recommended.

5.2.3   Data recording and on-board processing

The two channels of high bandwidth analog radar data are first of all digitized at 220 MHz in 8 bits. The resulting high bitstream cannot be handled by single channel digital circuits. Therefore the data is split up and treated in parallel.

Four presummers are available to process the data of one or two channels. Four output channels are needed in the polarimetric modes, but in single polarisation mode only one output channel is needed. To comply with these varying needs, the datastreams can be configured as necessary in a matrix switch.

After presumming the datarate is reduced, but still high. In the design new high capacity cassette recorders are foreseen for the digital storage on tape. This type of recorder accommodates a 100 Mbit/s datastream. The application of on-board pulse compression is not strictly necessary in this design and was still under discussion when the design was stopped.

5.2.4   Ground segment

For operational purposes it is important to have a flexible and efficient groundsegment. In the design two items received particular attention, the data conversion system and the SAR processor.

The dataconversion system should be capable of playing back the datatapes from the aircraft and transferring the data to computer compatible tapes. The Data Conversion System at the National Aerospace Laboratory needs an upgrade to enable this function. A play-back tape-recorder has to be acquired, and several digital circuits and software have to be updated.

The SAR processing facilities actually will consist of two processors in this plan. A flexible research processor at FEL-TNO and an efficient production processor at NLR. The processors are to be developed at general purpose supercomputers, without additional acceleration hardware. Both processors will be able to handle polarimetric data. The research processor also accepts data for the experimental MTI and spotlight modes.

5.2.5   Documentation

The documentation consists of technical, maintenance and user manuals. The production of such an extensive set of documentation takes much time. The workpackage starts early in the project to ensure a sufficient level of detail in the documentation.

5.3 The final PHARUS design

5.3.1 general

The approved predesign of the PHARUS system compares well to the high resolution design. At various levels in the system and in the project reductions have been introduced, without altering the nature of the system.

The number of modules in the radar is reduced by a factor of 4 to 32, probably configured as 2 x 16 elements. The transmitted power is now 600 Watt. The range resolution is reduced to 4 meter. The system has polarimetric capability. Most of the imaging modes are conserved. The widescan mode is no longer of interest because of the reduced maximum range of the radar. The experimental MTI and spotlight modes were also left out, though experiments in this direction will be feasible in a later stage. A summary of the key properties of the PHARUS system can be found in table 5.2.

mode	res (m)	numb.of looks	swath (km)	max.dist (km)	min.γ (dB)	flight alti.(m)	aperture time (s)
1 channel lin.pol (VV or HH)	4 8 16	3 8 20	8 12 18	15 19 26	-30 -30 -30	6000 6000 6000	1.06 0.67 0.46
4 channel polarimetr	4 8 16	3 6 12	1.8 3.8 6.5	7 9.8 13	-40 -40 -40	4500 5000 6000	0.5 0.35 0.23

Table 5.2: Key features of the PHARUS design

The reduced range resolution offers the possibility to simplify the digital data handling and the storage chain (lower speeds and less data to handle). An important factor is the continued use of the existing NLR datarecording chain, which also reduces the costs of updating the dataconversion facility in the groundsegment.

The production SAR processor is no longer part of the project. As a result the research processor will have to be used for production as well. There will probably be a restriction on the volume of data that can be handled by the processor, but since the intention of operational use has been abandoned in the project, this will not cause serious problems.

Finally the documentation of the system will be limited to the level needed by the designers and technicians to build the system and to do maintenance and repairs. Thus the amount of documentation is greatly reduced.

5.3.2 the radar

The radar is highly comparable to the high resolution design (see chapter 5.2.2). The reduction of the number of microwave modules to 32 facilitates the thermal control in the system.

The reduced radar bandwidth has no implications for the design. The PHARS was designed to accommodate the large bandwidth necessary in a high resolution radar. Now this central node design exists, it will be used again, without actually exploiting its high bandwidth capabilities.

The radar will be set up in such a way that extensions in a later stage will be possible. The use of a larger bandwidth as discussed above, is one example. Another one is the enlargement of the radar by combining antenna panels of 2 x 8 elements into one larger radar of 2 x 16, 4 x 16, 2 x 24 or 4 x 24 elements. The result is a more powerful radar, capable of imaging larger area's, longer ranges or at higher resolutions.

5.3.3 Data recording and on-board processing

The two channels (co- and cross polar) of the analog radar data may be digitized at a maximum speed of 100 MHz in 8 bits. The resulting bitstream is handled as discussed in 5.2.3.

After presumming pulse compression will be applied on board. This is necessary for the following reasons: the lower range resolution would lead to a high amount of extra samples at the end of the recorded range, if the pulse compression is not done on board. The limits of the current datarecording unit forces us to compress the data as much as possible, especially in the polarimetric mode, which is very demanding on datarate.

Unfortunately the capabilities of the digital hardware cannot be extended so easily, when the radar would be extended to more TR modules. A larger bandwidth will force us to redesign large parts of the data acquisition unit with components capable of handling higher speeds. The current design fully exploits the speed of the hardware applied. This bottle-neck will be further studied during the PHARUS design phase.

5.4   Conclusions

The predesign phase of the PHARUS definition study led to a plan for a polarimetric, medium to high resolution (4 meter), state of the art SAR system. An earlier, more costly design of a high resolution (1.5 meter) operational system was turned down for budgetary reasons.

The current plan has been accepted and will lead to a sophisticated radar system in a couple of years time. With a strong emphasis on the radar system, the ground segment (dataconversion and processing) and the documentation had to be limited. Consequently the radar is an experimental system rather than an operational one. On completion it will be possible (it may turn out to be necessary as well) to complete the system with facilities that were foreseen earlier.

The definition study PHARUS, consisting of three preparatory studies has provided the experience and insight to design the PHARUS system with confidence. The realisation of PHARUS does not have to take more than a couple of years. A state of the art polarimetric SAR will soon be available.

6   GENERAL CONCLUSIONS

The PHARUS definition study was carried out within the budgetary limits (time and financial) and was successful when compared to the initial objectives. The study has led to a tremendous increase in knowledge on SAR technology, patch antenna technology, high accuracy aircraft motion compensation and SAR processing. The successful development of a SAR testbed formed part of the study. It's images have been widely received with enthusiasm. Internationally, the project received much attention. This enables the partners in this study to contribute with their knowledge in other, international studies and programs, both airborne and spaceborne. The development and approval of plans for the PHARUS polarimetric SAR means a successful conclusion of the definition study and, more important, the outlook on a continued SAR program, ending with the availability of a state of the art SAR facility in The Netherlands, both important for Civil Remote Sensing and Defense research. From the preparatory studies in the PHARUS definition study the following executive conclusions can be drawn:

The antenna design study has increased the knowledge in patch antenna technology sufficiently to enable the design of the PHARUS antenna.
A very promising calibration method is developed to calibrate distributed transmitters and receivers.
Special near-field measurement facilities are realised for low-PRF measurements.

In the study of motion and motioncompensation, a raw SAR data simulator is developed to analyse the degradation of the image under user-defined flight conditions.
A motion measurement system is realised in the SAR testbed and has performed to satisfaction.

In the third study a modern, compact airborne radarsystem for experimental and verification purposes is realised. With the use of CAD/CAM programs and modern components like MMIC's, PLA's, etc. a high level of integration is obtained.

In general, the experimental SAR system has functioned as is specified. However, there are some minor details that require hardware and software adaptations. The processing of SAR data from the first flight of PHARS has resulted in very good images.

REFERENCES

L. Krul (ed.), 1986,
"Voorstudie Coherente radar", BCRS report nr. BCRS 86-03 (in Dutch).

Bahl, I.J. and P.Bhartia,
"Microstrip Antennae", Artech House, Dedham Massachussetts, 1980.

Van de Capelle, A. et al.,
"Microstrip Antennae and Arrays, Internal Research Report of the KU Leuven", Oct. 88,
Katholieke Universiteit Leuven, Dept. of Elec. Eng., U.D.C. 621.296.67.

Caverly, R.H. and G.Miller
"The Frequency-Dependent Impedance of Pin Diodes"
IEEE-MT, vol. 37 No. 4, April 1989, pp. 787-790

Pozar D.M., B.Kaufman,
"Design Considerations for Low Sidelobe Microstrip Arrays", IEEE Trans. on Antennae and
Propagation, Vol. 38, no. 8, August 1990, pp 1176-85.

Paquay M.H.A.,
"PHARUS WP1.1F/T, Studie naar microstrip antennes als basiselement voor de PHARUS-
antenne", PHARUS report PH9068FEL, Oct. 1990, FEL-xx-Cxxx. (In Dutch).

A.P. de Hek,
"C-band fasedraaier voor PHARUS", FEL-TNO

Visser, H.J.:
"Planar Near-Field Measurement of Non-Reciprocal Antennae", Physics & Electronics
Laboratory TNO, Report No. FEL-90-B092, April 1990.

Visser, H.J.:
*"Measuring Low-PRF Pulsed Signals With a Standard HP 8510B Vector Network Analyzer
Within Milliseconds"*, Physics & Electronics Laboratory TNO, Report No. FEL-90-B238,
August 1990.

Visser, H.J.:
"First Pulsed Near-Field MEasurement Results", Physics & Electronics Laboratory TNO,
Report No. FEL-90-B262, August 1990.

Otten, M.P.G.,
'Aircraft SAR simulation SARGEN 1.0' report nr. FEL-89-44, Physics and Electronics
Laboratory, The Hague, The Netherlands, February 1989

Otten, M.P.G.,
'A MOTION COMPENSATION STUDY FOR THE PHARUS PROJECT', paper no. 24 of
the AGARD Conference Proceedings No.459, High resolution air- and spaceborne radar,
May 1989, The Hague, The Netherlands

Otten, M.P.G.,
'Extended aircraft SAR simulation: SARGEN 2.0' PHARUS nr. PH8953FEL

Otten, M.P.G.,
'SAR processing methods' report nr. FEL-89-131, Physics and Electronics Laboratory, The Hague, The Netherlands, April 1989

Otten, M.P.G.,
'Alternative solutions for Hilbert filtering in a pulse compression radar' report nr. FEL-89-C226, Physics and Electronics Laboratory, The Hague, The Netherlands, August 1989

Otten, M.P.G.,
'Alternative solutions for Hilbert filtering in a pulse compression radar' Proceedings of the IEEE 1990 International Radar Conference, May 1990, Arlington, VA, p.86-89

Wood, J.W.,
'The removal of azimuth distortion in synthetic aperture radar images', Int. Journal of remote sensing, vol.9, no.6, 1988

Otten, M.P.G.,
'Phase error estimation for PHARUS: a review of autofocus and related algorithms' report nr. FEL-89-C243, Physics and Electronics Laboratory, The Hague, The Netherlands, September 1989

Brown, W.D., Ghiglia, D.C.,
'Some methods for reducing propagation-induced phase errors in coherent imaging systems' Journal of the Optical Society of America, A 5, p.924-957, June 1988

Eichel, P.H., Ghiglia, D.C., Jakowatz, C.V.,
'Speckle processing method for synthetic aperture radar phase correction' Optics letters, vol. 14, No.1, January 1989, p.1-3

Otten, M.P.G.,
'Comparison of SAR autofocus algorithms', Proceedings of the Military Microwaves Conference, 11-13 July 1990, London, p.362-367

Madsen, S.N.,
'Estimating Doppler Centroid of SAR data' IEEE trans. on Aerospace and Electronic systems, vol AES-15, no. 2, March 1989, p.134-140

H. Pouwels and L.J. Aartman:
A modular and versatile acquisition, recording and preprocessing system for airborne remote sensing; proceedings ISPRS symposium "Progress in Imaging Sensors"; ESA SP 252, Nov 1986, p113-121.
(also available as NLR MP86069U, NLR Nov 1986).

J. de Goede:
PHARS digitaliserings systeem, deel I t/m IV (in Dutch); NLR Contract Report CR 91079 L, NLR 910402

A.R. Vellekoop, P. Snoeij and M. Tian,
"Interne calibratie aspecten in het PHARUS project", PHARUS report PH-9106TUD, Feb. 1991 (in Dutch).

Otten, M.P.G.,
'PHARS data processing and evaluation' report nr. FEL-91-C101, Physics and Electronics Laboratory, The Hague, The Netherlands *(forthcoming)*.

P. Hoogeboom
(project manager)

P.J. Koomen
(for all authors)

REPORT DOCUMENTATION PAGE   (MOD-NL)

1. DEFENSE REPORT NUMBER (MOD-NL) TD91-3982	2. RECIPIENT'S ACCESSION NUMBER	3. PERFORMING ORGANIZATION REPORT NUMBER FEL-91-A375
4. PROJECT/TASK/WORK UNIT NO. 22340.0	5. CONTRACT NUMBER -	6. REPORT DATE NOVEMBER 1991
7. NUMBER OF PAGES 107 (EXCL RDP & DISTR.LIST)	8. NUMBER OF REFERENCES 27	9. TYPE OF REPORT AND DATES COVERED FINAL REPORT

10. TITLE AND SUBTITLE
DEFINITION STUDY PHARUS: FINAL REPORT

11. AUTHOR(S)
SEE PAGE 2

12. PERFORMING ORGANIZATION NAME(S) AND ADDRESS(ES)
TNO PHYSICS AND ELECTRONICS LABORATORY, P.O. BOX 96864, 2509 JG THE HAGUE
OUDE WAALSDORPERWEG 63, THE HAGUE, THE NETHERLANDS

13. SPONSORING/MONITORING AGENCY NAME(S)
NIVR/BCRS

14. SUPPLEMENTARY NOTES

15. ABSTRACT (MAXIMUM 200 WORDS, 1044 POSITIONS)
This report describes the results of the PHARUS definition stage, which can be distinguished in three main parts:
- Antenna technology study,
- Motion compensation study,
- Realisation of a SAR testbed.
The antenna technology study was mainly focussed on the theory and design of patch antennae. Further the study included the theory of internal calibration of SAR systems, microwave components under pulsed conditions and measurements of phased arrays under operational conditions.
The second study was focussed on finding a solution for the motion compensation in PHARUS. The study included the development of a SAR data simulator to evaluate the degradation of the SAR image by the motion of the aircraft. A motion sensor package for PHARUS was proposed. For verification, this motion sensor package was used in the SAR testbed.
The third study consisted of the design and development of a SAR testbed and processor to gain experience with airborne SAR technology. The SAR testbed had an active eight element antenna with distributed solid state power generation. Innovative microwave technology was used in the design of the radarsystem.
A real time digital azimuth filter was developed to reduce the large data stream to such a level that maximum recording capacity was not overdrawn. A personal computer enabled full control over the radarsystem. Algorithms are developed for the use in the SAR processor. In combination with the results of the motion compensation study the requirements for PHARUS were met.
The results of the definition study are used for the pre-design of the PHARUS system.

16. DESCRIPTORS	IDENTIFIERS
SYNTHETIC APERTURE RADAR ANTENNA MOTION SIMULATION PROCESSING SIGNAL PROCESSING HARDWARE SYSTEM DESIGN	PHARUS

17a. SECURITY CLASSIFICATION (OF REPORT) UNCLASSIFIED	17b. SECURITY CLASSIFICATION (OF PAGE) UNCLASSIFIED	17c. SECURITY CLASSIFICATION (OF ABSTRACT) UNCLASSIFIED

18. DISTRIBUTION/AVAILABILITY STATEMENT UNLIMITED AVAILABILITY	17d. SECURITY CLASSIFICATION (OF TITLES) UNCLASSIFIED